MODELLING AND VERIFICATION OF TiO_2/ZnO/EGW NANO COOLANT ON THE TiN MILLING TOOL PERFORMANCE

LINGENTHIRAN A/L SAMYLINGAM

DOCTOR OF PHILOSOPHY

UNIVERSITI MALAYSIA PAHANG

UNIVERSITI MALAYSIA PAHANG

DECLARATION OF THESIS AND COPYRIGHT

Author's Full Name : LINGENTHIRAN A/L SAMYLINGAM

Date of Birth : 29 SEPTEMBER 1988

Title : MODELLING AND VERIFICATION OF TiO_2/ZnO/EGW NANO COOLANT ON THE TiN MILLING TOOL PERFORMANCE

Academic Session : SEM 2 2018/2019

I declare that this thesis is classified as:

☐	CONFIDENTIAL	(Contains confidential information under the Official Secret Act 1997)*
☐	RESTRICTED	(Contains restricted information as specified by the organization where research was done)*
☑	OPEN ACCESS	I agree that my thesis to be published as online open access (Full Text)

I acknowledge that Universiti Malaysia Pahang reserves the following rights:

1. The Thesis is the Property of Universiti Malaysia Pahang
2. The Library of Universiti Malaysia Pahang has the right to make copies of the thesis for the purpose of research only.
3. The Library has the right to make copies of the thesis for academic exchange.

Certified by:

_______________________ (Student's Signature)

_______________________ (Supervisor's Signature)

880929-10-5417
Date:

ASSOC.PROF.DR.KUMARAN A/L KADIRGAMA
Date:

NOTE : * If the thesis is CONFIDENTIAL or RESTRICTED, please attach a thesis declaration letter.

SUPERVISOR’S DECLARATION

We hereby declare that we have checked this thesis and in my opinion, this thesis is adequate in terms of scope and quality for the award of Doctor of Philosophy.

____

(Supervisor’s Signature)

Full Name : DR. KUMARAN A/L KADIRGAMA

Position : ASSOCIATE PROFESSOR

Date :

____

(Co-Supervisor’s Signature)

Full Name : Dr. MD MUSTAFIZUR RAHMAN

Position : PROFESSOR

Date :

STUDENT’S DECLARATION

I hereby declare that the work in this thesis is based on my original work except for quotations and citations which have been duly acknowledged. I also declare that it has not been previously or concurrently submitted for any other degree at Universiti Malaysia Pahang or any other institutions.

____

(Student’s Signature)

Full Name : LINGENTHIRAN A/L SAMYLINGAM

ID Number : PMM16001

Date :

MODELLING AND VERIFICATION OF TiO_2/ZnO/EGW NANO COOLANT ON THE TiN MILLING TOOL PERFORMANCE

LINGENTHIRAN A/L SAMYLINGAM

Thesis submitted in fulfillment of the requirements
for the award of the degree of
Doctor of Philosophy

Faculty of Mechanical Engineering

UNIVERSITI MALAYSIA PAHANG

APRIL 2019

ACKNOWLEDGEMENTS

First and foremost, the deepest sense of gratitude to my mother and the God, who guide and gave me the strength and ability to complete this research successfully. Infinite thanks I brace upon my mother and Him. I would like to express my sincere gratitude to my supervisor Associate Prof. Dr. Kumaran Kadirgama and Associate Prof. Dr. Devarajan for their continuous guidance, support and encouragement, which gave me huge inspiration in accomplishing this research. Their supports encourage me to become confident and competent person to work individually as well as in group.

Not forgot to thank the panels who critics the outcome of this research besides providing some suggestions to improve the discussion and conclusion as well. I would also like to express my deepest appreciation to my family whom always support and motivate me to complete this research and thesis. I also owe a depth of gratitude to my university friends Yoges, Arvind and Mohanesen who shared their knowledge and ideas that lead to the completion of this thesis.

Finally, to individuals who has involved neither directly nor indirectly in succession of this research with thesis writing. Indeed I could never adequately express my indebtedness to all of them. Hope all of them stay continue support me and give confidence in my efforts in future. Thank you

ABSTRAK

Kekasaran permukaan, hayat alat dan mekanisme haus memainkan peranan utama untuk mengoptimumkan prestasi alat dalam proses pemesinan. Memperkenalkan nanopartikel menjadi penyejuk telah terbukti dapat meningkatkan pengoptimuman prestasi alat. Kajian ini telah dijalankan untuk mengkaji kesan penyejuk berasaskan zarah nano (TiO_2/EGW) dan penyejuk berasaskan zarah nano hibrid (TiO_2/ZnO/EGW) pada penambahbaikan alat Titanium Nitrat (TiN). Persamaan model linear kekasaran permukaan dan hayat alat dibangunkan menggunakan kaedah permukaan respon (RSM). Daripada RSM, parameter yang paling penting adalah kadar suapan, maka kedalaman paksi dipotong dan akhirnya memotong kelajuan. Operasi pengilangan akhir dengan menggunakan penyejuk berasaskan zarah hibrid nano (TiO_2/ZnO/EGW) memperoleh kekasaran permukaan yang lebih rendah dan hayat alat yang tinggi. Operasi pengilangan akhir dengan menggunakan penyejuk berasaskan zarah nano (TiO_2/EGW) dan penyejuk larut air (EGW). Penggantian berasaskan zarah hibrid nano (TiO_2/ZnO/EGW) menurunkan kekasaran permukaan 38% daripada EGW dan 17% daripada (TiO_2/EGW). Menurut ISO 8688-2-1989 (E) kriteria pemakaian untuk penggilingan dengan penyejuk larut air mencapai purata jarak pemotongan 885 mm. Jarak pemotongan untuk penggilingan dengan penyejuk berasaskan zarah nano (TiO_2/EGW) dilakukan dengan lebih baik pada jarak 55.55% untuk mencapai kriteria pemakaian pada purata jarak pemotongan 1450 mm. Sementara itu, jarak pemotongan untuk penggilingan dengan penyejuk berasaskan zarah hibrid nano (TiO_2/ZnO/EGW) bertindak lebih baik pada 80% untuk mencapai kriteria pemakaian pada jarak pemotongan purata 1585 mm. Nanofluid hibrid dan kekonduksian terma nanofluid tunggal lebih tinggi daripada EGW 13% dan 11%. Nanofluid dan kapasiti tunggal khusus nanofluid tunggal lebih tinggi daripada EGW kira-kira 30% dan 22%. Model antara pemotongan parameter dan tindak balas untuk kekasaran permukaan dan alat alat telah ditubuhkan. Untuk kekasaran permukaan kesilapan untuk nilai yang diramalkan berbanding nilai sebenar ialah 7%. Sementara itu, untuk kegunaan alat kesilapan untuk nilai ramalan berbanding nilai sebenar adalah 11%. Kelajuan pemotongan yang tinggi, kadar suapan rendah dan kedalaman paksi rendah akan memberikan kekasaran permukaan halus. Kelajuan pemotongan rendah dan kadar suapan rendah akan meningkatkan hayat alat. Pengoptimuman pelbagai objektif bagi parameter telah ditubuhkan. Di mana kelajuan pemotongan optimum = 2166 rpm, Feedrate = 0.02 mm/tooth dan kedalaman paksi dipotong = 0.1 mm yang menghasilkan hayat alat = 37.07 min dan kekasaran permukaan = 0.1452 µm. Keutamaan adalah hampir 1 (0.713), dan ia memenuhi matlamat pengoptimuman.

ABSTRACT

Surface roughness, tool life and wear mechanism plays major role for optimizing tool performance in machining process. Introducing nanoparticles into coolant has been proved to improve the optimization of the tool performance. This research has conducted to study the effect of nano particle based coolant (TiO_2/EGW) and hybrid nano particle based coolant (TiO_2/ZnO/EGW) on the Titanium Nitrate (TiN) tool enhancement. The linear model equation of surface roughness and tool life are developed using response surface methodology (RSM). From the RSM the most significant parameter is feed rate then axial depth of cut and lastly cutting speed. The end-milling operation by using hybrid nano particle based coolant (TiO_2/ZnO/EGW) obtains lower surface roughness and high tool life. End-milling operation by using nano particle based coolant (TiO_2/EGW) and water soluble coolant (EGW). Hybrid nano particle based coolant (TiO_2/ZnO/EGW) lower the surface roughness 38% than EGW and 17% than TiO_2/EGW. According to ISO 8688-2-1989 (E) the wear criteria for milling with water soluble coolant reached at average of cutting distance of 885 mm. Cutting distance for milling with nano particle based coolant (TiO_2/EGW) performed better at distance of 55.55% to reach the wear criteria at average cutting distance of 1450 mm. Meanwhile for the cutting distance for milling with hybrid nano particle based coolant (TiO_2/ZnO/EGW) perform better at 80% to reach the wear criteria at average cutting distance of 1585 mm. Hybrid nanofluid and single nanofluid's thermal conductivity higher than EGW 13% and 11%.Hybrid nanofluid and single nanofluid specific heat capacity higher than EGW about 30% and 22%. The models between cutting parameters and response for surface roughness and tool life have been established. For surface roughness the error for the predicted value vs the actual value is 7%. Meanwhile for tool life the error for the predicted value vs the actual value is 11%. High cutting speed, low feed rate and low axial depth will provide fine surface roughness. Low cutting speed and Low feed rate will increase the tool life. The multi objective optimization for the parameters has been established. Where the optimum cutting speed= 2166 rpm, Feedrate = 0.02 mm/tooth and axial depth of cut = 0.1 mm which produces tool life = 37.07 min and surface roughness = 0.1452 µm. The desirability is nearly 1 (0.713), and it satisfy the goal of the optimization.

TABLE OF CONTENTS

LIST OF TABLES

LIST OF FIGURES

LIST OF SYMBOLS

R_a	Roughness Average
R_z	Roughness Depth
k	Thermal Conductivity of Nanofluid
k_0	Thermal Conductivity of based liquid
L	Sampling Length
Y	Ordinate of the Profile Curve
K	Kelvin
γ	tool rake angle
l_c	tool-chip contact distance
l_s	shear plane length
a_c	undeformed chip thickness
a_o	deformed chip thickness
ϕ	shear angle
α	clearance angle
V	Volts
ω	weight percentage
φ	volume percentage
F_m	Feed Rate in mm/min
TL	Total Length to reach Flank Wear Criterion 0.3mm

LIST OF ABBREVIATION

TiO_2	Titanium Oxide
SiO_2	Silicon Oxide
ZnO	Zinc Oxide
TiN	Titanium Nitrite
BUE	Build- Up- Edge
CVD	Chemical Vapor Deposition
RSM	Response Surface Method
SEM	Scanning Electron Microscope
EG	Ethylene Glycol
TEM	Transmission Electron Microscope
Al_2O_3	Aluminum Oxide
CrN	Chromium Nitride
Cr_2O_3	Chromium(iii) oxide
DOE	Design of Experiment
CCD	Central Composite Design
BBD	Box-Behnken Design
CBED	Convergent Beam Electron Diffraction
EDX	Energy Dispersive X-ray

CHAPTER 1

INTRODUCTION

1.1 Research Background

Machining plays a major role in manufacturing industries. Machining is a versatile manufacturing process where the desired shape, size and surface finish can be acquired by excess material removal process. The material removal process includes the removal in the form of small chips. There are some important parts in machining operation which are cutting tools and machine tools. Cutting tool is a device which removes the excess materials through direct mechanical contact whereas machine tool provides the necessary relative motion between the workpiece and the cutting tool.

During machining process, the temperature will rise with speed and weakens the tool which will lead to tool wear and tool failure (Shaw & Cookson, 2005). To produce a fine product, higher cutting speed should be used but it will cause faster tool wear and lessen the tool life due to the excessive heat produced. Poor surface finished product will be result from the excessive heat produced. Thus, it is essential to reduce the heat produced during machining so that the work piece and cutting tool can be kept under controlled temperature. Thus, it is essential to cool down the heat generated at the tool and work piece interface for a better tool life and consequent improvement in the surface roughness for instances the usage of cutting fluid.

Metal working fluid is the common cutting fluid that been used widely in a lot of sectors. According to Grand View Research (June 2018), the global metalworking fluids market used in 2017 was valued at USD 10.3 Billion. The figure 1.1 shows the usage of metalworking fluid per year. The usage of metal working fluid has been forecast until 2025 where the research said it will increase by 4.4% by the end of 2025. The metalworking fluid been categorized in figure 1.2 according to the sectors by Grand

View Research. Machinery sector used about 43% of total global metalworking fluid per year (Grand View Research, June 2018). The figure 1.2 shows how important metalworking fluid in machinery sectors.

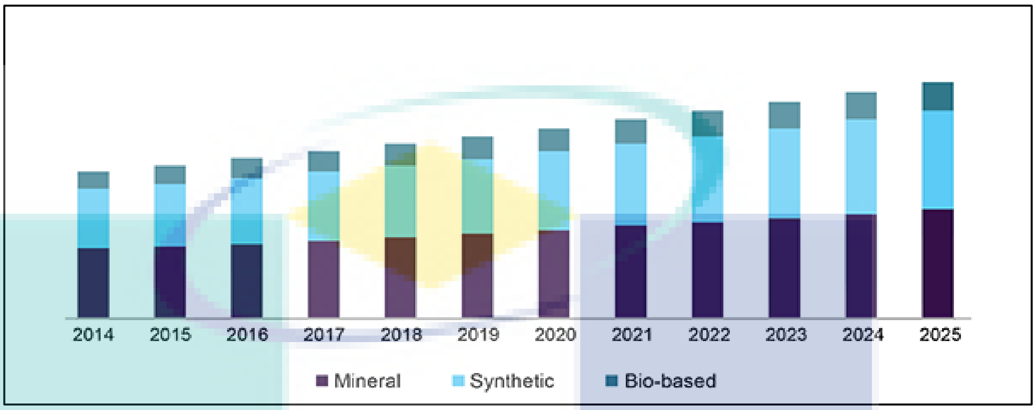

Figure 1.1: Metalworking fluids market size per year

Source: Grand View Research, June (2018)

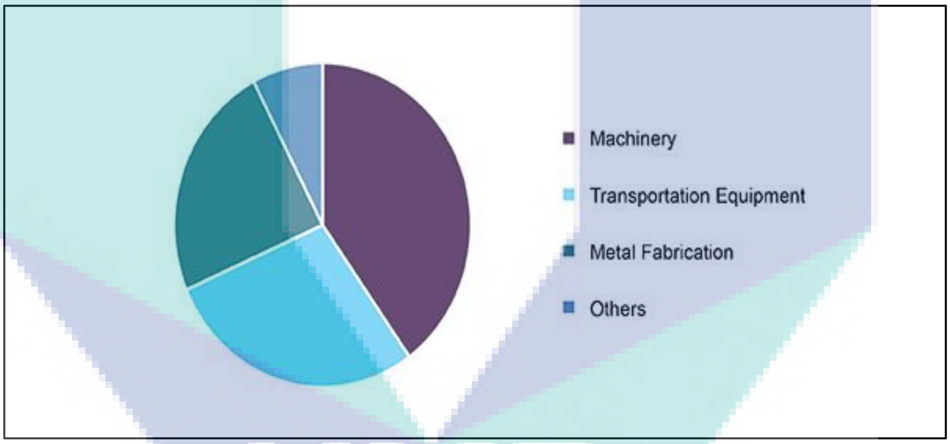

Figure 1.2: Metalworking fluids market size according sector

Source: Grand View Research, (June 2018)

The cutting fluid is very crucial in machining process because it acts as a cooling system. The main role of cutting fluid is to remove heat generated from friction between cutting tool and workpiece which eventually reduce temperature rise in cutting tool. Besides that, cutting tool is also useful to remove chip. Lowering cutting tool temperature also helps to reduce cutting force during machining and increase the life span of the cutting tool. The temperature rises in cutting tool is caused by chip deformation and friction force between tool and work material (Shaw & Cookson, 2005).

However, many manufacturing industries are facing a real challenges even though use metalworking fluid as coolant in the machining process. There are still thermal damages occur on the work-piece surfaces which affect the manufacturing cost of the industry. This is due to the high cutting temperature still occurs during the milling process when using metalworking fluid as coolant. Build-up-edge (BUE) still occurs due to the high temperature on the cutting flank face. BUE will contribute a rises in tool wear and reduce the surface integrity of workpiece (Hsien, 2015). Moreover, having a low thermal conductivity which is 50% lower than carbon steel, increases the rates of tool wear and damages on the workpiece due to high absorption of heat in cutting tool and workpiece (Wit Grzesik, 2008).

Many researchers have conducted various researches on alternating the cutting fluid as coolant. Most of the investigation of alternating the cutting fluid is mainly focused on minimum quantity lubricant technique and there are very few research and publication about using nanofluid as a milling machine coolant Yazid, CheHaron, Ghani, Ibrahim, and Said (2011). On the other hand, it is reported that the dispersed nanoparticle additives (TiO_2, ZnO, SiC, etc) in the based liquid exhibits higher load carrying capacity, anti-wear and friction reduction properties (Murshed, Leong, & Yang, 2008) Therefore, these features can make the nanofluid very attractive in usage of machining coolant.

The concept of nanocoolant or nanofluid is referred to dispersions of nano particle into the based liquid which is water or ethylene glycol. Nanofluids are the next generation heat transfer fluid due to their higher thermal conductivity than those of based liquid (S. Lee, Choi, Li, & Eastman, 1999). From the viewpoints hybrid nanofluid show better performance in term of heat transfer rate, compare to conventional coolant for machining. Besides that, the cutting temperature could also be reduced in both work-piece and cutting tools due to its high heat transfer rate. Therefore, the tool life and the surface integrity considered to be much improved compared with normal commercial coolant (Sarkar, Ghosh, & Adil, 2015).

The most common cutting tool used for machining is coated tool with Titanium Nitrate (TiN). The application of TiN coated tools is made with one of two processes; chemical vapor deposition (CVD) and physical vapor deposition (PVD). The thickness of the coating material makes a significant difference in the life of tools, as well as their performance (Jawaid, Sharif, & Koksal, 2000). Generally, the CVD coatings are noticeably thicker than PVD coatings, thus allowing a quality surface on steel alloy as well as cast iron applications. The TiN coating is used to reduce the friction between tool and workpiece which resulting resistance to tool wear. The significant advantages of TiN in machining process are, increasing the tool life, improve the surface quality of the product and increase the rate of production (Jawaid et al., 2000).

SUS 304 stainless steel is the most common form of stainless steel used around the world, largely due to its excellent corrosion resistance and value. Besides, this alloy also categorized as non-magnetic and it can only hardened by natural cold working process. It contains between 16 and 24 percent chromium and up to 35 percent nickel, as well as small amounts of carbon and manganese. It is also common in buildings, site furnishings, air craft fitting, aerospace component and some component in chemical environment (Hong & Koo, 2005). SUS 304 stainless steels also are an alloy with high fracture toughness, high tensile strength high ductility, low heat conductivity and high work hardening rates (Shao et al., 2007).

1.2 Problem statement

Cutting tool is a device which removes the excess materials through direct mechanical contact whereas machine tool provides the necessary relative motion between the workpiece and the cutting tool. When the machining operation is carried out, the temperature rises with the speed and the tool strength decreases, leading to faster wear and tool failure. A higher productivity can be achieved through higher cutting speed but it will cause faster tool wear. Thus, it is essential to reduce the heat produced during machining so that the work piece and cutting tool can be kept under controlled temperature.

During cutting process, friction force and high thermal load between interface causes tool wear to occur especially at the edge of cutting tool (Schuldt, Arnold, Kowalewski, Schneider, & Rohm, 2016). In matter of fact, the existence of tool wear and thermal load is caused by excessive friction force which subsequently shortens the cutting tool’s life span. The wear formation at the cutting tool results in poor surface roughness and product with less dimensional accuracy.

Formation of Build-up edge (BUE) and Build-up layer (BUL) defects which causes bad appearance on the workpiece (Jayal & Balaji, 2009; Najiha, Rahman, & Kadirgama, 2015). Overheating of the cutting tool can results in its sharpness reduction. Eventually it will lead to poor surface finished product and consumption of higher power. Thus, it is essential to cool down the heat generated at the tool and work piece interface for a better tool life and consequent improvement in the surface roughness for instances the usage of cutting fluid (Jayal & Balaji, 2009; Muthukrishnan & Davim, 2011).

Cutting fluid act as a coolant and remove heat generated from friction between cutting tool and workpiece which eventually reduce temperature rise in cutting tool. Lowering cutting tool temperature helps to reduce cutting force during machining and increase the life span of the cutting tool. The temperature rises in cutting tool is caused by chip deformation and friction force between tool and work material. Cutting fluid helps by washing away chips during machining (Avila & Abrao, 2001). Even though current cutting fluid, metalworking fluid helps to reduce the heat generated between the tool and work piece, but it is not sufficient enough to produce fine surface roughness (Benardos & Vosniakos, 2003). Thermal damages still occur on cutting tool due to poor thermal conductivity of the metal working fluid.

Nevertheless, the cutting fluid represents a considerable proportion of the total costs of production. Furthermore, in the United States (period from 1994 to 1999), Independent Lubricant Manufacturers Association (ILMA) accounted that, the 95 to 103 million gallons of cutting fluids were formed on a yearly premise (Gupta, Sood, & Sharma, 2016). Conventionally, conventional coolant is used as cutting fluid in flood cooling. The disposal of large amount of cutting fluid brings some serious environmental issues. The exposure of machine operators to this cutting fluid leads to serious health hazards such as skin and human respiratory problems (Lawal, Choudhury, & Nukman, 2012). The economic, environmental and human exposure issues associated with conventional flood machining have prompted researchers to explore ways of either minimizing the amount of cutting fluids applied in machining.

To enhance the cutting fluid thermal conductivity and reduce heat generated between cutting tool and workpiece, study on nanofluid and hybrid nanofluid conducted. Many studies proved that the nanocoolant or nanofluid reduce the heat generated at tool tip drastically and enhance the tool life by reducing the tool wear much better than metalworking fluid (S. K. Das, Choi, & Patel, 2006). The nanoparticles in nanofluid boost the thermal conductivity of the fluid which can reduce the friction force of the tool and workpiece. Nanofluids and hybrid nanofluids provide a potential way to enhance tool life, reduce tool wear and produce a fine surface roughness (Khandekar, Sankar, Agnihotri, & Ramkumar, 2012; P.-H. Lee, Nam, Li, & Lee, 2012)

1.3 Objective

The objectives of research are as follows;

1. To analyses the thermal properties (thermal conductivity and specific heat capacity) of the hybrid nanofluid (TiO_2/ZnO/EGW) and nanofluid (TiO_2/EGW)
2. To establish predicted models between cutting parameter and responce (surface roughness and tool life) during milling operation of SUS 304 stainless steel using nanofluid.
3. To establish multi objective optimization for the parameters (cutting speed, federate and axial depth.
4. Morphology analysis of tool wear of base fluid (EGW), nanofluid (TiO_2/EGW) and hybrid nanofluid (TiO_2/ZnO/EGW)

1.4 Scope of Study

To achieve the research objectives, end milling type was used to cut the work piece. The material that was used as work piece to conduct the research experiment is SUS 304 stainless steel. The mill holder diameter that was used to conduct the experiment is 16mm. Besides that, the insert type that was used to cut the work piece is coated carbide tool. The inserts coating specification with single layer 1mm TiN coated. Furthermore, the nano particles that have been chosen for to produce the coolant are TiO_2 and ZnO with size range between 30 nm to 50 nm. The volume concentration of the nano coolant will be 0.5, 1.0 and 1.5 volume percentage. The milling parameter has been chosen according to the insert catalog which the cutting speed used are 1500 rpm, 2000 rpm and 2500 rpm, feed rate used 0.02 mm/tooth, 0.03 mm/tooth and 0.04 mm/tooth and the axial depth of cut used are 0.1 mm, 0.2 mm and 0.3 mm. the radial depth of cut of 0.4 mm is constant on this study. In this study the response surface method used is Box-Behnken Design (BBD).

1.5 Thesis Outline

This thesis contains five chapters which is every chapter have its own purpose. After viewing the entire chapter in this thesis hopefully viewer can understand the whole system design for this project.

Chapter one contains of the introduction or the overview of this project, the problem statement of this project, the objectives of the project, the scopes of the project and the outline of this thesis for every chapter.

Chapter two contains all the theory of milling operation, tool life; tool wear, surface roughness, and milling temperature are discussed. The behavior and properties of nanoparticle also discussed in this chapter. The application of some statistical modelling are discussed in the end this chapter.

In chapter three the experimental procedure and development of statistical modelling created with response surface method (RSM). This chapter will explain about the detail of the project. It also includes the information about the progress of the experiment and the specification of the apparatus used throughout the project.

Chapter four discusses the result and the analysis for this project. The results between experimental with ethylene glycol based TiO_2/ZnO nanocoolant and experimental with normal conventional coolant are compared and analyzed. The model obtain from RSM are also compared and analyzed in this chapter.

Chapter five will explain the conclusion of the project. It also includes the future recommendation of the project.

CHAPTER 2

LITERATURE REVIEW

2.1 Introduction

The main purpose of this chapter is to deliver the information about milling process; cutting parameter, hybrid nanocoolant, and tool wear mechanism. Information from this chapter will provide a huge point from other researcher's results and findings. This information can be linked with the finding of this research that has been discussed in chapter five.

2.2 Milling

In milling processes, material is removed from the workpiece by a rotating cutter. The two basic milling operations are peripheral (or plain) milling and face (or end) milling. Peripheral milling generates a surface parallel to the axis of rotation, while in face milling generates a surface normal to the axis of rotation. Face milling is used for relatively wide flat surfaces (usually wider than 75 mm) (Wit Grzesik, 2008). End milling, a type of peripheral milling operations, is used for profiling and slotting operations. The basic geometry of the end milling process is shown in Figure 2.1, where v is the cutting speed of the cutter (m/min), D is the diameter of the cutter (mm), Ns is the rotational speed of the cutter (rev/min), fz is the feed per tool (mm/tooth), fm, is the feed per minute (mm/min) = $fz \, X \, z \, X \, Ns$, z is the number of teeth in the cutter, aa, is the axial depth of cut (m) and ar is the radial depth (width) of cut (mm) (Ng, Aspinwall, Brazil, & Monaghan, 1999).

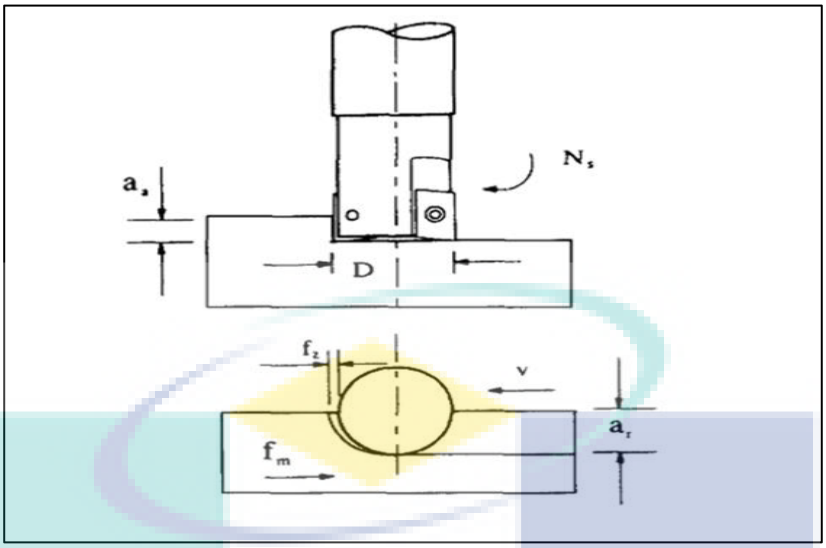

Figure 2.1: The basic geometry of the end-milling process

Source: Ng et al. (1999)

The most common general – purpose milling machine is the knee and column milling machine or knee milling. The major components of the knee mill are the column, spindle, knee, saddle and table. The uncut chip thickness varies continuously in milling. Cutting is also not continuously in milling, rather is periodically interrupted as cutting edges enter and leave the part. This lead to cyclic thermal and mechanical loads on the tool, which leads to a number of fatigue failure mechanisms not encountered in continuous cutting. The cutting action of each cutting edge on a milling cutter is similar to that of a single point tool. The cutting speed and the federate *fr*, and feed per revolution *f*, are related by an equation (Lima, Avila, Abrao, Faustino, & Davim, 2005):

$$fr = Nf \tag{2.1}$$

The variation of the uncut chip thickness in milling is complicated. Exact analyses have shown that the uncut chip thickness varies trochoid ally as the cutter rotates. For small feeds, however, a sinusoidal approximation is adequate. The uncut chip thickness *ai* at an engagement angle of *vi*, maximum uncut chip thickness, *amax* and average uncut chip thickness, *aavg* are given by (Masmali & Mathew, 2016):

$$ai = ft \cos \kappa \sin vi \tag{2.2}$$

$$amax = ft \cos \kappa \sin vm \tag{2.3}$$

$$aavg = ft \cos \kappa \sin (vm/2) \tag{2.4}$$

where κ is the lead angle equivalent to the lead angle in turning. In peripheral milling, $\kappa = 0$. The metal removal rate Q is given by (Masmali & Mathew, 2016):

$$Q = frbd \tag{2.5}$$

where d and b are the axial and radial depth of cuts for end milling, while radial and axial of cuts for peripheral milling.

In milling, tools are subjected to cyclic thermal and mechanical loads and may fail by mechanisms not observed in continuous cutting. The cyclic variations in temperature in milling induce cyclic thermal stresses as the surface layer of the tool expands and contracts. This can lead to the formation of thermal fatigue cracks near the cutting edge. In most cases, such cracks are perpendicular to the cutting edge and begin forming at the outer corner of the tool, spreading inward as cutting progresses. The growth of these cracks eventually leads to edge chipping or tool breakage (Masmali & Mathew, 2016).

Thermal cracks form and grow more rapidly as peak temperatures during the cutting cycle increase and as the difference between peak and low temperatures increases. When using coated WC tooling, the coating may fail by spalling due to a similar thermal fatigue mechanism (Balint & Hutchinson, 2005). Edge chipping is also common in milling. Chipping may occur when the tool first contacts the part or more commonly when it exits the part. Entry and exit failures have been most widely studied for face milling steel with WC tooling, but fracture mechanisms and countermeasures are applicable to other materials combinations. Entry failures most commonly occur when the outer corner on the insert strikes the part first. This is more likely to occur when the cutter rake angles are positive rather than negative. The finish in milling is also affected by a number of factors not present in turning; these factors result mainly from differences in tooling and process kinematics (Benardos & Vosniakos, 2003).

Reducing spindle run out and cutter grinding or setup errors reduces the average roughness. Reducing these errors causes all cutting edges to cut at more uniform depth. The radial cutting force will contribute to the shape of the surface because end mills are generally the most flexible part in the machine tool system due to low aspect ratio. The form errors on the surface become more complex for helical end mills than straight flutes (Altintas, 2012; Budak, 1992; Kline, DeVor, & Shareef, 1982; Smith, 1991; Sutherland & Devor, 1986). The tool static deflection is affected by the number of teeth cutting simultaneously. For example , if there is only one tooth in contact with the workpiece at any time, the surface form error is small in end milling because the uncut chip thickness becomes zero when the cutting edge passes a line perpendicular to the machine surface.

The history of metal cutting dates from the latter part of eighteenth century. Before that time, machine tools did not exist, and the diary of an English engineer, Richard Reynolds, dated October 1760, has given some insights of the manufacturing problems that Reynolds has faced, particularly when attempting to produce a cylinder for a fire engine to draw water from a coal pit (Inspektor, Oles, & Bauer, 1997). First successful steam engine was built in 1776 by James Watt. During the development of machine James Watt found some difficulties which were the boring of the cylinder casting. He could not make his sheet metal cylinder into steam tight. This problem has been later solved by John Wilkinson who has invented the horizontal boring machine (Inspektor et al., 1997).

Most of the study has been focused on down-to-earth reduction machining cost with an unsatisfactory accuracy and surface quality. Actual modern fundamental of metal cutting study has been carried out in 1945 by Merchant when he revealed the vision of metal cutting phenomena. However, Merchant failed to develop the predictive skills. Therefore, the objective of metal cutting research became unclear. Then later the actual fundamental of metal cutting experiment was started in 1960s (Boubekri & Shaikh, 2015). Metal cutting starts in concept with the introduction of machine tool. Today in modern civilization, for the manufacturing process of all products, machine tools are widely used.

2.2.1 Orthogonal and Oblique Cutting

The picked geometry gives a sensibly decent displaying of the chip arrangement on the significant front line of metal expulsion procedures, for example, turning, milling, drilling, sawing, grinding, and so forth. One of the vital parameters in the orthogonal metal cutting procedure is the rake point, α, characterized between the substance of the cutting apparatus and the plane opposite to the cutting bearing. The extent of rake point significantly affects the execution of the cutting device, the chip arrangement and the nature of the cut surface (Astakhov, 1998). On the off chance that the front line is slanted at an edge under 90 degree to the workpiece speed, the cutting activity is known as oblique cutting (Ostwald & Munoz, 2008). The oblique cutting procedure is the focal point of the present work. At the point when correlation is made between the orthogonal cutting and oblique cutting procedure, oblique cutting has a greater number of favorable circumstances than orthogonal cutting in light of the fact that for a similar feed rate and profundity of cut, the power follows up on a bigger region of the apparatus in-oblique cutting (Ostwald & Munoz, 2008).

The tool in oblique cutting will subsequently have a more extended life as the heat created per unit zone because of friction along the tool-workpiece interface is decreased. On the other hand, a tol utilized as a part of oblique machining will by and large expel more metal for a similar life expectancy of the device utilized as a part of orthogonal cutting. Genuine orthogonal cutting is bound fundamentally to tasks, for example, proposing and opening though other cutting procedures are primarily sideways.

2.2.2 Mechanic of Metal Cutting

There are two diverse perspective of mechanic of metal cutting which is another surface are shaped by plastic deformation on the tip of cutting tool and the measure of energy required to cutting because of plasticity and friction forces (Atkins, 2003). Be that as it may, the energy required for arrangement of new surface is viewed as insignificant.

The energy shaped amid the metal removal is changed over to thermal energy which is discharged from crafted by plastic deformation and friction force. The mechanical thermal in the tool chip interface is critical for consider the metal removal process. The thermal mechanical energy in the tool– chip interface is essentially critical for the plan of metal cutting procedures. This thermal mechanical energy is for the most part dictated by the stress of plastic deformation and grinding power which is delegated essential and auxiliary shear zone.

The sliding velocity on the tool-chip interface combined with stress of plastic deformation and friction force generate a very high temperature until reach the melting point of the workpiece material. This temperature is sufficient enough to plastic deformation happens on the workpiece surface. The area where the metal deforms area called primary shear zone as shown in Figure 2.2 where, γ is the tool rake angle, l_c is the tool-chip contact distance, l_s is the shear plane length, a_c is undeformed chip thickness, a_o is deformed chip thickness, ϕ is shear angle and α is the clearance angle (Furner, Yahya, & Duffy, 2005).

As the temperature at this point reach yield point, a chip break away from the workpiece material and slips away the primary shear plane. On the other hand, on the cutting tool surface the secondary shear zone occurs. Once the chip slip away along the up direction of the cutting tool, friction force raises the temperature in this zone.

Previous studies reported that the temperature on the secondary zone can reach up to 1200 °C when machining tool steel. During machining process, the cutting edge moves through the workpiece and deforming the workpiece material to shear a chip, a third shear zone formed under the leading edge. A material spring back is the outcome of this zone.

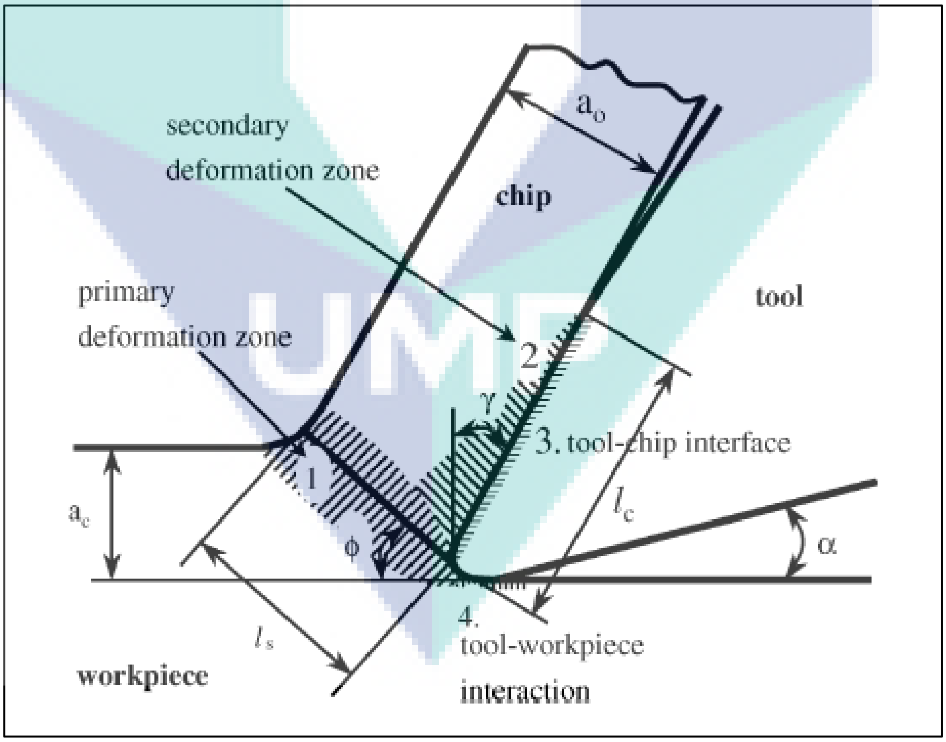

Figure 2.2: The primary and secondary shear zone during machining
Source: Furner et al. (2005)

2.2.3 Formation of Build-up-Edge

During low cutting speed the build-up-edge (BUE) tends to occur. The BUE is formed by the particle of the workpiece material which is stick to the rack face and cutting face as shown in Figure 2.3. These particles have been highly deformed and subject to strain-hardened. Previous research has been concluded that BUE is much harder than the workpiece material (Behrens et al., 2007). Previously an investigation has been done to found the possibilities of BUE occur during machining (Gökkaya, 2010). This investigation concluded that BUE only occur as stated below:

a. Strain hardening has been occurring on workpiece material.
b. A stable and stationary chip formation.
c. A low temperature during the chip formation which do not allow for recrystallization.
d. There is a stationary zone in the material flow on the cutting edge.

The geometry of the cutting edge is affected by BUE. It will drag along the workpiece material which leads to an adhesive wear on cutting tool. During the machining process the BUE is unwanted since it will affect the formed surface integrity. At high cutting speed BUE does not occurs as previous researchers stated that there is no strain hardening at high cutting speed if the recrystallization temperature is higher during the deformation process (Shaw & Cookson, 2005).

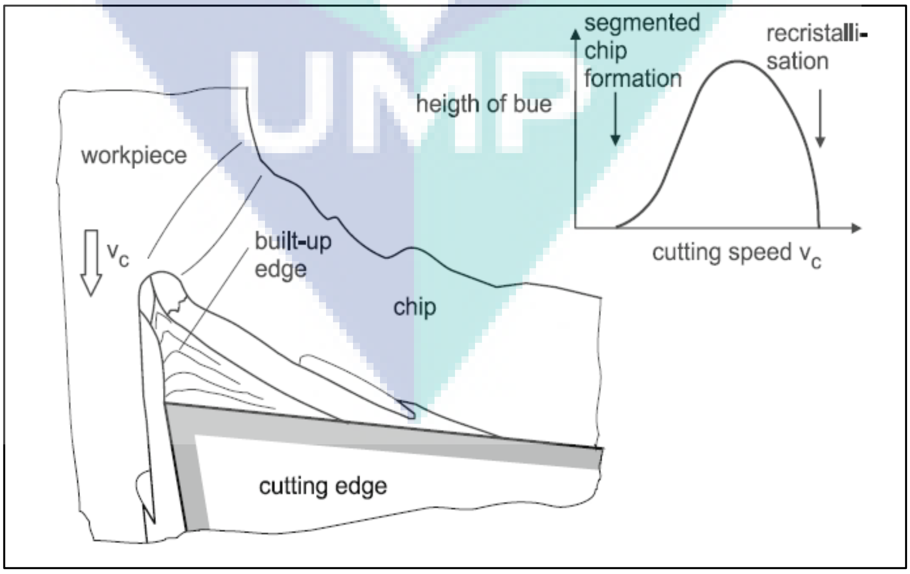

Figure 2.3: Formation of build-up-edge

Source: Behrens et al. (2007)

2.2.4 Chip Formation

There are four types of chips that can be formed in metal cutting process, as shown in Figure 2.4. During low cutting speed condition, if the brittle materials are cut a fracture mechanism will occur where the discontinuous chip is formed. The continuous chips are formed without a built-up edge on the tool. This occurs when cutting ductile material under steady–state conditions. However, long continuous chip causes handling and removal problems in practical operations. Under conditions of low cutting speeds where the friction between the chip and the rake face of the tool is high, the chip may be welded to the tool face. This accumulation of chip materials is known as build-up edge. Finally the last type of the chip is macroscopically continuously chip, consists of a narrow band of heavily deformed material alternating with larger regions of relatively undeformed material. These shear localized chips can be formed when the yield strength of the work piece decreases with temperature. Under the proper conditions, rapidly heated material in a narrow band in front of the tool can become much weaker than the surrounding material, lead to localized deformation (Kadirgama, Abou-El-Hossein, Mohammad, Noor, & Sapuan, 2008).

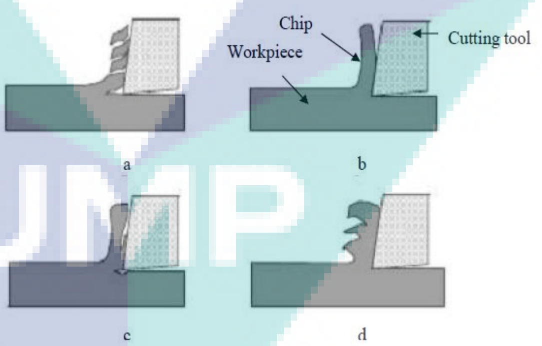

Figure 2.4: Four basic types of chips: (a) discontinuous (b) continuous (c) continuous with built -up edge and (d) shear localized.

Source: Kadirgama, Abou-El-Hossein, et al. (2008)

However, two issues are important for the determination of fracture: (1) where the fracture occurs; and (2) what type of fracture (brittle or ductile). It is shown that the limiting stress in the workpiece material may occur in one of the two regions, as shown in Figure 2.5. They are region A, the surface separating the workpiece and the layer being removed, and region B, the surface of maximum combined stress.

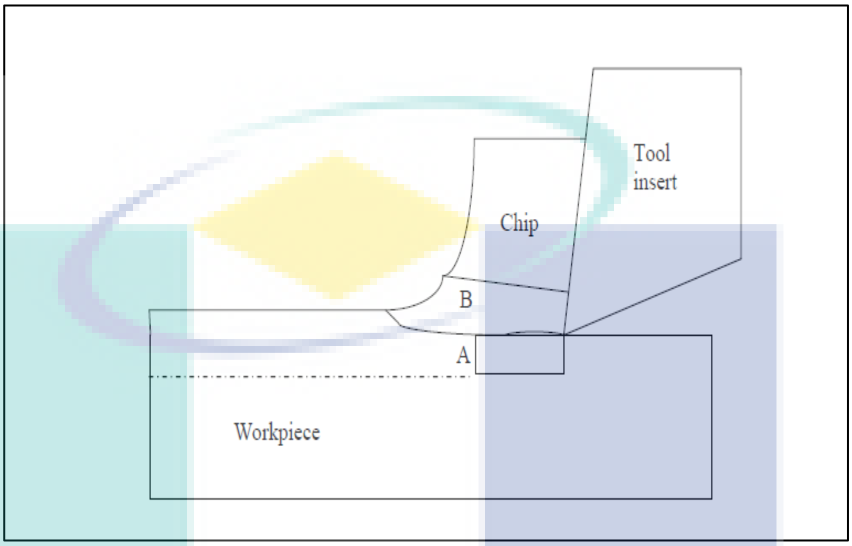

Figure 2.5: Zones where limiting stress can occur

Source: Ostwald and Munoz (2008)

Region A is a region of high combined shear and normal stress. The shear stress stems from the direct action of the cutting edge whereas the normal stress is due to the "tearing off" of metal layer when the material of the chip is forced upwards. Consequently, the deformation level here is high due to the high intensity of plastic flow in the presence of crack. It is believed that fracture in metal cutting starts from region A, and its further development depends on a given combination of the mechanical properties of workpiece material, tool geometry and cutting regime used (Ostwald & Munoz, 2008).

2.2.5 Tool Life and Wear Mechanism

Tool wear is gradual process occur with combination of prime wear mode. It is extremely dependent on cutting conditions, workpiece material, cutting tool type and the tool geometry. However, using insert as a cutting tool always can detect some kind of wear on it. It is highly depending on the cutting parameter used and different type of wear can be observed and the tool life of the insert will be varying too. To determine the failure criteria of an insert, normally it is set to be 0.35 mm as worn tool (Coromant, 1994). It is not depend on the type of wear that makes the insert to be worn. The most common wear types on insert reviewed in this section.

The fundamental nature of the wear mechanism can vary under different conditions. In metal cutting, six primary forms of wears are known to occur: adhesion wear, abrasion wear, diffusion wear, oxidation wear, crater wear, flank wear, notch wear, edge chipping, and built-up edges (Astakhov, 1998). In adhesion wear, the wear is caused by the fracture of welded asperity junctions between the two metals. In metal cutting, junctions between the chips and tool material are part of the friction mechanism; when these junctions are fractured, small fragments of tool material can be torn out and carried away from the underside of the chip or the new workpiece surface.

The conditions that exist in metal cutting are well suited for adhesive wear as new surfaces uncontaminated with oxide films are continually produced, and this facilitates the formation of welded asperity junctions (Ostwald & Munoz, 2008). The form of wear known as abrasion wear occurs when hard particles on the underside of the chip pass over the tool face and remove the tool material by mechanical action. These hard particles may be the highly strain-hardened fragments of an unstable built-up edge, fragments of the hard tool material removed by adhesion wear, or hard constituents in the work material (Astakhov, 1998).

The most common wear is flank wear. It is an abrasive wear and also can be predictable. The edge of the insert is changing its structure and the quality of workpiece surface is not satisfactory. The greater the flank wear, the higher the cutting force needed for the cutting process since the insert becomes blunt at the edge of the inserts. Figure 2.6 shows the sample of flank wear developed on cutting insert (Bjurka, 2012). The measurement of flank wear is done from the unworn edge to the worn edge as shown in Figure 2.7. The W in Figure 2.7 shows where the flank wear measured. The failure criteria of flank wear is 0.3 mm (Coromant, 1994).

Solid-state diffusion occurs when atoms in a metallic crystal lattice move from a region of high atomic concentration to one of low concentration. This process is dependent on the existing temperature, and the rate of diffusion increases exponentially with the increase of temperature. In metal cutting, where intimate contact between the work and tool materials occurs and high temperatures exist, diffusion can occur where atoms move from the tool material to the work material (Ostwald & Munoz, 2008).

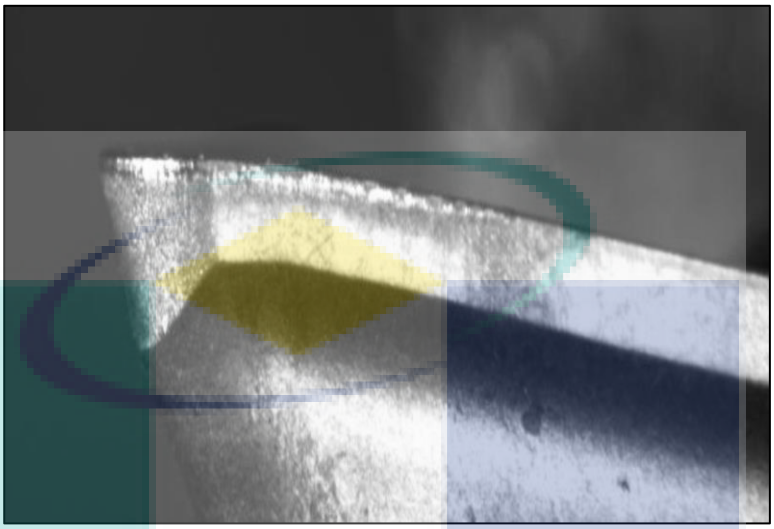

Figure 2.6: Flank wear developed on cutting insert

Source: Bjurka (2012)

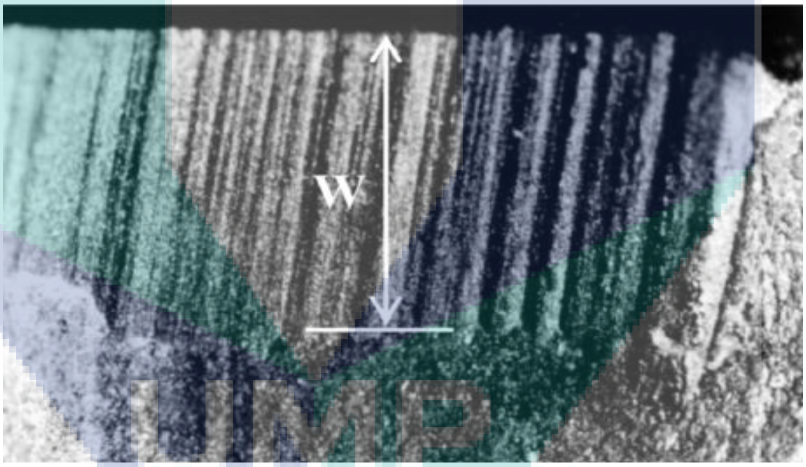

Figure 2.7: Flank wear

Source: Coromant (1994).

Oxidation wear occurs when the atoms in the cutting tool and work material form new molecules at the contact boundary where the area is exposed to the air (i.e., oxygen). This depends on the tool work materials, tool geometry and cutting conditions. A particular wear mechanism may be dominant, but all of them may occur simultaneously but at different rates. In general, the wear of the tool normally occurs at regions where the tool is in contact with the work material (W. Chen, 2000; Trent & Wright, 1991).

Besides that, crater wear is another type wear which commonly observed in machining. The cause of this wear is due to an abrasive wear on the chip surface of the insert. Crater wear occurs at the tool chip contact area where the tool is subjected to the friction force of moving chip under heavy load and high temperature conditions. As the cutting speed increases, the temperature due to friction increases, causing the atoms to diffuse continuously. The high temperature occurs near the midpoint of the tool chip contact length, where the great amount of crater wear occurs due to intensive diffusion. As the crater wear approaches the cutting edge, it weakens the edge and causes chipping of the tool (Astakhov, 1998; Ostwald & Munoz, 2008).

Furthermore, crater wear also cause by the chemical diffusion between chips and the cutting insert. This is due to relatively high temperature on the cutting zone. Therefore, cavity appears on this zone where the highest temperature point in the cutting zone in combination with chip as well. The feed rate of the machining determine how far into the insert the crater begin. At high feed rate, the crater start far from the edge of the insert. The distance from the edge of the insert is measured to find the crater wear (De Oliveira & Diniz, 2009). Crater wear can be minimized by selecting a tool material that has the least affinity to the workpiece material in term of diffusion. The use of lubricants is advantageous since during cutting, the lubricant penetrates the chip and the tool, thus reducing the friction and temperature. Additionally, coating material has a low friction coefficients and good chemical stability at high temperature condition, and this could assist in reducing the crater wear (Ostwald & Munoz, 2008). Figure 2.8 shows the common crater wear.

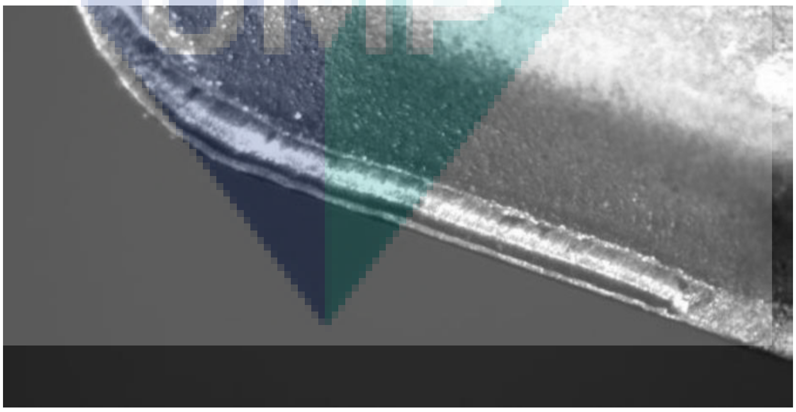

Figure 2.8: Crater wear
Source: Ostwald and Munoz (2008)

Notch wear is another wear which is ussually occur at during machining at high depth of cut. Besides that, it is also occurs during maching a harder material that will cause deformation hardening on the surface. This hard workpiece surface will then tear the the insert. Notch wear occurs locally at the primary cutting edge where the tool is in contact with the workpiece surface. This wear is normally caused by hard surface layers and work-hardened burrs, especially on stainless austenitic steels (Bawa, 1995; Stirnimann & Kirchheim, 1997). Figure 2.9 shows the notch wear which is due to machining hard material (Bruni, d'Apolito, Forcellese, Gabrielli, & Simoncini, 2008).

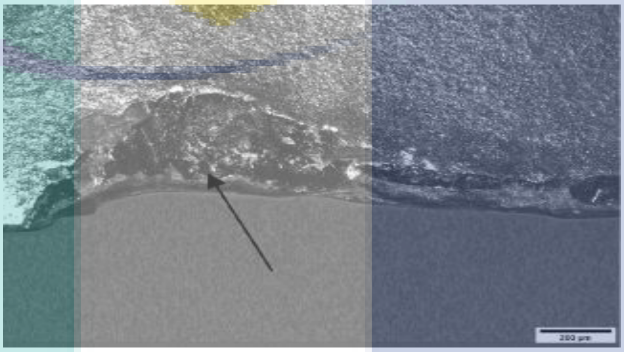

Figure 2.9: Progression of notch wear

Source: Bruni et al. (2008)

Chipping is type of wear which the fracture occurs on edge due to exist of comb cracks. The chipping wear is totally randomized based on the composition of the workpiece material. Therefore, it is very hard to determine whether the insert is worn or not. Normally the chipping criteria also been fixed as 0.35 mm to found the wear insert (Cormier, Young, Johnson, & Daddona, 2011). Figure 2.10 shows the example of chipping wear.

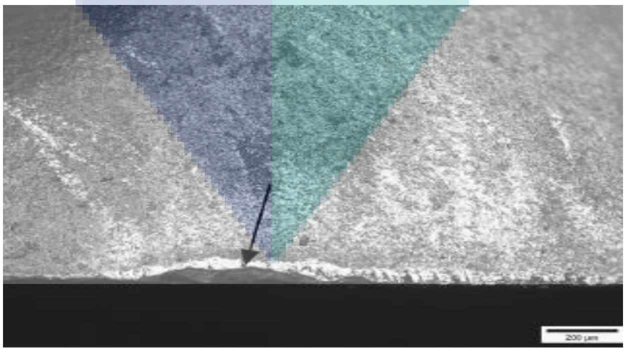

Figure 2.10: Chipping

Source: Cormier et al. (2011)

Comb crack are usually formed initially on the tip of the cutting edge, on a height that equals half of the axial depth of cut. This is because the yielding temperature is greatest here (Ulutan & Ozel, 2011). After the crack has been occurred, a different crack will tend to form on the half of the height from the initial comb crack. The coating of the insert will be grind down after the comb crack occurred. Generally, the crack will turn into cavity. Previously, a research has been concluded that comb crack can lead to the formation of BUE. the development of comb crack is inflicted by the sudden temperature variation. Therefore, using a proper coolant can reduce the possibilities of comb crack during machining (Diniz & Ferreira, 2003). Figure 2.11 shows the comb crack on the edge of cutting insert.

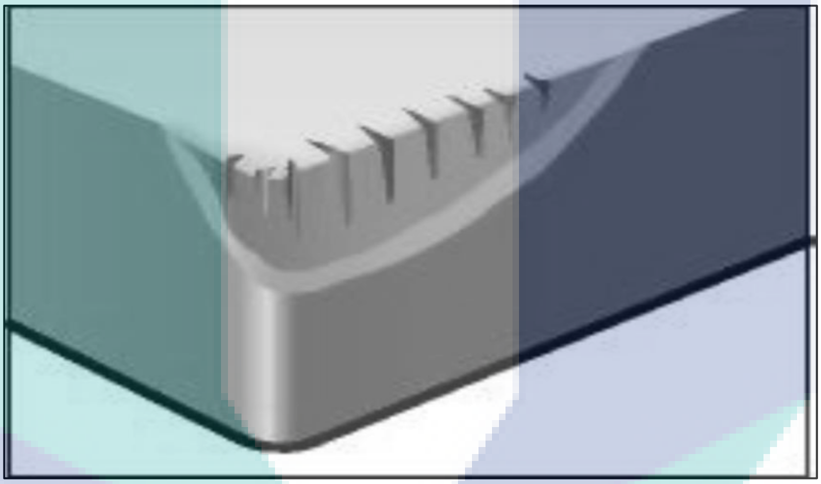

Figure 2.11: Comb crack
Source: Bjurka (2012)

Tool wear has significant impact on the quality of the machined surface as well as the economics of machining. Thus, it can be regarded as the most important aspect of machining operation (M Rahman, Kumar, & Salam, 2002). Wear type, in general, depends on tool and workpiece material, tool geometry and property of cutting fluid (Ozcelik & Bayramoglu, 2006).

2.2.6 Surface Roughness

Surface roughness influences not only the dimensional accuracy of machined part, but also the mechanical properties of the part, especially the fatigue strength. The surface roughness describes the geometrical feature of surface which in turn determines the fatigue life and corrosion life. The factors that influence the surface roughness are (Benardos & Vosniakos, 2003):

a. Temperature generated during processing
b. Residual stresses
c. Metallurgical transformation
d. Plastic deformation, tearing, and cracking of the surfaces

Several methods for inspecting and characterizing the surfaces have been developed. Inspection equipment based on both contact and non-contact principles is available. Contact–type instruments, generally employing styluses, are commonly used. Non-contact instruments are usually based on optical interferometry or electron beam principle. A large relief angle may reduce friction between the tool and workpiece, but excess relief angle reduces the support under the cutting edge, thereby causing failure under heavy-duty operation, and may result in inferior surface roughness on machined parts (Kiyak & Çakır, 2007).

Surface finish and surface roughness are widely used term in industry. It is used to measure the smoothness of the machined surface (Dhar, Kamruzzaman, & Ahmed, 2006). Surface finish could be stated in many dissimilar parameters. A large number of recently developed surface roughness parameter due to the variety of machining operation. The most common parameter for surface roughness described follows:

- Roughness average (R_a): This parameter is known as arithmetic mean roughness value. R_a is the universal recognized and most commonly used throughout international as surface roughness parameter. Therefore,
-

$$R_a = \frac{1}{L}\int_0^L |Y(x)|dx \qquad (2.6)$$

Where, R_a is the arithmetic average deviation from the mean line, L is the sampling length and y is the ordinate of the profile curve. It is the arithmetic average deviation from the mean of the roughness profile from the mean line.

Previously a research has been conducted to find the surface roughness on end-milling process for stainless steel with different cutting parameter. Mostly, the surface roughness increases with increases in cutting speed. But, this theory is only the cutting speed reach 104 m/min. Beyond this cutting speed the surface roughness seen to be decreases even the cutting speed increases. Besides that surface roughness also increases gradually with increases in feed rates. It has been concluded that the finest surface roughness can be produced at highest cutting speed and lowest feed rate.

A number of approaches for inspecting and characterizing the surfaces have been developed. Inspection equipment based on both contact and non-contact principles is available. Contact–type instruments, generally employing styluses, are commonly used. Non-contact instruments are usually based on optical interferometry or electron beam principle. A large relief angle may reduce friction between the tool and workpiece, but excess relief angle reduces the support under the cutting edge, thereby causing failure under heavy-duty operation, and may result in inferior surface roughness on machined parts (Astakhov, 1998).

Previous research conducted by Baradie (1993) and Stefanescu, Upadhya, and Bandyopadhyay (1990) have shown that the surface quality can be improved at high cutting speed. According to Gorlenko (1981), surface roughness can be characterized by various parameters. Numerous roughness height parameters such as average roughness (Ra), smoothening depth (Rp), root mean square (Rq), and maximum peak-to-valley height (Rt) can be closely correlated. The present study uses average roughness (Ra) for the characterization of surface roughness, due to the fact that it is widely adopted in the industry for specifying the surface roughness. Mital and Mehta (1988) have conducted a survey of the previously developed surface roughness prediction models and factors influencing the surface roughness. They have found that most of the surface roughness prediction models have been developed for steels.

2.2.7 Tool Geometry

In metal cutting, the modification of the tool edge geometry is referred to as edge preparation. Figure 2.12 illustrates three major types of edge preparation design that are used in most of the commercial cutting inserts. A chamfer edge combined with additional hone is also available. The purposes of edge preparation are to strengthen the cutting edge and to prepare a surface for deposition of coatings. Chamfer edges are used when cutting with heavy chip loads (roughing) and interrupted cuts (Astakhov, 1998).

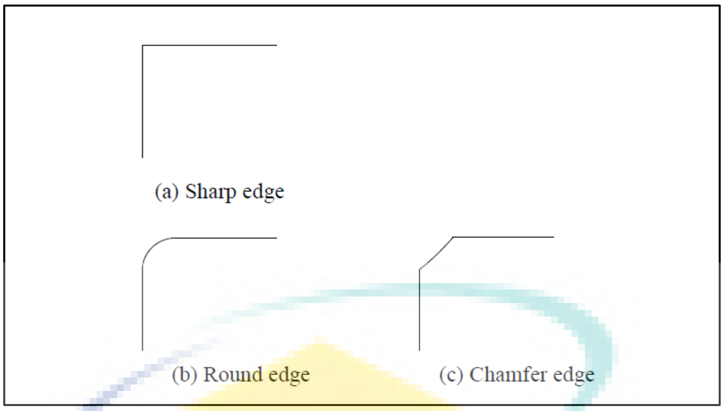

Figure 2.12: Typical cutting edge preparation designs

Source: Astakhov (1998)

The design of tool edge geometry influences process parameters such as the shape of deformation zones, distributions of temperature and stresses on the tool face, and cutting forces. Following this, the changes in chip flow, machined surface integrity (e.g. residual stress), tool wear resistance, and tool life (or machinability) are affected (Ostwald & Munoz, 2008).

Due to its large influence, the design of edge preparation has been playing an important role in the finishing applications of hardened steels. In a study performed by Kishawy and Elbestawi (1998), they have revealed that for a sharp tool, the magnitude of the tensile residual stress on the machined surface and the penetration depth of the stressed layer can be reduced with the increasing of cutting speed. An opposite trend, however, has been observed for hone tools.

Shintani, Ueki, and Fujimura (1989) have analyzed the effect of tool geometry on the cutting performance of CBN tools for carburized hardened steel (600-720 HV) under both continuous and interrupted cutting conditions. Based on their experimental results, the optimum tool geometry for continuous cutting is specified to have a negative chamfer angle of 35°, a chamfer width larger than the tool-chip contact length of 0.2 mm, a nose radius of 0.8 mm, and a hone radius of 0.05 mm. From the ANOVA analysis of turning hardened SUS 52100 steel with low-CBN inserts, Thiele and Melkote (1999) have observed that the material hardness with edge preparation can impose a significant effect on surface roughness. Increasing the edge hone radius tends to increase the average surface roughness due to the increase of ploughing force. Matsumoto, Hashimoto, and Lahoti (1999) have investigated four different tool edge designs (sharp, honed, single chamfered & double chamfered) on residual stress in bar turning. They have concluded that with the honed and double chamfered tools, the residual stress on the machined surface becomes more compressive and the affected zone extends to a deeper sublayer.

Endres (2002) have proposed an analytical orthogonal cutting model that includes the effect of the edge radius by conducting the force balance analysis on the lower boundary of the primary deformation zone. The cutting forces are thus derived as a function of edge radius and shear angle. In a recent report published by Manjunathaiah and Endres (2000), the authors have investigated the effect of nose radius on tool flank wear. They have reported that for sharp tools, there exists a moderate nose radius that minimizes the tool flank wear both at the lead edge and at the tool tip.

Ren and Altintas (2000) have proposed an analytical cutting model for chamfer tools, based on the Oxley's slip-line field model designed for sharp tools (Oxley, 1989). They have proposed to minimize the cutting energies in the deformation zones by analyzing the influence of chamfer angle and cutting condition on the cutting force and temperature. An extrusion model has been applied to the trapped dead metal zone near the chamfer edge.

From the results of the tool wear measurement and the proposed model, they have found that the optimal chamfer angle to be -15° when dry cutting is performed on P20 model steel (34 HRC) with uncoated carbide tools. Melkote and Thangaraj (1994) have derived a surface texture model including the influences of radial rake, primary end tooth relief angles, tool nose radius, flank width and the cutting conditions on residual stress and surface roughness.

Generally the presence of compressive residual stress is beneficial. Tensile stress, however, is detrimental (Bailey, Jeelani, & Becker, 1976; El-Khabeery & Fattouh, 1989). Earlier works (Fuh & Wu, 1995b; M'Saoubi, Outeiro, Chandrasekaran, Dillon Jr, & Jawahir, 2008) have revealed that the residual stresses are induced from thermal strain. The elastic-plastic strain and microstructure change that are dependent on machining state, however, are affected by the tool geometry, the cutting condition, and the property of the work material.

2.2.8 Cutting Tool Materials

One of the breakthroughs in the machining of metals is the heat treatment process of high speed steel cutting tools reported by Taylor Hoyle (1964). The use of these cutting tools facilitates higher metal removal rates, mainly due to the improved tool wear behavior. Since Taylor's discovery, research works in the field of metallurgical science and technology have been intensively carried out. This had led to the development of new tool materials such as cast alloys, cemented carbides, sintered oxides and ceramics (Stirnimann & Kirchheim, 1997).

The proper selection of tool material is not a simple task, as no set of standard rules are available. The selection of material is sometimes based on the experience of tool designer. In many cases, the number of failures may be high, especially when dealing with new tool materials. Past experience and basic knowledge enable a designer to make optimum selection of material (Ostwald & Munoz, 2008).

Cutting tool design has a strong impact on machining performance (Thiele, Melkote, Peascoe, & Watkins, 2000). Properly designed tools produce parts of consistent quality and have long and predictable useful life. An improperly designed tool may wear or chip rapidly, reduce productivity, increase cost and result in an inferior product. Cutting tool can be classified as single point tool, which has one active cutting edge, and multipoint tool, which has multiple active cutting edges. Single point tool is used for turning and boring, while multipoint tool is used for milling and drilling. Cutting tools must be made of materials, which are capable of withstanding high stress and temperature generated during chip formation.

High-speed steels may contain combinations of tungsten, chromium, vanadium, molybdenum and cobalt. They are capable in taking heavy cuts, withstanding shock and maintaining a sharp cutting edge under red heat. High-speed steel tool bits generally consist of two types: molybdenum-base (group M) and tungsten base (group T). The most widely used tungsten-based tool bit is known as TI which is sometimes called 18-4-1 because it contains 18% tungsten, 4% chromium and 1% vanadium. General purpose molybdenum-based high speed steel tool bit is designated as MI or 8-2-1, (i.e. 8% molybdenum, 2% tungsten, 1% vanadium and 4% chromium). If more red hardness is desired, a tool containing more cobalt element shall be selected (Parashar & Mittal, 2002).

Cast alloy tool bit usually contains 25% to 35% chromium, 4% to 25% tungsten and 1% to 3% carbon while the remainder is cobalt (Reen, 1966). These tool bits have high hardness, high resistance to wear, and excellent red hardness properties. Since they are cast, they are weaker and more brittle compared to high speed steel tool bits. Stellite tool bits are capable to withstand high cutting speed and high feed rate operating conditions (deep uninterrupted cut). They may be operated at about 2.0 to 2.5 times higher than the speed of high speed steel tool bits.

Cemented- carbide tool bits are capable to withstand cutting speed of 3 to 4 times higher than those of high speed steel tool bits. They have low toughness but high hardness and excellent red-hardness properties. Cemented-carbide consists of tungsten carbide sintered in a cobalt matrix. Sometimes other materials such as titanium or tantalum may be added before sintering to produce the desired properties on a given tool. Straight tungsten carbide tool bits are used to machine cast iron and non-ferrous materials. Since they crater easily and wear rapidly, they are not suitable to machine steel. Crater-resistant carbides, which are used for machining steel, are produced by adding titanium or tantalum to the tungsten carbide and cobalt (Stirnimann & Kirchheim, 1997).

Coated carbide tool bits are made by depositing a very thin layer of wear resistant material such as titanium nitride, titanium carbide or aluminum oxide on the cutting edge of the cutting tool. This layer decreases friction, improves the wear resistance of cutting edge by 200-500% and enhances the breakage resistance of the tool while providing longer life and increased cutting speeds. Titanium-coated inserts offer greater wear resistance at speeds below 500 ft/min whereas ceramic coated tips are suited for operations involving higher cutting speed. Both types of inserts may be used for cutting steels, cast irons and nonferrous materials (McEachron, Connors, & Slutz, 1993).

Ceramic is a heat resistant material produced without a metallic bonding agent such as cobalt. Aluminum oxide is the most popular material used to produce ceramic cutting tools. Titanium oxide or titanium carbide may be used as an additive, depending on the application of cutting tool. Ceramic tool permits operations of higher cutting speeds, possesses longer tool life and produces better surface roughness than carbide tool. However, they are brittle as compared to carbide or coated carbide and must be used in shock-free or low shock situation (Davis, 1995).

Cermet is a cutting insert, consists of a combination of ceramics and metal. Most cermets are made of aluminum oxide, titanium carbide and zirconium oxide compacted and compressed under intense heating operation. There are several advantages of cermeted tool bits: (1) they exceed the equivalent tool life of coated and uncoated carbide; (2) they can be used for machining at high temperatures; (3) they produce better surface roughness; and (4) they can machine steel up to 66 Rockwell (Rc) hardness (Stirnimann & Kirchheim, 1997). Diamond tools are used mainly to machine nonferrous metals and abrasive nonmetallic materials. Single-crystal diamonds have high wear but low shock resistance.

The new type of diamond tooling (polycrystalline diamond) consists of tiny synthetic diamonds fused together and bonded with a suitable carbide substrate (Farkas, 1972). Polycrystalline cutting tools offer greater wear and shock resistance, hence, the allowable cutting speed is enhanced greatly. Polycrystalline diamond tool offers better surface finish, better part-size control up to 100 times greater tool life than that of carbide tool. These cutting tools are made by bonding a layer of polycrystalline cubic boron nitride to a cemented carbide substrate. They are good in shock / wear resistance and high in edge life; hence, they can be used to machine high-temperature alloys and hardened ferrous alloys (Ezugwu, Wang, & Machado, 1999)

2.3 Coolant

Coolant or cutting fluid is a liquid which is used to produce cooling and lubricant between the cutting tool and the work piece. Cutting fluid also reducing the contact processes in the chip formation zone. Cooling and lubrication is very important in cutting process. According to Kakaç and Pramuanjaroenkij (2016) the lubricant action is very important and low cutting speed and the cooling is important at higher cutting speed due the high increases in heat in cutting zone.

Historically, water was used as a cooling medium in various machining operation. However, water is an excellent cooling medium due to its high thermal conductivity but it corrodes the part and poor lubrication. Nowadays, oils and synthetic fluids are used as coolant in machining. There are four types of cutting fluid used nowadays which consist of straight or neat oils, soluble oil, synthetic fluids and semi-synthetic fluids. Around 80% of cutting fluids in industries are using water based oil and synthetic fluids as a coolant in machining (Khamsehzadeh, 1991).

The presence of coolant during machining may reduce the process of fatigue arising from irregular contact of the hot chip and the cutting tool (Khamsehzadeh, 1991). This will in turn reduce the tendency of crack propagation and limit the plucking action of the cutting tool during machining. Coolant may intermittently penetrate into the flank and rake face of the tool and induce rapid changes in temperature. Due to the presence of high cutting temperature and periodic penetration of the coolant into the surface, the cutting tool will be subjected to continuous expansion and contraction. A tool material with adequate thermal conductivity and low thermal expansion coefficient will therefore minimize the temperature fluctuation at the cutting edge.

There are several advantages of using coolant in machining. First, using a proper coolant will increase the tool life. As reported by Kakaç and Pramuanjaroenkij (2016) improvement in the machining coolant causes some reduction in temperature. The tool wears extremely sensitive to the small changes of temperature in the region where the tool in contact with the work piece. Besides that, coolant also will reduce the thermal distortion caused by temperature gradient generated within the work piece during machining. They're also some books stated that using coolant will easier to handle the finished work piece. However, Benardos and Vosniakos (2003) stated that by using a suitable cutting fluid will improve the surface quality and also useful for clear the chips from cutting area.

Large machining centers often have a coolant station that is very complex. The coolant station provides coolant through the tools in order to increase the amount of fluid for cutting operation. Coolant stations are usually made up of a series of filters to remove impurities and chips that have been carried in the coolant and pumps. Some coolant stations provide pressures of more than 1000 psi to the cutting operation. The relatively high pressure value allows good removal of chips, significant cooling, and better surface roughness (Kadirgama, Noor, & Rahman, 2008).

2.3.1 Nanofluid

Nanofluid is fluid which suspended with nanoparticle. The nanoparticle will suspend with the conventional fluids such as water, ethylene glycol (EG) and engine oil. Nanofluid are thought to be next generation heat transfer fluids due to its existing properties (X. Chen, Engle, Wang, & Yu, 2009). Nanofluid have attracted great interest various industries such as micro electric, automotive, manufacturing and so on. According to Murshed, Leong, and Yang (2005) the advantages of nanofluids are performing better stability than micro-sized and mili size particle. Additionally, nanofluids obtain higher thermal conductivity than the based liquid.

More than twenty laboratories in worldwide have published the data regarding the thermal conductivity of nanofluids. All the results shows that the thermal conductivity of nanofluids exhibits higher thermal properties even the concentration of liquid is less than 5% in volume percentage (Murshed et al., 2005). The viscosity of the nanofluids is another important property for heat transfer application. As reported by Murshed et al. (2005) the pH value and the viscosity of the nanofluids are considered as factors that affect the stability of the nanofluid at room temperature.

2.3.1.1 Stability of Nanofluid

Stability of nanofluid is a key parameter for consistent functioning of a thermal system at designed capacity. Therefore, preparation of stable nanofluid is a technical difficulty to the researchers due to strong Vander Waal and cohesive forces among the nanoparticles. These forces are the root cause for agglomeration. The agglomerated hybrid nanofluid loses its potential to transfer heat by diminishing the Brownian motion of particles. It also deteriorates the flow behavior by amplifying frictional resistance and consequently increases the pressure drop. Therefore, stable suspension of the nanoparticles is essential to get desired properties. Underlying principles of stable suspension of nanoparticles are Diffusion Principle: nanoparticles are scattered by fluid medium and hence dispersed into it by electric double layer repulsion. Zeta Potential Principle: the absolute zeta potential value of the nanofluid must be more to the extent possible. As the zeta potential diverges from the iso-electric point, strong repulsive forces develop among particles and reduce agglomeration. Suresh, Venkitaraj, Selvakumar, and Chandrasekar (2011) produced stable Al_2O_3-Cu/ water hybrid nanofluid by maintaining the pH value 6.

Typical instruments that are used to check the relative stability are sedimentation photographs, zeta potential, centrifugation, UV–Vis spectrophotometer, SEM (Scanning Electron Microscope), light scattering, TEM (Transmission Electron Microscope). From the literature, it is found that there are different effective strategies developed to minimize the agglomeration. Among all, most common methods are (i) adding surfactant (ii) electrostatic stabilization by controlling the pH value and (iii) ultrasonic vibration. Most of the researchers prepare stable nanofluid by adding suitable surfactants.

2.3.1.2 Surfactant Addition

Surfactant is a surface-active agent, which creates an affinity between the nanoparticles and base fluids. These surfactants are the complex chemical compounds, which lowers interfacial tension between base fluid and suspended nanoparticles. In addition, it helps to stabilize the suspension by increasing the electric double layer repulsion between nanoparticles (one layer is formed on the surface of particles by the corresponding ions within the crystal lattice and second diffusion layer is formed on the base fluid. When these double-layered particles come, closer, repulsive forces develop and thereby diminish the agglomeration). Surfactants chemically convert nanoparticles from hydrophobic to hydrophilic or vice versa, based on the type of host fluid and nanocomposite/nanoparticle. On the other hand, surfactant can also increase the zeta potential of nanofluid, which magnifies the surface charge of dispersed nanoparticles in the host fluid (Manjunathaiah & Endres, 2000; Ren & Altintas, 2000).

The conventionally used surfactants are Sodium Dodecyl Benzene Sulfonate (SDBS) (Melkote & Thangaraj, 1994; Oxley, 1989), Sodium Dodecyl Sulphate (SDS) (Bailey et al., 1976; El-Khabeery & Fattouh, 1989), Cetyl Trimethyl Ammonium Bromide (CTAB) (Okushima, Kakino, Hagihara, & Hashimoto, 1971), Dodecyle Trimethyl Ammonium Bromide (DTAB) (Liu & Barash, 1982), Hexa decetyl trimethyl ammonium bromide (HCTAB), Salt and OlicAcid (Matsumoto, Barash, & Liu, 1986) Sodium Octonate (SOCT) (Melkote & Thangaraj, 1994; Oxley, 1989), Poly Vinyl Pyrolidone (PVP) (Dewes, Ng, Chua, Newton, & Aspinwall, 1999; Usui & Shirakashi, 1982), Gum Arabic (Tieu, Fang, & Zhang, 1998) and Octylsilane (Ng et al., 1999). To obtain the favorable results, selection of appropriate surfactant should be made in conjunction with the combination of nanoparticles and base fluid.

2.3.1.3 Electrostatic Stabilization

The stability of nanofluid is directly related to the electro kinetic properties of nanoparticles. An electric charge would exist in the atoms at the outer most orbital. This charge is the root cause of kinetic behavior of nanoparticles in base fluids. In Electrostatic stabilization, stable suspension can attain by forming an electric static double layer by the ions of particles and host fluid. The diffusion layer is initiated at the isoelectric point at which zeta potential is zero. As the pH values of solution move away from this isoelectric point, these repulsive force increases and hence stability of nanofluid improves. This electrostatic stabilization method is pH sensitive (Alauddin, El Baradie, & Hashmi, 1997).

2.3.1.4 Ultrasonic Vibration

It is a typical nanofluid stabilization method. Because of its easiness, many researchers are using this technique. The key principle of this technique is nanoparticles disperse uniformly in the base fluid under the influence of high frequency vibrations. It is to be noted that the surface properties of suspended nanoparticles are not changed as the case with previous methods. The optimized duration of sonication depends on the size, type and concentration of nanoparticles. Ultrasonic bath, ultrasonic vibrator and homogenizers are the most common devices to impart ultrasonic vibrations. The stability of the nanofluid can be measured by the sedimentation rate in terms of particle velocity in host fluid. According to Stokes law (Muraka, Barrow, & Hinduja, 1979) speed of nano particle sedimentation can decrease by decreasing the nanoparticle size (R), increasing host fluid viscosity (μ), and decreasing the density gradient between the nanoparticle and host fluid (ρp-ρf). Among all parameters, the most significant parameter is R, according to the Brownian motion principle of nanoparticle, the sedimentation will be zero if the particle size reaches the critical size (Rc).

2.3.1.5 Thermal Conductivity

From the Figure 2.13, the thermal conductivity of nanofluid increases with the increases of temperature, since the enhanced ratio is almost constant and the thermal conductivity of nanofluids tract the thermal conductivity of base liquid which was similar to conclusion of Timofeeva et al. (2007). However, the temperature has a very small effect on the thermal conductivity of nanaofluid because of the high viscosity of the base liquid and large aggregates of the nanoparticles.

In a previous study Afrand, Toghraie, and Ruhani (2016), shows that the thermal conductivity of nanofluids is sensitive to the particle volume fraction and temperature and weak sensitivity to clustering size. This means that the size of particle has very little influence on the properties of nanofluids. The thermal conductivity ratio graph as shown in Figure 2.13 for TiO_2 shows that the TiO_2 nanofluids are much more sensitive to temperature. But, the thermal conductivity of TiO_2 nanofluids is lower than water at a temperature below 10 °C. Afrand et al. (2016) stated that this is due to experimental uncertainty of the measurement.

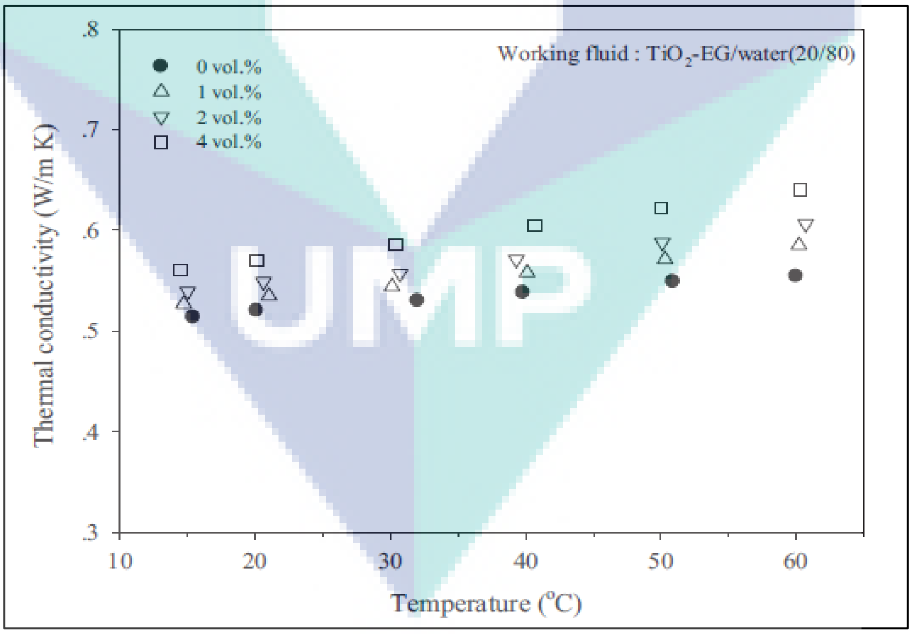

Figure 2.13: Thermal conductivity versus temperature for TiO_2/EG nanofluids at different volume percentage.

Source: Afrand et al. (2016)

Murshed et al. (2005) prepared nanofluid by dispersing TiO_2 nanoparticles in rod-shapes of Ø10 nm×40 nm (diameter by length) and in spherical shapes of Ø15 nm in deionized water. A transient hot-wire apparatus with an integrated correlation model is used to measure the thermal conductivities of these nanofluids more conveniently. The pH value and viscosity of the nanofluids are also characterized. The experimental results show that the thermal conductivity increases with an increase of particle volume fraction. The particle size and shape also have effects on this enhancement of thermal conductivity. For TiO_2 particles of Ø10 nm × 40 nm and Ø15 nm dimensions with maximum 5% volume fraction, the enhancement is observed to be nearly 33% and close to 30%, respectively over the base fluid.

In recent study on the mixture of ethylene glycol and ZnO nanoparticles at 1.5% volume concentration in water: ethylene glycol for mixtures of 80:20, 60:40, and 40:60 over a temperature range, researcher found that the highest increment of thermal conductivity of 32.26% occurred in the 80:20 ratio at 60 ºC (Sundar, Ramana, Singh, & Sousa, 2014). Sundar et al. (2014) also mentioned that ethylene glycol has poorer thermal conductivity than water, and the addition of ethylene glycol will only suppress the thermal conductivity of the base fluid. The same base fluid ratio of 40:60 (water: ethylene glycol) has also been studied by Vajjha and Das (2009) by dispersing ZnO at higher volume concentrations of up to 10% in a temperature range of 298–363 ºC. They also observed that the thermal conductivity increases with the increase of particle size. Apart from particle size, the effects of other factors such as temperature, nanoparticle shape, base fluid materials, additives, and aggregation on the thermal conductivity of nanofluid have also been reviewed by Philip and Shima (2012). Most of the research done in this area has focused on thermal conductivity in the calculation of nanofluids because scholars believe that when the thermal conductivity of nanofluids increases, their heat transfer property increases too.

The studies of thermal conductivity is conducted by Afrand (2017) that is to investigated experimental study on thermal conductivity of ethylene glycol containing hybrid nano-additives and development of a new correlation. An experimental investigation on the effects of hybrid nano-additives, composed of magnesium oxide (Mg O) and functionalized multi-walled carbon nanotubes (FMWCNTs), on the thermal conductivity of ethylene glycol (EG) is presented. The experiments performed at temperatures ranging from 25 ºC to 50 ºC and the solid volume fraction range of 0–0.6%. The measurements revealed that the thermal conductivity of nanofluids significantly enhances with an increase in the percentage of the solid volume fraction. Moreover, the thermal conductivity of EG considerably increased with increasing temperature, while thermal conductivity of hybrid nanofluid slightly enhanced (Afrand, 2017).

The thermal conductivity measurements showed that the maximum enhancement of thermal conductivity of nanofluid is 21.3%, which occurred at solid volume fraction of 0.6% and temperature of 25 ºC. Finally, efforts were made to provide an accurate correlation for estimating the thermal conductivity at various temperatures and concentrations. Deviation analysis of the thermal conductivity ratio was performed. The comparison between experimental results and correlation outputs showed a good agreement. So, In the present study, the thermal conductivity of MgO-FMWCNTs/ EG hybrid nanofluid at temperatures ranging from 25 ºC to 50 ºC for various suspensions at volume fraction of 0.05%, 0.1%, 0.15%, 0.2%, 0.4% and 0.6% have been examined. Experimental results indicated that the thermal conductivity significantly enhances with an increase in the percentage of the solid volume fraction (Afrand, 2017).

Moreover, the thermal conductivity of EG increased with increasing temperature considerably, while the thermal conductivity of hybrid nanofluid slightly enhanced. Results revealed that at higher solid volume fractions (0.2–0.6%), the thermal conductivity enhancement is lower than that at low solid volume fractions (0.05–0.2%). The thermal conductivity measurements showed that the maximum enhancement of thermal conductivity of nanofluid is 21.3%, which occurred in a solid volume fraction of 0.6% and temperature of 25 ºC. Using experimental results, in order to predict the thermal conductivity of MgO-FMWCNTs/ EG hybrid nanofluids, a correlation has been proposed. Deviation analysis of the thermal conductivity ratio showed that the maximum value of margin of deviation was 1.2%. Comparison between experimental results and the correlation outputs demonstrated that the correlation has a high accuracy. Hence, this correlation can estimate the thermal conductivity of MgO-FMWCNTs/EG hybrid nanofluids at solid volume fractions ranging from 0.05% to 0.6% for the temperature range of 25–50 ºC (Afrand, 2017).

2.3.1.6 Viscosity

Consequently, the viscosity of nanofluid plays a vital role in determining the thermal performance in heat transfer, especially factors like aggregation and sedimentation of nanoparticles (Ghadimi, Saidur, & Metselaar, 2011; Yu, Xie, Chen, & Li, 2010). Sundar, Singh, and Sousa (2013) extensively investigated the viscosity of an ethylene glycol-water mixture based Fe_3O_4 nanofluid. The effects of volume fraction of nanoparticles (0.0022–0.0055), temperature (15-70 ºC) and shear rate on the viscosity of nanofluid were calculated. The results reported that increasing shear rate leads to a reduction of viscosity. They suggested that the formation of aggregates contributed to the increase in viscosity of the nanofluids. Murshed et al. (2008) indicated that the dispersion of 5% Al_2O_3 or TiO_2 nanoparticles in water based, causing the viscosity to rise by 82% and 86%, respectively.

The rise of nanofluids' viscosity can cause a serious constraint in heat transfer application. S. K. Das et al. (2006) conducted a study on the effect of nanoparticles concentrations and size on nanofluids viscosity under various temperature ranges. They reported that viscosity drops sharply with temperature, notably for high concentration of nanoparticles. Abu-Nada and Oztop (2009) conducted a simulation to implement models for nanofluid properties to predict heat transfer refinement in natural convection and developed a mathematical correlation based on the experimental results from the literature. The correlation particularly, for nanofluid viscosities is the function of temperature and nanoparticle concentrations.

Mintsa, Roy, Nguyen, and Doucet (2009) evaluated the viscosity of CuO nanoparticles in water based. They reported that the viscosity of the nanofluid would decrease with a rise in temperature. They also acknowledged that unwanted pressure drop as a consequence of viscosity signification (by increasing the concentration) could impact thermal properties enhancement in nanofluids. Chandrasekar, Suresh, and Bose (2010).investigated the viscosity of Al_2O_3/water nanofluids with a change in shear rate. According to their results, the viscosity of the nanofluid would rise with the concentration of nanoparticles. In addition, effects of carbon nanotubes (CNT) on the viscosity of deionized water and ethylene glycol with the presence of Sodium dodecyl sulphate (SDS) as surfactant were experimentally conducted by Yang, Ding, Chen, and Li (2007). They indicated that the viscosity rose when the particles concentration is increased. While the viscosity of the nanofluid decreased when the temperature rose to between 30 ºC and 60 ºC. Based on their results, low nanoparticles concentration influenced the viscosity notably with significant temperature ranges.

The study of viscosity is conducted by (Minea, 2017) that is investigated about effects of temperature and particles concentration on the dynamic viscosity of MgO-MWCNT/ethylene glycol hybrid nanofluid: Experimental study. The effect of temperature and particles concentration on the dynamic viscosity of MgO-MWCNT/ethylene glycol hybrid nanofluid is examined. The experiments carried out in the solid volume fraction range of 0 to 1.0% under the temperature ranging from 30 ºC to 60 ºC. The results showed that the hybrid nanofluid behaves as a Newtonian fluid for all solid volume fractions and temperatures considered. The measurements also indicated that the dynamic viscosity increases with increasing the solid volume fraction and decreases with the temperature rising.

The relative viscosity revealed that when the solid volume fraction enhances from 0.1% to 1%, the dynamic viscosity increases up to 168%. Finally, using experimental data, in order to predict the dynamic viscosity of MgO-MWCNT/ethylene glycol hybrid nanofluids, a new correlation has been suggested. The comparisons between the correlation outputs and experimental results showed that the suggested correlation has an acceptable accuracy. Furthermore, the results reveal that for nanoparticles volume fractions of 0.8% and 1.0% the effect of temperature on the viscosity of nanofluid is more noticeable.

2.3.2 Hybrid Nanofluid

Within decades, a lot of research has been conducted on nanofluids including preparation, characterization, modeling, convective and boiling heat transfer and applications, and more than 50 review articles have been published till date (Choi, Singer, & Wang, 1995; S. K. Das et al., 2006; Pozhar, 2000; Pozhar & Gubbins, 1997). But the hybrid nanofluids are very new kind of nanofluids, which can be prepared by suspending different types (two or more than two) of nanoparticles in base fluid, and hybrid (composite) nanoparticles in base fluid. A hybrid material is a substance which combines physical and chemical properties of different materials simultaneously and provides these properties in a homogeneous phase. Synthetic hybrid nanomaterials exhibit remarkable physicochemical properties that do not exist in the individual components. Many researches has been conducted regarding the properties of these composites (Sarkar et al., 2015) and hybrid materials consisting of carbon nanotubes (CNTs) have been used in electrochemical-sensors, bio-sensors, nanocatalysts, etc. but the use of these hybrid nanomaterials in nanofluids has not developed as such. Work on hybrid nanofluids is very limited and a lot of experimental study is still being done (Sarkar et al., 2015).

The main objective of synthesizing hybrid nanofluids is to obtain the properties of its constituent materials. A single material does not possess all the favorable characteristics required for a particular purpose; it may either have good thermal properties or rheological properties. A trade-off between several properties and that is where the use of hybrid nanofluid comes in many practical applications. Hybrid nanofluid is expected to yield better thermal conductivity compared to individual nanofluids due to synergistic effect. Carbon nanotubes have a multitude of unique properties like its physical strength, chemical stability, mechanical resistance, very high electrical and thermal conductivity, etc (Sarkar et al., 2015). These characteristics have attracted the researchers towards carbon nanotubes as well as in development of a new category of hybrid nanomaterials consisting of a composite of carbon nanotubes with metallic, semi-conductive or non-conductive nanoparticles.

With methods such as one-step, two-step and other novel methods hybrid nanofluids can be prepared. Quality and stable hybrid nanofluids can be prepared through these methods for researches and applications such as heat transfer.

2.3.2.1 Two-step method

To prepare nanofluids researchers widely use the two-step method. Initially in this method most of the nanoparticles, nanotubes, nanofibres and other nanomaterials produced as dry powders (synthesizing process) either by chemical or physical methods (Yu & Xie, 2012). With the help of magnetic stirrer, ultra-sonication, high shear mixing and homogenizing, the synthesized dry nanopowder will be suspended into a fluid in the next processing step. This strategy is the most financial readiness of nanofluid particularly in extensive scale in light of the fact that the blending of nanopowder have been mass fabricated underway levels. In conjunction with the high surface area of nanoparticles (relies upon the extent of the molecule) and other surface activity, nanoparticles tend to residue and in addition influencing the thermal properties of the nanofluids (Yu & Xie, 2012).

Afrand et al. (2016) showed that for strong volume division higher than 1%, clustering phenomenon was observed, which prompted deposition and sedimentation of nanoparticles and nanofluid was not dispersed. In this way, the solidness of the nanoparticles can be enhanced by adding the surfactant to the liquids to maintain a strategic distance from the accumulation. Adding surfactant to the liquid may enhance the stability of the nanoparticles dispersion, anyway the adequacy of the surfactant weakens under high temperature of thermal exchange application. What's more, sedimentation of the nanoparticles may bring about the settlement or obstructing as well as lessening the thermal conductivity of the nanofluids. Suresh et al. (2011) used two-step technique to create Al_2O_3 – Cu/water hybrid nanofluid of volume part of 0.1%. Sodium lauryl sulfate (SLS) was utilized as a surfactant. Before that, the nanocrystalline alumina-copper (Al_2O_3– Cu) hybrid powder was set up by a thermochemical combination strategy through a few phases, which was splash drying, oxidation of antecedent powder, diminishment in hydrogen climate and homogenization.

Dry f-MWCNT and Fe_3O_4 nanoparticle were set up with an equivalent volume blend (B. Das et al., 2014). Two-step technique has been locked in to deliver hybrid nanoparticles (f-MWCNT-Fe_3O_4) and dispersed in ethylene glycol (Sundar, Ramana, Singh, & De Sousa, 2012). Esfe et al. (2014) utilized two-step technique to yield MWCNT-ZnO (10% volume of MWCNT and 90% volume of ZnO) hybrid nanoparticles and dispersed in SAE40 oil. Esfe et al. (2014) delivered Cu-TiO_2 hybrid nanoparticles utilizing a two-step strategy and included into ethylene glycol (EG), alongside no surfactant introduced in the liquid. Prior to that, they synthesized the nanofluid by dispersed into seven diverse concentrations (0.1, 0.2, 0.4, 0.8, 1.0, 1.5 and 2%) and certain measures of Cu and TiO_2 were included into the base liquid for every concentration. MWCNT-ZnO was set up with proportion of 15% and 85%, individually. The nanoparticles were produced by utilizing two-step technique and included into oil, without use of any surfactant to frame crossover nanofluid (Wilborn, 2014).

MWCNT and ZnO were orchestrated mechanically like Esfe et al. (2014) incorporating ventures aside from the quantity of strong volume portions figured.

Afrand et al. (2016) figured the nano-added substances which were creation of FMWCNTs and MgO nanoparticles to be scattered in unadulterated ethylene glycol. The hybrid nanoparticles with various strong volume parts were set up by utilizing two-step strategy.

2.3.2.2 One-step method

In one-step preparation method, both syntheses of nanoparticles and the preparation of the nanofluids are performed concurrently. It is commonly a process of mixture of the nanoparticles with the synthesis of the nanofluids for which the nanoparticles are directly prepared by physical vapor deposition (PVD) technique or liquid chemical method. There are many one-step techniques for preparation of nanofluids, for example Physical vapor deposition (PVD) technique or Liquid chemical method, VEROS (Vacuum Evaporation onto a Running Oil Substrate) technique, direct evaporation system and vacuum-SANSS (submerged arc nanoparticles synthesis system). In these methods, the processes of drying, storage, transportation, and dispersion of nanoparticles are avoided, so the agglomeration of nanoparticles is minimized and the stability of fluids is increased (Eastman, Choi, Li, Yu, & Thompson, 2001). Eastman et al. (2001) implemented a one-step physical method to prepare nanofluids, in which Cu vapor was directly condensed into nanoparticles by contact with a flowing low vapor pressure liquid (ethylene glycol).

One-step physical method however, unable to synthesize nanofluids in large scale due to excessive cost, therefore the one-step chemical method was developed. Kumar, Meenakshi, Narashimhan, Srikanth, and Arthanareeswaran (2009) utilized a novel one-step chemical method for the preparation of stable, non-agglomerated copper nanofluids by reducing copper sulphate pentahydrate with sodium hypophosphite as reducing agent in ethylene glycol as base fluid by means of conventional heating. They indicated an in situ, one-step method which yield high amount of product with less time consumption. Zhu, Lin, and Yin (2004) prepared a novel one-step chemical method for prepping copper nanofluids by contracting $CuSO_4.5H_2O$ with $NaH_2O.H_2O$ in ethylene glycol as base fluid under microwave irradiation. Deshmukh and Sangawar (2016) used chemical route one-step method to prepare polyethylene microspheres. They indicated images from scanning electron microscopy proved that the concentration of polyglycolic acid reduced the agglomeration and increased the degree of sphericity of the polyethylene microspheres. In a one-step method, carbon was heated and vaporizes simultaneously in the chamber, the carbon vapor and particles were then produced and dispersed in water (base fluid), to form desired carbon/water nanofluid.

Teng, Cheng, and Pai (2011) prepared this nanofluid by the plasma arc system which belongs to one-step method and the magnetic stirrer and stainless steel mesh thoroughly mix the resulting nanofluid, which will be induced out to form stable carbon/water nanofluid. Aberoumand and Jafarimoghaddam (2016) utilized a single step method known as Electrical Explosion of Wire (E.E.W). The nanofluid will be produced via an explosion in a container of base fluid and thin metal wire. High current and electric voltage is the main operators of the explosion. Then, produced Tungsten (III) oxide (W_2O_3)/transformer oil (base fluid) nanofluid was used as the base fluid for suspending silver (Ag) nanoparticles with E.E.W again, to produce Ag-W_2O_3/transformer oil hybrid nanofluids. Wei, Zhu, Kong, and Wang (2009) prepared copper dioxide nanofluids by a single-step method called submerged arc nanoparticles synthesis system (SANSS). The established SANSS were shown to be effective in diminishing particle aggregation and producing uniformly distributed, along with well-controlled size of CuO nanoparticles dispersed in a deionized water suspension.

Munkhbayar, Tanshen, Jeoun, Chung, and Jeong (2013) presented on nanofluids preparation by a one-step physical technique using the pulse wire evaporation (PWE) method. The apparatus used consists of four main components: a high-voltage DC power supply, a capacitor bank, a high-voltage gap switch, and an evaporation/condensation chamber. MWCNTs were polarized by chemical treatment to allow for better dispersion. A plain method for purifying MWCNTs via nitric acid (HNO_3) and sulfuric acid (H_2SO_4) were prepared to improve its hydrophobic nature (optimize characterization of MWCNTs). A deionized water-based Ag nanofluid with a nanoparticle concentration was prepared and maintained by the one-step PWE method and by controlling the wire explosion number respectively. The dispersion rate and thermal conductivity of these nanofluids were evaluated by UV spectrophotometry and a transient short hot wire method. Mineral oil-based nanofluids containing silver nanoparticles with a narrow-size distribution were also prepared by one-step method. Henglein (1993) presented that the particles could be stabilized, which arranged to the silver surfaces via two oxygen atoms forming a dense layer around the particles. The silver nanoparticles suspensions were stable for 1 month. Angayarkanni and Philip

(2015) extensively reviewed that the laser ablation is another one-step method to yield and disperse nanoparticles straightaway in base fluid.

Xia et al. (2003) presented that gold nanoparticles that was suspended in water were due to pulsed laser ablation in liquids. Under this method, the average size of the Au-NPs was ranged from 7.1 to 12.1 nm while their size-distribution tended to become narrower with effects of laser-induced fragmentation. Therefore, nanofluid showed significant colloidal stability even after 1 month although no surfactant was used. However, due to high rate of reactivity of nanoparticles, they have the tendency to sediment, resulting on residual reactant being left in the nanofluid due to incomplete reaction or dispersion. Therefore, the surfactant or stabilizer was used as a stabilizing agent who prevents particles aggregation.

2.4 Machining of SUS 304 Stainless Steel

The most common form of 304 stainless steel is 18-8, or 18/8, stainless steel, which contains 18 percent chromium and 8 percent nickel. 304 can withstand corrosion from most oxidizing acids. Stainless Steel SUS 304 offer high strength, and also extremely workable, with the ability to be deep drawn into shape without the need for annealing, making 304 perfect for the manufacture of bowls, sinks, pans and a range of different medical vessels and hollow ware (Hong & Koo, 2005). SUS 304 stainless steels are an alloy with high fracture toughness, high tensile strength high ductility, low heat conductivity and high work hardening rates. These undesirable properties contributed to a number of difficulties such as poor surface integrity and short tool life (Ouchi, 2001).

The main applications of SUS 304 stainless steel are used in air craft fitting, aerospace component and some component in chemical environment. Besides that, it was also being used for welded construction in aerospace structural component. Most of this application needs certain machining process with different machines. All the machining process of SUS 304 stainless steel come across with huge number of difficulties such as poor surface roughness due to high temperature in the cutting zone (Anijdan, Madaah-Hosseini, & Bahrami, 2007). The properties of SUS 304 stainless steel that contribute to the defect in the machining can be shortened as follows:

a. Low thermal conductivity contributes to massive heat at the cutting zone which will
effects the surface integrity (Yoon et al. 2006).

b. High deformation hardening of SUS stainless steel will cause wear on the flank of the cutting tool.

c. It is also classified as alloy with higher tendency of build-up-edge (BUE) which affects the life span of the cutting tool and the surface roughness (Senevirathne & Ranaweera, 2018).

d. It is also classified as high hardness and wear resistant which contribute to poor surface roughness during machining.

Furthermore, during the machining of this alloy, there a strong bong has been form between the workpiece and the cutting tool and when the chip is formed, it may bring with it a fragment of the tool and cause a flank wear. This is mainly for cemented carbide tool. Basically, machining SUS 304 stainless will encounter a lot of problem and this is very 2004 common in industry. Therefore according to machining with optimum cutting parameter will reduce the defects on machining. The best cutting speed and feed rate were determined according to flack wear, BUE, chip form and also surface roughness (Kadirgamaa et al. 2008).

2.4.1 Cutting Tool Material for SUS 304 Stainless Steel

Since SUS 304 stainless steel has been classified as “difficult-to-cut” material, the cutting tool material used to cut this material must be good in strength, thermal properties, wear resistant and also adequacy of chemical stability at high temperature. According to Kumar et al. (2009) modern cutting tool are coated with ceramic and providing lower attraction to tool and lower thermal conductivity of the tool which rise the chip temperature and enabled flow of the chip (Yazid et al. 2012).Various alloys have been added to the coating element to advance the properties of the cutting tool.

Tungsten cobalt (Wc-Co) is one of the protective hard coating materials for carbide cutting tool. But, according to and Kumar et al. (2009) chromium nitride (CrN) is consider superior than TiN in term of corrosion and wear resistant, friction behavior and toughness. However, TiN and CrN are limited up to 500 ºC and 600 ºC respectively. Besides that, (Ti,Al)N and (Al,Cr)N coating showed a great improvement thermal resistant up to 900 ºC which can withstand huge amount cutting temperature. This is due to the formation of steady oxidation layer of Al_2O_3, Cr_2O_3 and TiO_2 layers. On the other hand, (Ti, Al)N coating have enhanced abrasive wear resistant but (Al, Cr)N coating are more recommended has thermally stable.

2.4.2 Machining with Nanofluid

From previous study by (Azwadi et al. 2017) is he explained about applications of nanofluids in machining processes. In addition to reviewing the various conventional and advanced cooling techniques during machining, the paper also discusses the preparation methods, factors for enhancing thermal conductivity and properties of nanofluids. In line with fast development of nanofluid in machining process, the purpose of this paper is to review recent progress on the application of nanoparticles in lubricants especially for MQL technique. The conclusions and important summaries were also presented according to the data collected. However, application of conventional cutting fluids would cause health and environmental problems. Prolonged contacts with cutting fluids have proven to lead skin and respiratory diseases. Cutting fluids also contaminate air, water and ground during huge disposal (Singh et al. 2016).

In a different study by (Jerold & Kumar 2012), they have compared in the turning experiment of SUS1045 steel with cryogenic LN_2 and CO_2 cooling. They have found that the use of cryogenic LN_2 reduced the cutting temperature about 3–17% when compared to CO_2coolant. On the other hand, the application of CO_2 reduced the cutting forces about 2–12% when compared to the use of cryogenic LN_2 coolant. In addition, tool wear was found to be less on the application of CO_2 compared to the cryogenic LN_2 coolant and wet machining conditions. The cooling abilities of the cutting fluids were assessed by carrying out the machining tests using the fluids with and without nanoparticle (carbon nanotubes) inclusions. The nodal temperatures that represented the cooling capabilities of the fluid decreased with the CNT content. However, the change was less beyond 2% of the CNT inclusion, corresponding to the change in thermal conductivity. In another study, nanographene-enhanced vegetable oil fluid provided better results in terms of wettability and a reduced friction coefficient. The results were verified by applying the nanographene-enhanced coolant in MQL. Better performance was achieved in terms of tool wear and edge chipping. The nanoboric acid inclusion in coconut oil showed reduced cutting temperatures and better performance in terms of tool flank wear and surface roughness (Sodavadia & Makwana, 2014). The improvement was based on the increased thermal conductivity and enhanced heat transfer coefficient. A lot of researches on the application of nanocutting fluids have been reported in the literature about the use of nanoparticles as additives to the traditional oil-based lubricants and improved machining performance in terms of reduced wear and decreased friction.

The research on the application of nanoparticles as a water-based cooling/lubricating medium is still very rare (Najiha, Rahman, & Kadirgama, 2016). The application of water-based Al_2O_3 and diamond nanofluids in the MQL grinding showed promising improvements in surface roughness, a reduction in the grinding force, and an improved G-ratio with high concentrations of nanofluids as compared to pure water application (Najiha et al., 2016). Research has been carried out to investigate the wheel wear and the tribological characteristics in wet, dry and MQL grinding of cast iron. The tribological properties and application performance of water-based TiO_2 nanofluid were investigated in the MSR 10D four ball tribotester and bench drilling operation (Lu, Wei, Gu, Liu, & Park, 2014). It was found that the surface-modified TiO_2 nanoparticles can effectively reduce the load-carrying capacity, friction reducing and anti-wear properties of pure water. Water-based nanofluids can serve as more sustainable and environment-friendly cutting fluids, given the toxicity and non-biodegradability of the oil-based fluids (MM Rahman, Kadirgama, & Ab Aziz, 2014). The manufacturing practices and technologies adopted as a part of sustainable machining were evaluated, analyzed and optimized for sustainability impacts. Even though sustainable machining is a critical aspect of sustainable manufacturing, the studies carried out to assess the ecological and social effects of sustainable machining are insufficient.

Most of the researches that have analyzed the effects of sustainability conducted so far are limited to the economic aspects i.e. from discovering the newer techniques of material removal as a substitute to the conventional machining as well as to the optimization of various variables contributing to the machining process. Some of the researchers have attempted to analyze the environmental impacts. In a study carried out by Gautier, Priarone, Rizzuti, Settineri, and Tebaldo (2015), the milling process of a non-conventional material γ-TiAl alloy was analyzed for ecological and environmental effects with three cooling and lubricating conditions i.e., flooded cooling, MQL and dry machining. Shao, Kibira, and Lyons (2010) have proposed a methodology that uses a virtual model of a machining system to analyze the environmental impact of the process. The objective of the simulation system, scope, model elements, and its input and output requirements were discussed. This approach allows assessing the environmental impact in the virtual environment using the real world, specification, and simulation data as input and provides a platform to evaluate different options for an optimal decision making.

2.5 Modelling

Response surface method (RSM) is a collection of statistical techniques for empirical model building. By careful design of experiments, the objective is to optimize a response (output variable) which is influenced by several independent variables (input variables). An experiment is a series of tests, called runs, in which changes are made in the input variables in order to identify the reasons for changes in the output response. RSM has been firstly developed to model experimental responses and then migrated into the modeling of numerical experiments. The difference is in the type of error generated by the response. In physical experiments, inaccuracy can be due to measurement errors whereas in computer experiments, numerical errors are due to incomplete convergence of iterative processes, round-off error or the discrete representation of continuous physical phenomena. In RSM, the errors are assumed to be random (Konermann & Douglas, 1997). The Response surface method (RSM) is a methodology of constructing approximations of the system behavior using results of the response analyses calculated at a series of points in the variable space. Optimization of RSM can be solved in the following three stages:

- Design of experiment.
- Building the model.
- Solution of minimization problem according to the criterion selected.

RSM is a combination of experimental and regression analysis and statistical inferences. The concept of a response surface involves a dependent variable *y* called the response variable and several independent variables *x1*, *x2*, . . .,*xk* (Khuri & Cornell, 1996). If all of these variables are assumed to be measurable, the response surface can be expressed as:

$$y = f\,(x1;\, x2;\, .\,.\,.\,;\, xk) \tag{2.7}$$

Usually a low order polynomial (first-order and second-order) is employed in some regions of the independent variables. The first-order model:

$$y = \beta_0 + \sum_{i=1}^{k} \beta_i x_i + \varepsilon \tag{2.8}$$

and the second–order model:

$$\sum_{i=1}^{k} \beta_i x_i \;+\; \sum_{i=1}^{k} \beta_{ij}\, x^2{}_i + \sum_i \sum_j \beta_{ij} x_i x_{\,j} + \varepsilon \text{ for i<} \tag{2.9}$$

are generally utilized in RSM problems. The β parameters of the polynomials are estimated. The RSM is practical, economical and relatively easy to use and it has been employed by many researchers for modeling machining processes (Baradie, 1993). Mead and Pike (1975) and Hill and Hunter (1966) have reviewed the earliest works on RSM. In order to institute an adequate functional relationship between the surface roughness and the cutting parameters (speed, depth of cut and feeds), a large number of tests are needed, requiring a separate set of tests for each combination of cutting tools and workpiece materials.

Fuh and Wu (1995a) have proposed prediction models based on the Takushi method and RSM. By using factors such as cutting speed, feed and depth of cut, Alauddin, El Baradie, and Hashmi (1995) have developed surface roughness models and determined the cutting conditions for 190 BHN steel and Inconel 718. They have found that the variations of both tool angles have important effects on surface roughness. In order to model and analyses the effect of each variable in minimizing the number of cutting tests, surface roughness models based on RSM and experimental design have been determined in this investigation.

Mishra and Prasad (1985) has derived a relationship to study the residual stresses based on a moving heat source under various simulated cutting conditions, but the predicted trend is not in good agreement with the results of actual machining. RSM has been utilized to determine the residual stresses under different cutting conditions and materials (El-Khabeery & Fattouh, 1989). Whilst the properties of the materials are not identical except for tensile strength, some materials machined by a tool with a chamfer have been subjected to microstructure change due to temperature effect (Matsumoto et al., 1986).

Wu and Matsumoto (1990) have been pioneering the application of RSM in tool life testing. The number of experiments required to develop a surface roughness equation can be reduced as compared to that of the traditional one-variable-at-a-time approach. Based on RSM and 23 factorial designs, first- and second-order models have been developed in this project. Only 12 tests are required to develop the first-order model, whereas 24 tests are needed for the second-order model. Choudhury and El-Baradie (1999) has pointed out that for accurate rating of machinability, three factors, namely, tool life, surface roughness, and power consumed during cutting, must be considered. Similar opinions have been contributed by Giovanola (1988).

Taraman (1974) has used the RSM approach to predict surface roughness. Families of mathematical models for tool life, surface roughness and cutting forces have been developed in terms of cutting speed, feed, and depth of cut. Hasegawa, Seireg, and Lindberg (1976) have conducted 34 factorial designs to conduct experiments for the development of surface roughness prediction model. They have found that the surface roughness increases with the increase of cutting speed. Sundaram and K Lambert (1981)have considered six variables i.e. speed, feed, depth of cut, time of cut, nose radius and type of tool, in order to monitor surface roughness.

Kadirgama, Noor, et al. (2008) stated that a survey on surface roughness prediction models and found that most of the models have been developed for steels. Boothroyd (1988) and Baradie (1993) have investigated the effect of speed, feed and depth of cut on steel and grey cast iron, and then emphasized the use of RSM in developing a surface roughness prediction model.

2.5.1 Full-factorial Design

In order to construct an approximation model that can capture the interactions between *N* design variables, a full factorial approach may be necessary to investigate all possible combinations. A factorial experiment is an experimental strategy in which design variables are varied simultaneously, instead of one at a time (Box & Draper, 1987; Montgomery, 2017). The lower and upper bounds of each design variable in the optimization problem must be defined. The allowable range is then discretized at different levels. If each variable is defined merely at the lower and upper bound (two levels), the experimental design is called 2*N* full factorial design. Similarly, if the midpoints are included, the design is called 3*N* full factorial design as schematically shown in Figure 2.14.

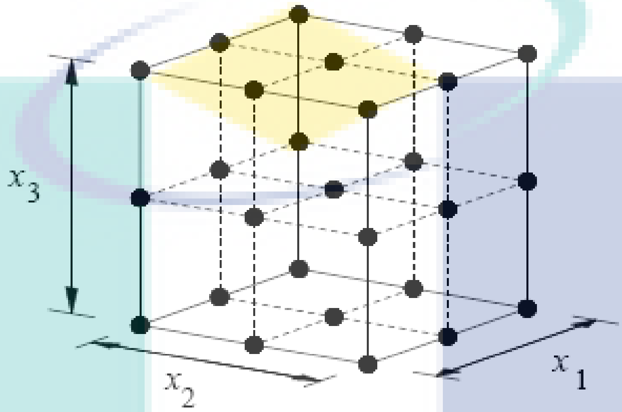

Figure 2.14: 3N full factorial
Source: Montgomery (2017)

Factorial design can be used for fitting the second-order models to improve the optimization process. A general second-order model can be defined as (Box and Draper 1987):

$$y = a_0 + \sum_{i=1}^{n} a_i x_i + \sum_{i=1}^{n} a_{ii} x_i^2 + \sum_{i=1}^{n} \sum_{i=1}^{n} a_{ij} x_i x_j \tag{2.10}$$

where *xi* and *xj* are the design variables and *a* is the tuning parameters.

The construction of a quadratic response surface model in *N* variables requires the study at three levels so that the tuning parameters can be estimated. Therefore, at least (*N*+1) (*N*+2) / 2 functional evaluations are necessary. Generally, for a large number of variables, the number of experiment grows exponentially (3N for a full factorial) and becomes impractical. A full factorial design is typically used for five or fewer variables (Box & Draper, 1987; Montgomery, 2017).

If the number of design variables becomes large, a fraction of full factorial design can be used at the cost of estimating only a few combinations of variables. This is called the fractional factorial design and is usually used for screening important design variables.

2.5.2 Central Composite Design

A second-order model can be constructed efficiently with Central composite designs (CCD). CCD is first-order (2N) design method augmented by additional center and axial points to allow estimation of the tuning parameters of a second-order model. Figure 2.15 shows the CCD for 3 design variables (Baradie, 1993).

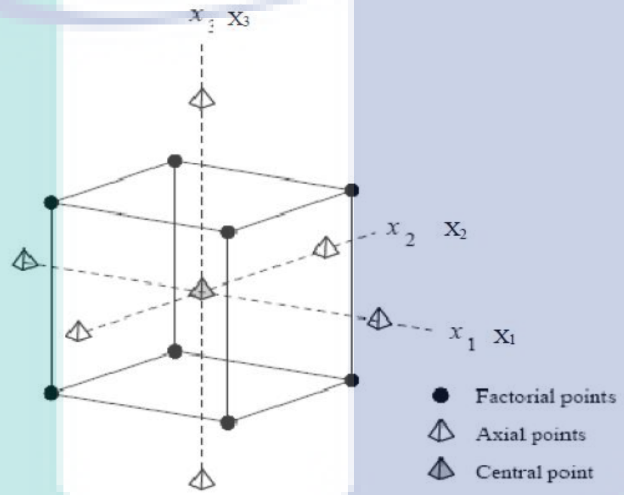

Figure 2.15: CCD for 3 design variables

Source: Baradie (1993)

2.5.3 Box Behnken Design

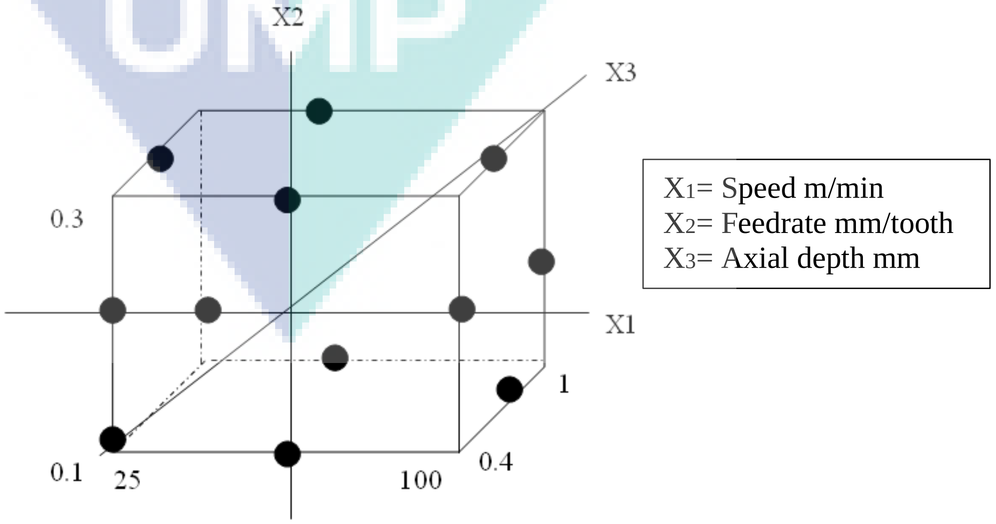

Figure 2.16: BBD for 3 design variables

Source: Montgomery (2017)

Some key features of BBD incorporated include:

1. Allow efficient estimation of first- and second-order terms.
2. Desirable design properties of orthogonal blocks.
3. Less expensive to run compared to CCD having the same number of factors. Additionally, BBD has fewer design points.
4. All the design points fall within the safe operation zones. BBD designs do not have axial points, which may be lying outside the region of interest or beyond the safe operating limits. Therefore, they are safer for such environments that involve high risk of tool and machine damage if more severe parameter is used.
5. All factors are never set to their extreme (low or high) levels simultaneously.

2.6 Micrographic Analysis

Transmission electron microscope (TEM) was used to monitor the dispersion, clustering and morphology of the nanoparticle in the base liquid. As stated by Murshed et al, the size of nanoparticle in the base liquid is higher than the actual size specified by the supplier. This is due to large nano particle density, higher number of particle, inter-particle attraction and agglomeration between the nano particle and base water. Figure 2.17 and Figure 2.18 shows clustering and agglomeration of TiO_2 nanofluids after the dispersion (Murshed et al., 2005).

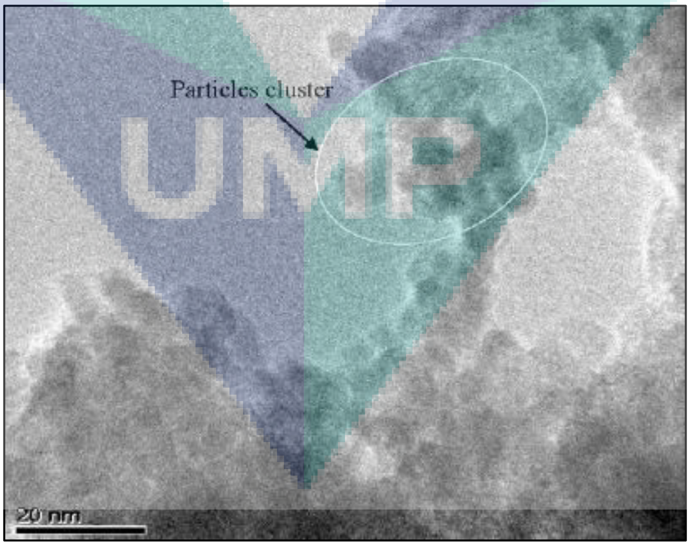

Figure 2.17: TEM photograph of TiO_2 nanofluid with particle size 15nm in diameter.
Source: Murshed et al. (2005)

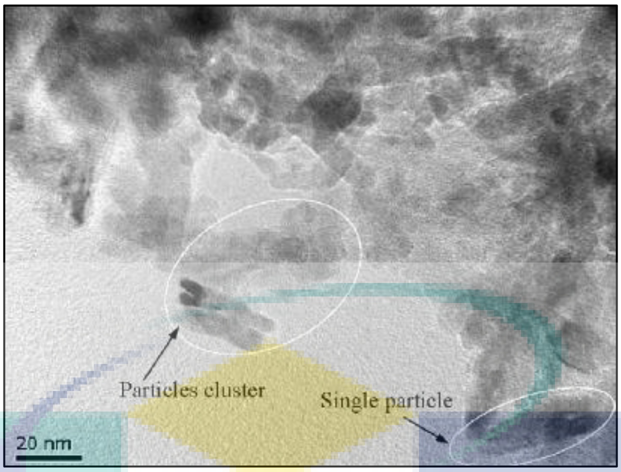

Figure 2.18: TEM photograph of TiO_2 nanofluid with particle size 10nm in diameter.
Source: Murshed et al. (2005)

Scanning electron microscope (SEM) was performed to investigate the cutting tool wear. Figure 2.19 shows that the tool tips wear on rake face and flank face (Byrne, Dornfeld, & Denkena, 2003). On the rake surface crater wear, the outer chip notch and the inner chip notch are seen (Byrne et al., 2003). In the crater area energy dispersive spectroscopy (EDS) microanalysis has found traces of work material (Fe and Cr). Byrne et al. (2003) found that on the flank in figure 2.19, the flank wear zone and the primary groove were recognized.

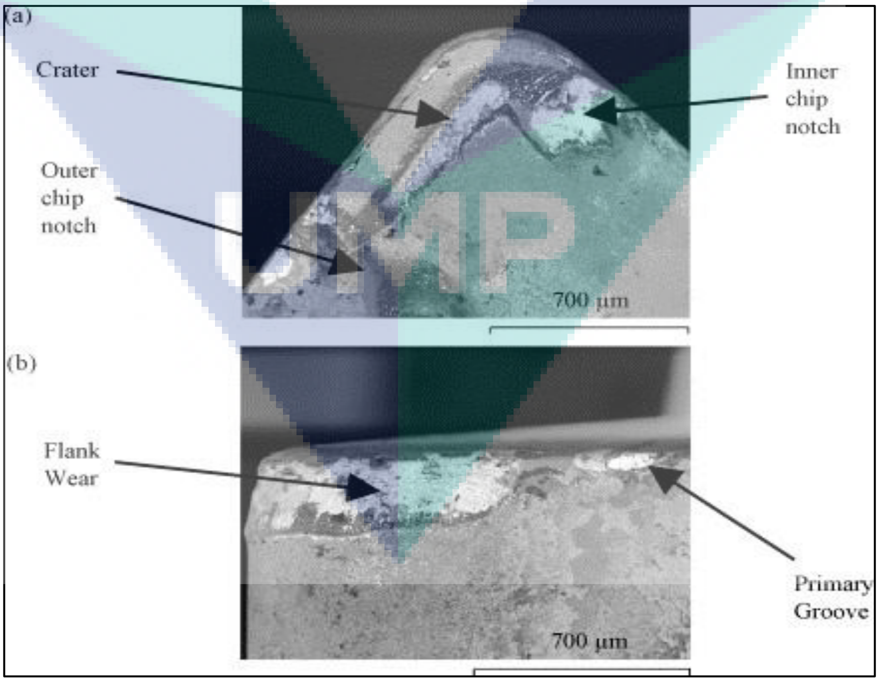

Figure 2.19: SEM analysis on rake face and flank face.
Source: Byrne et al. (2003)

2.7 Summary

1. In most cases, the tangential cutting force is the largest of the three components, although in finishing operation the radial thrust force is often the largest, while the feed force is the smallest.

2. The cutting force decreases with increasing cutting speed, whereas cutting force increases with increasing feedrate and axial depth of cut.

3. The fundamental nature of the mechanism of wear can be very different under different conditions. In metal cutting, six main forms of wear are known to occur: adhesion, abrasion, diffusion wear, oxidation wear, crater wear, flank wear, notch wear, edge chipping, and built-up edges.

4. The build-up-edge (BUE) can occur during the low cutting speed and does not occur at high cutting speed because there is no strain hardening if the recrystallization temperature is much greater during the deformation process.

5. Machining process of SUS 304 stainless steel come across with huge number of difficulties such as poor surface roughness due to high temperature in the cutting zone.

6. The most common type of tool wear for milling SUS 304 stainless steel is flank wear, crater wear, notch wear, chipping and comb crack. The failure criteria of flank wear which is 0.3 mm.

7. The tool coating is the main factor affecting tool life followed by cutting speed and workpiece angle. An increased in the cutting speed, feedrate and axial depth of cut would decrease the tool life.

8. The surface roughness increases when the cutting speed and feed rate increases and the surface roughness decreases when the axial depth of cut increases.

9. All the results shows that the thermal conductivity of nanofluids exhibits higher thermal properties even the concentration of liquid is less than 5% in volume percentage.

10. The thermal conductivity of TiO_2 nanofluids and ZnO nanofluid increases with increases in temperature.

11. Two step methods is the most financial readiness of nanofluid particularly in extensive scale in light of the fact that the blending of nanopowder have been mass fabricated underway levels.

12. Response surface method (RSM) is a collection of mathematical and statistical techniques for empirical model building. The objective is to optimize a response (output variable) which is influenced by several independent variables (input variables).

13. RSM was developed to model experimental responses and then migrated into the modelling of numerical experiments. The difference is in the type of error generated by the response. In physical experiments, inaccuracy can be due to measurement errors whereas, in computer experiments numerical errors are due to incomplete convergence of iterative processes, round-off errors or the discrete representation of continuous physical phenomena.

14. The RSM is practical, economical and relatively easy to use and was employed by many researchers for modeling machining processes.

15. Transmission electron microscope (TEM) was used to monitor the dispersion, clustering and morphology of the nanoparticle in the base liquid. Scanning electron microscope (SEM) was performed to investigate the cutting tool wear.

CHAPTER 3

METHODOLOGY

3.1 Introduction

The purpose of this chapter is to provide the information regarding the design of experiment, equipment used throughout the experiment, cutting tool material, workpiece material that has been used in this research. The experiment has been carried out in two stages which is preliminary run and real experiment. The aim of preliminary run is to find excellent range of cutting parameter. The real experiment will carry out by using the detailed base on the preliminary run.

3.1.1 Flow Chart

Figure 3.1 shows the flow chart of the thesis. The first step of this thesis is the nanofluid preparations with selection of volumes. Then the nanofluids evaluated. Once the preparation done with nanofluids, the next step is material and equipment preparations. Then the milling process is done with selected parameters and three type of coolant (ethylene glycol, nanofluid and hybrid nanofluid). The data for tool life, surface roughness, and flank wear are collected and discussed.

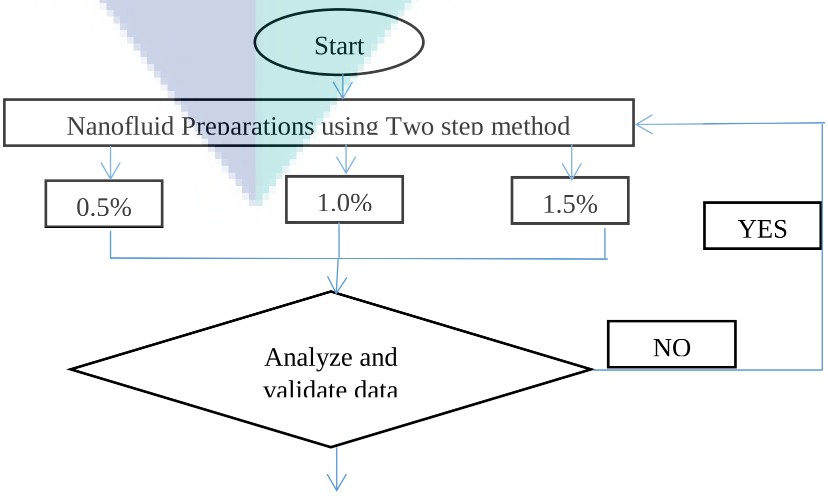

Figure 3.1: Continued

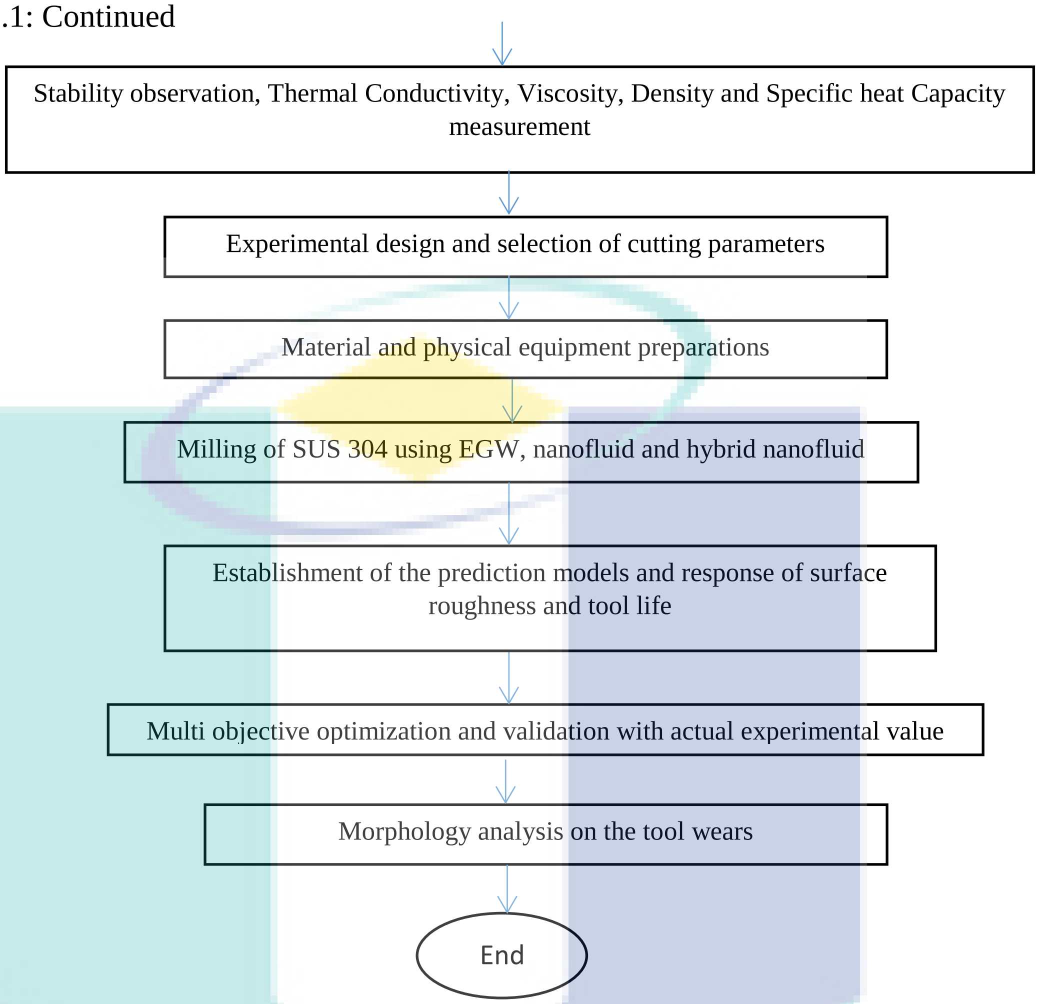

Figure 3.1: Flow chart

3.2 Nanofluid Preparation

3.2.1 Selection of Nanoparticles

Previous study reported that nanoparticles have a good convection heat transfer rate compared to its based liquid (Duangthongsuk and Wongwises, 2010) (Vajjha et al., 2010). The bonding between the pure metallic particles with oxide will tend to increase the stabilization in based liquid. Titanium oxide (TiO_2) and zinc oxide (ZnO) are among the nanoparticles which having a superlative heat transfer rate and stabilization (Zhou et al., 2010). Therefore, TiO_2 and ZnO nanoparticle was purchased from US Research Nanomaterials. Inc. These nanoparticles having a purity of 99.9 % and having an average particle size less than 50 nm. These two nanoparticles will be diluted according to the volume percentage for the further properties study. The properties study among these two nanoparticles will support to choose the preeminent nanoparticle which will selected to use as nanocoolant for the end-milling process.

3.2.2 Selection of Volume Percentage

In previous reviews, shows that the thermal conductivity of nanofluids is sensitive to the particle volume fraction and temperature and weak sensitivity to clustering size. This means that the size of nano particle have little effect on properties of nanofluid compare to volume concentration. Yu et al. (2012) (Yu & Xie, 2012) stated that the thermal conductivity is greater at higher volume concentration above 0.5 volume percentage (Yu & Xie, 2012). Two step methods used the most financial readiness of nanofluid. The TiO_2 nanofluid is prepared using dilution method at volume percentage. For the hybrid nanofluid, 50% of TiO_2 and 50% of ZnO nanoparticle ratio diluted with the based liquid. Therefore, the weight percentage, ω need to be converted to volume percentage, φ by using Eq. (3.1). The volume of based liquid (60% ethylene glycol and 40% distill water), ΔV for preferred concentration, φ_2 can be found by using Eq. (3.2) with original condition of V_1 andφ_1.

$$\varphi = \frac{\omega \rho_w}{\left(1-\frac{\omega}{100}\right)\rho_p+\frac{\omega}{100}\rho_w} \qquad \text{where } \omega = \left[\frac{m_p}{m_p+m_w}\right] \times 100 \tag{3.1}$$

$$\Delta V = (V_2 - V_1) = V_1\left(\frac{\varphi_1}{\varphi_2} - 1\right) \tag{3.2}$$

Where;

V = change of volume (ml)

V_2 = total volume (ml)

V_1 = volume needed to be add (ml)

φ_1 = actual volume concentration (vol. %)

φ_2= desired volume concentration (vol. %

Next, the calculated base liquid (60% ethylene glycol and 40% water) quantity was used to dilute the 99.9% purity of nanofluid from supplier. The diluted nanofluid and hybrid nanofluid will be mechanical stirred for 3 hour by using digital motorized stirrer with 1200 rpm to ensure the nanoparticles fully dispersed into the based liquid and immersed in ultrasonic bath for 2 hours. Figure 3.2 shows the mechanical stirring process. Figure 3.3 shows the ultrasonic bath process.

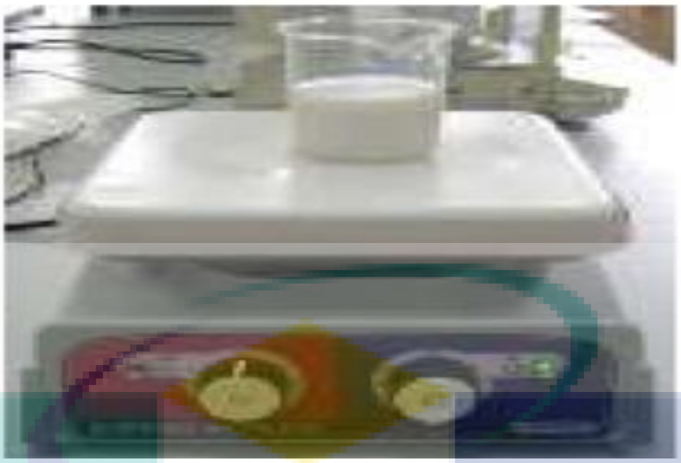

Figure 3.2: Magnetic stirring process

Figure 3.3: Ultrasonic bath process

3.3 Nanofluid properties measurement

3.3.1 Stability Evaluation

3.3.1.1 Sedimentation observation of nanofluid

Once the sonication is done, a 10ml of nanofluid will be poured into a test tube as shown in Figure 3.4 for each volume concentration for stability observation method for one month. The purpose of the stability observation method is to observe the visibility of the sedimentation processes within the nanofluid and estimating the stability of the nanofluid

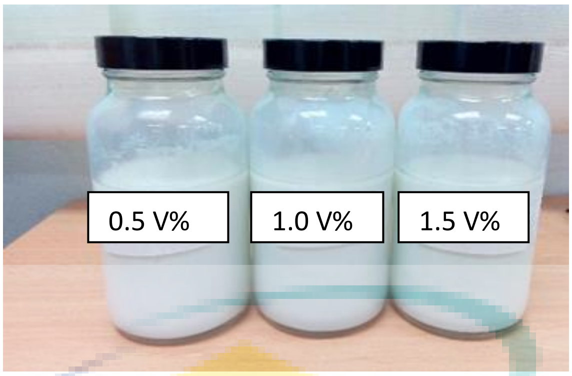

Figure 3.4: Nanofluid samples

3.3.1.2 Ultra Violet Visible Spectrometry

Besides sedimentation observation method, Ultra Violet- Visible (UV-Vis) test has been carried out in this research to prove the nanofluid stability quantitatively. In this test, the nanofluid samples will be poured in cuvette and absorbance drop will be measured for one month. As for first step, Shimadzu UV-2600 Spectrophotometry is used to find peak wavelength of nanofluid to be used for absorbance value determination as shown in Figure 3.5, used the same method to determine stability of nanocellulose based nanofluid. Once peak wavelength is obtained, it is used to determine the absorbance value drop for the lowest and highest volume concentration of nanofluid for nearly one month.

Figure 3.5: Shimadzu UV-2600 spectrometer

3.3.2 Thermal Conductivity Measurement of Nanofluid

Thermal conductivity of the nanofluid is the important factor in this study. The thermal conductivity of the nanofluid is measured with thermal property analyzer which uses the transient line heat source to detect the thermal properties of the liquid. The thermal analyzer model is KD2 Pro as shown in Figure 3.6. The range of the measurement for this equipment is 0.2 W/m.K to 2.0 W/m.K. KS-1 sensors is used to measure the thermal conductivity of liquids. The measurement of thermal conductivity is validated by measure the thermal conductivity of distill water and glycerin. At room temperatures the thermal conductivity of distill water and glycerin was 0.610 and 0.280 W/m.K, respectively. This result is agreed with the literature which thermal conductivity of distill water and glycerin is 0.613 W/m.K and 0.285 W/m.K, respectively, within ± 5% accuracy.

The measurement was conducted under controlled temperatures ranging from 30 ºC to 70 ºC. The measurement of the thermal conductivity will recorded at 1 sec interval for 90 sec total 90 sec cycle. After the 90 sec cycle, the thermal conductivity value will calculated by the controller. The value of the thermal conductivity was validated by theatrical equation. As stated by Sharma et al. (2012) (Sharma, Sarma, Azmi, Mamat, & Kadirgama, 2012), regression equation to predict the thermal conductivity has deviation of less than 11%. The thermal conductivity measurement also is validated compare the value obtained with the predetermined values from American Society of Heating, Refrigerating and Air- Conditioning Engineers (ASHRAE).

$$K_{nf} = K_w \left[0.8938\left(1+\frac{\varphi}{100}\right)^{1.37}\left(1+\frac{T_{nf}}{70}\right)^{0.277}\left(1+\frac{d_p}{150}\right)^{-0.0336}\left(\frac{\alpha_p}{\alpha_w}\right)^{0.01737}\right] \quad (3.3)$$

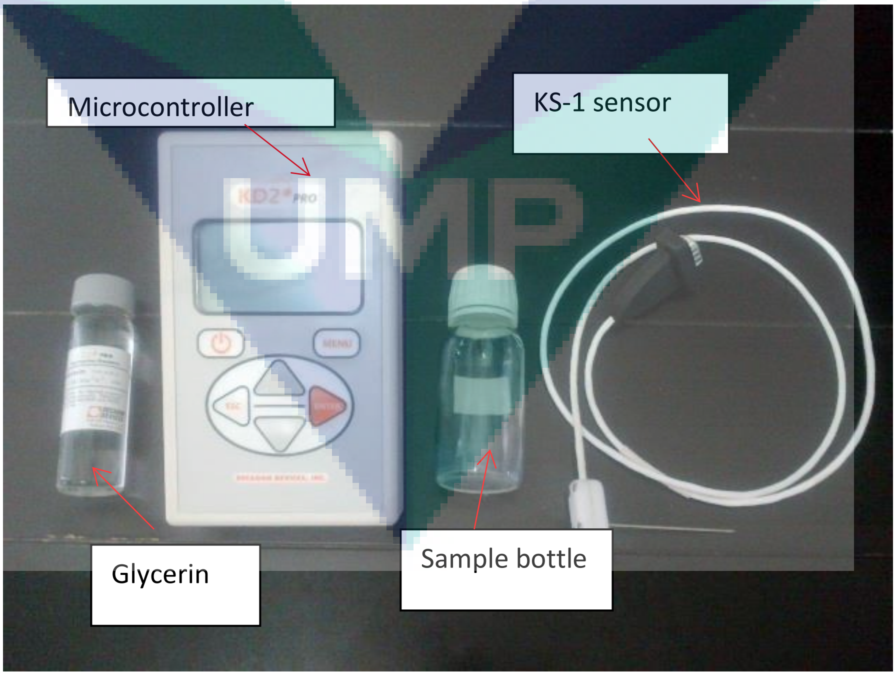

Figure 3.6: KD2 Pro used to measure the thermal conductivity of nanofluid

3.3.3 Viscosity Measurement of Nanofluid

Before measuring the viscosity of nanofluid, the viscometer is validated with measurement of distill water at room temperature. The measured viscosity of nanofluid is validated by using Eq. (3.4). As detailed by Sharma et al. (2012) (Sharma et al., 2012), the regression equation can be used to predict the viscosity of nanofluid.

The average deviation, standard deviation and maximum deviation for this equation is 3.18%, 3.8% and 13% receptively when compared with experimental data. The viscosity measurement also is validated compare the value obtained with the predetermined values from American Society of Heating, Refrigerating and Air-Conditioning Engineers (ASHRAE). With a good agreement between actual measurement and the predetermined values, the measurements were conducted for nanofluids.

$$\frac{\mu_{nf}}{\mu_w} = C_1\left[\left(1+\frac{\varphi}{100}\right)^{11.3}\left(1+\frac{T_{nf}}{70}\right)^{-0.038}\left(1+\frac{d_p}{170}\right)^{-0.061}\right] \tag{3.4}$$

The method of measurement starts by preparing a 16ml of nanofluid. The 16 ml of sample will be added into the UL (ultra-low) adapter and attached with the cylinder water jacket. The ULA spindle will be inserted into the jacket. Next, the jacket will be screwed to the rheometer. The water bath was switched on, and the temperature will be set at a specified temperature. The water bath helps to maintain the temperature of the sample in the range of 30 ºC–70 ºC.

The temperature of the nanofluids will be measured using the thermocouple connected with the rheometer. The nanofluids will be heated up about 5 min to reach a stable temperature. The measurements will be recorded using the Rheocalc software which is installed in the computer. The measurements will be repeated for about five times to obtain an average value to prevent errors. For this research, the experiment will be conducted at the nanofluid temperature of 30 ºC, 50 ºC and 70 ºC for each volume concentration. Figure 3.6 shows viscosity measurement equipment.

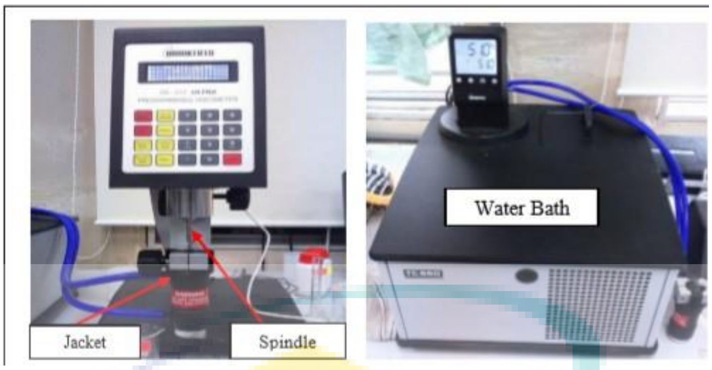

Figure 3.7: Viscosity measurement equipment

3.3.4 Specific heat capacity measurement

Specific Heat Capacity is measured by using Differential Scanning Calorimetry (DSC) by using Perkin Elmer model name DSC-8000 as shown in Figure 3.8. This equipment is very suitable to provide fusion heat and endothermic peak's property under various heat rates. Besides, DSC-800 has capability to provide real time analysis for heat flux by considering weight loss. It also has temperature accuracy of 0.0001mg and 0.01 ºC which able to provide very accurate data.

The specific heat capacity is measured by heating sample from 30 ºC to 80 ºC at rate of 10 ºC/minute under purged Nitrogen (N2) gas. The equipment validation is performed by using benzophenone and caffeine for better reading accuracy. Meanwhile, indium was used for heat flow calibration. Meanwhile, Zhou & Ni, (2008) used the same method to measure specific heat capacity and the results from the equipment are promising.

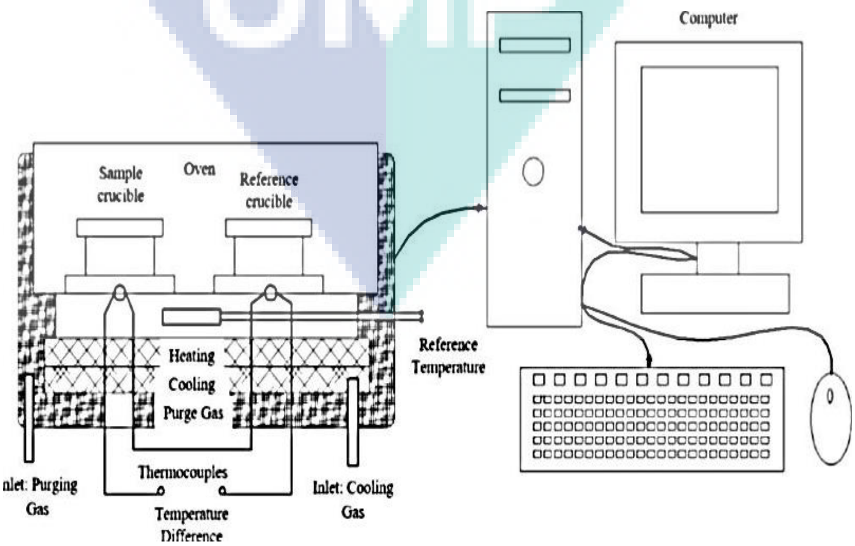

Figure 3.8: Differential scanning calorimetry

3.4 Experimental Design and Selection of Cutting Parameters

Based on the literature review, the process of discover a proper combination of cutting parameter is very high cost and time consuming. The results from preliminary test with different combination of cutting parameter which consist of cutting speed, feed rate, and depth of cut, it is decided to use design of experiment (DOE) to find the optimum range of cutting parameter of the cutting tool selected. Besides that, response surface method (RSM) is used to found the optimum cutting parameter for SUS 304 stainless steel.

3.4.1 Selection of response surface method

Response surface method (RSM) is used to design the experiment. The combination of factor which consists of cutting parameter has been generated by using RSM. Besides that RSM can generate the optimal parameter value based on the mathematical and statistical technique. The benefit of RSM as follow:

a. Clearly shows the relation between the factor and response in term of mathematical and statistical.
b. Find factor settings in which process specifications are satisfied.
c. Find factor settings that optimize the process response.
d. Identify new operating conditions that produce demonstrated quality improvement over the quality achieved by current condition.

Figure 3.9 shows the example of BBD for three different variables where X_1 = cutting speed, X_2 = feed rate and X_3 = axial depth of cut.

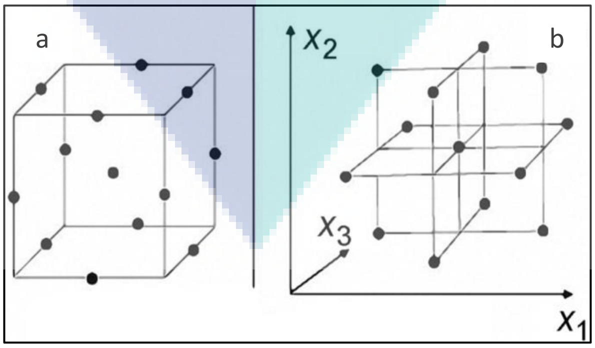

Figure 3.9: Example of BBD for three different variable

Source: Dureja, Gupta, Sharma, and Dogra (2009)

There are two type of DOE's which is central composite design (CCD) and box-behnken design (BBD). Throughout this study, BBD was chosen as the design of experiment. BBD produce a quadratic relationship between the experimental factor and response. The key reason for choosing BBD is to estimate the response in term of first-order and second-order. Besides that, BBD is much cheaper in term of cost compared to CCD.

3.4.2 Cutting Speed

The term of cutting speed is referring to the linear speed on the cutting zone. The measured unit for this speed is rpm. As stated before, three level of cutting speed is selected which is high, medium and low. However, the selected range of the cutting speed is based on the cutting tool supplier Catalog 8010, Kennametal to estimate the flank wear criteria for SUS 304 stainless steel. The three level of cutting speed are as follow:

a. 1500 rpm
b. 2000 rpm
c. 2500 rpm

3.4.3 Feed Rate

Tool feed rate is defined as the relative motion of the cutting tool during the cutting process. The feed rate is measured in millimeter per tooth (mm/tooth). Three level of feed rate is selected which is low, medium and high. The rate of the feed rate is in between the feeds suggested by the Catalog 8010, Kennametal. The three level of feed rate are as follow:

a. 0.02 mm/tooth
b. 0.03 mm/tooth
c. 0.04 mm/tooth

3.4.4 Axial Depth of Cut

The axial depth of cut is the distance of the tool along its axis in the workpiece as it makes a cut. The axial depth of cut in this study is focused on this finishing end-mill process. Previous study stated that finish cut for milling process is below than 0.4 mm of cut. Above this axial depth the roughness is considered ruthless and never considered as finishing process for austenite stainless steel (Zhou et al., 2015). Besides that, since austenite stainless steel is considered very hard material with hardness around Rockwell B 70 it is suggested to use low axial depth of cut during milling to avoid huge wear on cutting tool. Therefore three axial depth of cut which is selected for this study are as below:

a. 0.1 mm
b. 0.2 mm
c. 0.3 mm

3.4.5 Design of experiment

There are three type of experiment design has been created to conduct the end-milling process on SUS 304 stainless steel. The first set of experiment design was created for end-milling process by using ethylene glycol water based soluble coolant and the second set of experiment coolant was created for end-milling process by using ethylene glycol based TiO_2 nanocoolant and the third experiment using ethylene glycol based TiO_2/ZnO nanocoolant . However, the milling parameter used for each set of experiment set is similar as shown in Table 3.1. The range of cutting speed value was selected of 1500 rpm and 2500 rpm. The range of feed rate value was selected between 0.02 mm/tooth to 0.04 mm/tooth and the range of axial depth of cut value was selected between 0.1 mm to 0.3 mm.

Table 3.1: The value selected for each parameter

Parameter/ Coding level	**-1**	**0**	**+1**
Cutting speed (rpm)	1500	2000	2500
Feed rate (mm/tooth)	0.02	0.03	0.04
Axial depth (mm)	0.1	0.2	0.3

Source: Catalog 8010, Kennametal

The first set of end-mill experiment was conducted with water soluble coolant. Therefore the concentration of the coolant was not count for this experiment. By using Minitab 15, the experiment design was created with aid of Box-behnken design. The total end-milling test for this experiment was 15 with varying cutting speed, feed rate and axial depth of cut. Table 3.2 show the selected value for each parameter.

Table 3.2: DOE table for the experimental

Experiment	Cutting Speed, rpm	Feed Rate, mm/tooth	Depth of Cut, mm
1	2000	0.03	0.2
2	2500	0.03	0.3
3	2000	0.02	0.1
4	2500	0.04	0.3
5	2000	0.03	0.1
6	2000	0.02	0.3
7	2500	0.03	0.2
8	1500	0.04	0.3
9	2000	0.03	0.3
10	1500	0.02	0.1
11	2500	0.02	0.1
12	1500	0.03	0.2
13	1500	0.03	0.3
14	2000	0.04	0.3
15	2000	0.04	0.1

3.5 Material and physical equipments

3.5.1 Cutting Tool Material

The milling insert are made by Ceratizit on the basis of the ISO catalogue number of XDKT 11T308SR-F50. This milling insert is a coated carbide grade with TiN coating CVD. TiN is considered as very ductile because it's relatively very hard. The thickness TiN used for coating is 1 mm. TiN coating will increases the wear resistant and reduces the friction during machining process. This coating will form a metallurgical bond the cutting tool that will not peel easily during the machining process.

The shape of the insert used in this study is X-shaped insert which is slotted into a 32 mm diameter tool holder. This insert is specified to use under flooded machining.

Throughout this study, only one insert per experiment mounted to the tool holder to perform the milling experiment. The cutting tool implement in this experiment are shown in Figure 3.10. The specification of the insert shown in figure 3.11 where where d = 4.9 mm, l_1 = 1.2 mm, l = 7.8 mm, $\alpha = 15^o$, d_1 = 2.5 mm and s = 3.18 mm. Before the experiment, each cutting insert was observed for any defects. Then, the cutting tool will be screw together with the holder. Only one side on the holder will be attached with the insert to in order to study the performance of the cutting tool.

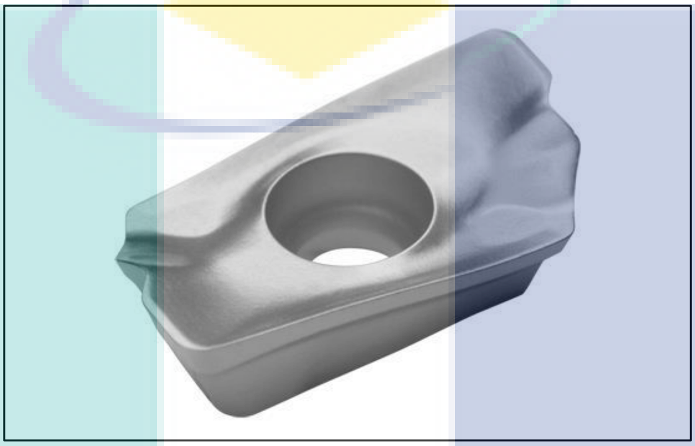

Figure 3.10: Cutting tool used in these experiment

Source: Dureja et al. (2009)

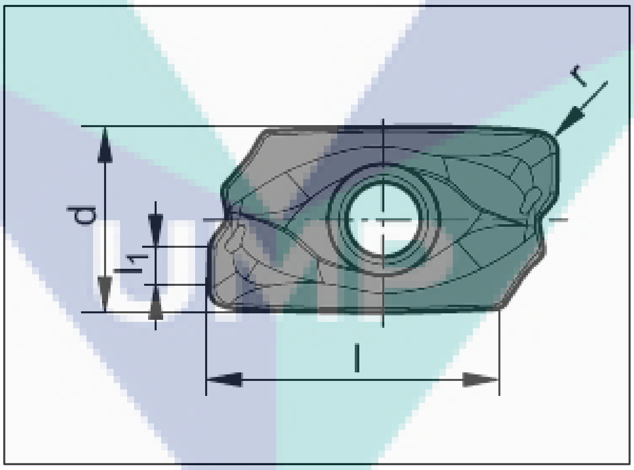

Figure 3.11: Geometry of the insert

Source: Dureja et al. (2009)

3.5.2 Workpiece Material

SUS 304 stainless steel block were used for the experiment as shown in Figure 3.12. The size of the block is 180×100×25 mm. The hardness of this block is around Rockwell B 70. The chemical and physical properties of the workpiece material are shown in Table 3.3 and Table 3.4. The SUS 304 stainless steel block were cleaned up with sandpaper 240 grit to removes the dust or any undesirable dust particle on surface of the workpiece. Then, the top layer of the workpiece was removed by face milling to make sure the surface of the workpiece is stable.

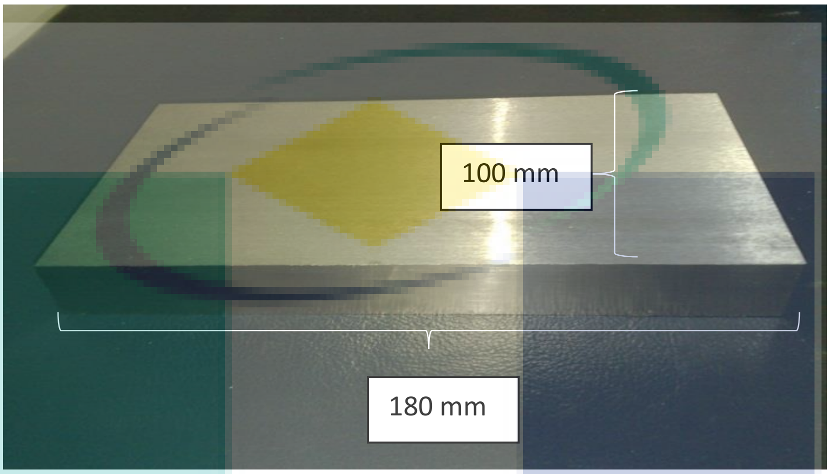

Figure 3.12: Workpiece material

Table 3.3: Chemical composition of workpiece material

Element	C	Si	Mn	Cr	Mo	P	S	Ni
Wt %	0.02	0.32	1.31	16.4	2.03	0.30	0.20	12.17

Table 3.4: Physical properties of workpiece material

Properties	**Value**
Density (kg/m^3)	8000
Elastic Modulus (GPa)	193
Mean Coefficient of Thermal Expansion (µm/m/^{o}C)	17.8
Thermal Conductivity at 100^{o}C	16.2
Thermal Conductivity at 500^{o}C	21.5
Specific Heat (J/kg.K)	500

3.5.3 CNC Machining Center

The machine center is driven by a 7.5 kW electrical motor which provides high torque. A vertical machine center OKUMA MX45-VA was used for all operations that preparing the workpiece or cutoff were required. This was a rigid and high precision machine that was suitable for milling as shown Figure 3.13. Specification of machine is shown in Table 3.5. Before run the milling experiment, the machine need to prepared. The table of the machined need to be clean up by using cloth to ensure there is no chip which will distract the stability of the workpiece. Then, place the vise on the table and put the t-slot nuts and bolts in position but it need to be loose. Before tighten up the nuts, the vise need to be square to make sure the workpiece clamped according to the dimension.

Figure 3.13: The Okuma CNC machine used in the present work.

Table 3.5: Specification of the Okuma CNC machining center MX-45 VA:

Control	OSP-U100M
X- axis	41.34"
Y- axis	20.08"
Z- axis	22.05"
Table surface to spindle nose	7.87" to 29.92"
Column to spindle center	22.05"
Table working surface	51.18" x 20.08"
Table load capacity	2,200 lbs
Spindle speed range	10 to 7,000 RPM
Spindle taper	cat no. 50
Rapid traverse	591 IPM for X-Y, 512 IPM for Z
Cutting feed	01 to 160 IPM
Tool storage capacity	20 Tools
Max tool diameter with adjacent tools	5.31"
Max tool diameter without adjacent tools	11.81"
Max tool length	15.75"
Max tool weight	44 lbs
Spindle drive	7.5 HP

First, the workpiece block were clamped on the vise which on the table on the machine. CNC programming was used to cut along the surface of the workpiece which is considered 1 pass. The program was stop after 180 mm of cut which is considered 1 pass to measure the flank wear and the surface roughness on the workpiece. After each pass of cut, the workpiece surface will flat by using face milling before proceed with the next pass. Once all the 15 experiments run out for ethylene glycol, the coolant replaced to single nanofluid and 15 experiments will run. Then the single nanofluid will replaced to hybrid nanofluid for another 15 experiments.

The end-milling process was carried out by using the CNC machine with ethylene glycol, ethylene glycol based TiO_2 nanofluid and ethylene glycol based TiO_2/ZnO separately. Only one edge of the cutting tool was used for the testing in order to study the performance of the cutting tool. After each pass of end-milling process, the insert is removed the tool holder in order to measure the tool wear and surface roughness accordingly. Each pass of cutting is 180 mm. The surface roughness, flank wears and tool wear is measured after each pass of end-milling process. The machining process and the measured of the flack wear will repeated until the flack wear reach the ISO wear criteria which is 0.3 mm. The wear growth on the cutting tool will be measured and recorded. Along with this, the surface roughness also been measured by using Pethometer S2 as describe in section 3.5.5. The progressive of the surface roughness will be measured and recorded until the wear reaches the ISO wear criteria.

3.5.4 Scanning Electron Microscope

Scanning electron microscope (SEM) model Zeiss EVO 50 is equipped with EDX X-ray was used for measuring the tool wear and to determine all the defects on the cutting tool after end-milling test. The composition and the chemical properties of the workpiece and cutting tool are tested by using the SEM with contribute an important detail for this research. Figure 3.14 shows the SEM that was used in this present study. The specification of the SEM is as follow:

a. The range of the acceleration voltage is from 0.2 to 30 kV.
b. Magnification range is from 5 to 1,000,000 times.
c. Resolution up to 3072×2304 pixel.
d. X-ray analysis is 8.5 mm AWD and 35° take off angle.

The measurement of the flank wear is done parallel together with surface roughness measurement. The flank wear measurement is the width from the original cutting edge to the limit of wear land. The measurement of flank wear is measured after each pass of end-mill process. As recommended by ISO 8688-2-1989 (E) the wear criteria for end-milling steel are 0.3 mm. The measured flank wear is recorded after each pass until the wear reaches the wear criteria. After recording the flank wear, the insert will tighten up again with tool holder to continue with next pass.

The measurement of tool life is measured by the total time taken of cuts by the milling inserts to reach the maximum flack wear criteria which is 0.3 mm. ISO 8688-2:1989 (E) stated that a recommended uniform wear criteria is 0.3 mm and the maximum wear criteria is 0.5 mm when end-mill austenite stainless steel (ISO 8688-2:1989 End mill testing. However, there is no specific ISO standard for end-mill SUS 304 stainless steel by using CVD TiN coated carbide inserts. The end-milling test will be conducted until anyone of the below criteria is achieved:

1. Flank wear reached 0.3 mm
2. Maximum wear criteria reached 0.5 mm
3. Major fracture or catastrophic failure

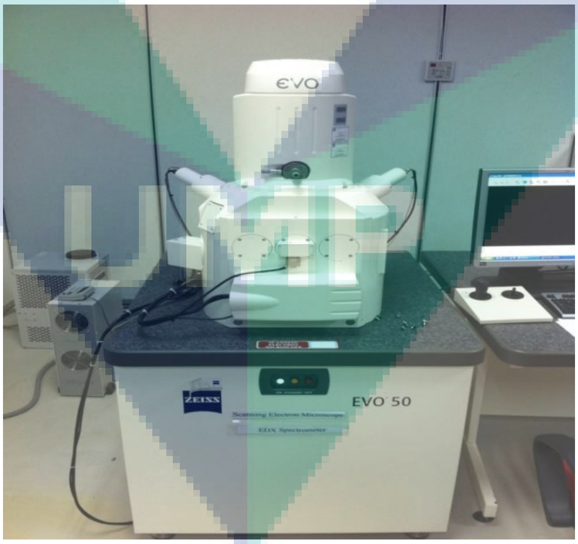

Figure 3.14: Scanning Electron Microscope (SEM) model Zeiss EVO 50

3.5.5 Surface Roughness Tester

A low weigh portable surface roughness tester model Mahr Pethometer S2 as shown in Figure 3.15 is used to measure the surface roughness of the workpiece after the machining done. The arithmetic average surface roughness (R_a) mean roughness depth (R_z) was measured by using this instrument. Table 3.6 shows the specification of Pethometer S2.

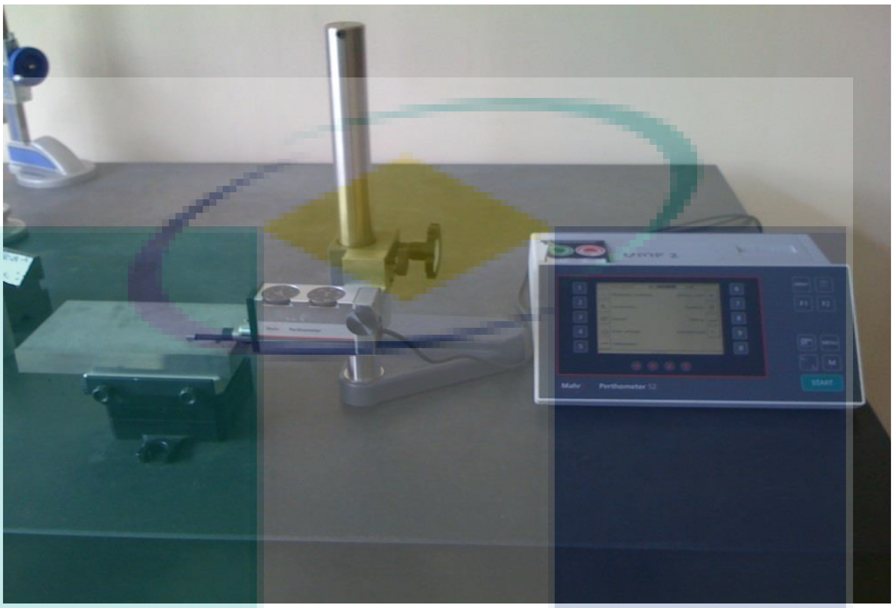

Figure 3.15: Pethometer S3

Surface roughness values were measured by using Pethometer S2. A total of 3 measured were taken to determine the average surface roughness of the end-mill surface. The surface roughness readings were taken in the center and both edge of the end-mill surface as shown in Figure 3.16. The 3 reading which is Ra_1, Ra2 and Ra_3 to determine the average surface roughness.

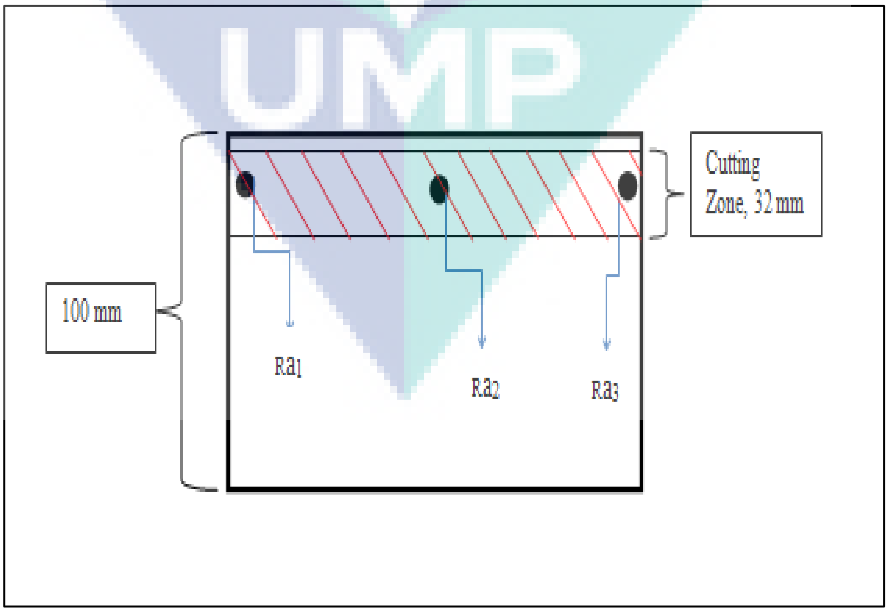

Figure 3.16: Surface roughness reading point on the milling zone

Table 3.6: Specification of Pethometer S2

Specification	Detail
Roughness parameter	Ra, Rq; Rz, Rt, Rp, Rv, RSm, Rdq
Standard	DIN EN IOS/JIS/ASME 46.B
Measurement	by means of a stylus instrument
Tracing length	1/2/4/8/12/16 mm
Software	S2Prog Windows program
Unit	Mm or inch (selectable)
Display	graphics LCD module with
Dimension	approx. 150 × 320 × 250 mm

3.5.6 Transmission Electron Microscope

Transmission electron microscope (TEM) model Philips CM-200 as shown Figure 3.17 was used to determine the size of nano particle and the agglomeration of nano particle in the based liquid with is ethylene glycol. It is equipped with a light element EDS X-ray detector and can detect the sample areas at the 10 to 20 nm scale. It is also capable of 0.27 nm resolution and has wide gap pole-piece to allow large tilt angles of specimen. The specification of the TEM as follow:

a. The acceleration is 200 kV with LaB6 cathode
b. It has 2.7 A resolution (twin lens) with about 70° sample tilt.
c. It has double-tilt, heating and cyro stages for specialized experiments
d. A fine probe and Convergent Beam Electron Diffraction (CBED)

Figure 3.17: Transmission electron microscope (TEM) model Philip CM 200

The TEM grid size is 3.05 mm diameter ring with thickness of 100 µm. the grid material is made of copper. The sample is placed into the inner diameter of the ring which is about 2.5 mm. First, the forceps are cleaned with 99.9% ethanol to remove any unwanted particle stick on the forceps which will distract the result. Forceps is used to grasp the carbon grid ring. Next, one drop of nanofluid sample solution dropped on the grid. Then, the drop will be dried with normal air for 15 min.

3.6 Modelling and Multi objective optimization

Linear equation generated using statistical method. Machining response optimized with three properties so that it will indicate the optimum parameters (Cutting speed, federate and axial depth of cut) for surface roughness and tool life using statistical method (minitab). The optimize criteria was selected as maximum tool life and minimum surface roughness. The value acquired for high desirability later compared with the actual experiment value for the selected parameters by the statistical method.

CHAPTER 4

RESULT AND DISCUSSION

4.1 Introduction

The main purpose of this chapter is to discuss the milling responses (surface roughness, tool life and tool wear) when the milling process is conducted with various cutting conditions and coolants (EGW, ethylene glycol based TiO_2 and TiO_2/ZnO nanofluid). The thermal properties of the TiO_2 and TiO_2/ZnO nanofluids were analyzed and evaluated in order to select the best nanofluid to use as a milling coolant. Mathematical models have been developed by using response surface method to find the connection between the variables and responses. The optimum cutting condition has been developed and analyzed by using surface optimizer. The kind of the wear and wear mechanisms, additionally been talked about in this part. The experimental result has been validated from previous research to support the results. Optimization of the tool life and surface roughness predicted using statistical method. The parameter suggested from statistical method used and the actual value compared with the statistical method value.

4.2 Characterizing of Nanofluids

4.2.1 Evaluation of Nanofluids

The prepared $TiO_{2,}$ TiO_2/ZnO nanofluids assessed and were characterized based on the criteria of pH value, nanoparticle size and the sedimentation time. Different concentrations were set up for the nanofluids which are 0.5 vol%, 1.0 vol% and 1.5 vol%. Table 4.1 shows the pH value and average size of each nanofluid. Figure 4.1 and Figure 4.2 shows the micrographic picture of TEM for TiO_2 and TiO_2/ZnO nanofluids. The average nanoparticle size and the agglomeration of the TiO_2 and TiO_2/ZnO nanoparticle in the based liquid can be observed through Figure 4.1 and Figure 4.2. The average size of the TiO_2 nanoparticle is about 30 to 50 nm while the average size of TiO_2 and ZnO nanoparticle is around 30 to 35 nm. The agglomeration prompts a higher sedimentation time for TiO_2/ZnO nanofluid which is over a month, while TiO_2 nanofluid sedimentation noticeable after a month.

The strong stability of TiO_2/ZnO nanofluid can be related with the particle agglomeration size. As per Philip, Shima, and Raj (2008) agglomeration happen amid the arrangement of nanofluid because of high surface contact between the particles. This particles form a strong van der Waals force which was very hard to break it into primary nanoparticle. Then again, Murshed et al. (2005). expressed that the surfactants will ensure the molecule completely scattered in the base fluid by electrostatic repulsive force among the nanoparticle and hydrobic surface force due to physical adsorption of surfactant in the liquid. TiO_2/ZnO nanofluid showed a steady suspension and able to sustain more than one month which prepared with mechanical stirring process without surfactants and sonication process. The stability of nanofluid is vital for consistent improvement in heat transfer and anticipates fouling in the coolant tank.

Table 4.1: Characteristic of nanofluid

Nanoparticle type	pH value	Average size (nm)
TiO_2	8.2-8.5	35-50
ZnO	9.3	< 40
TiO_2/ ZnO	8.6	-

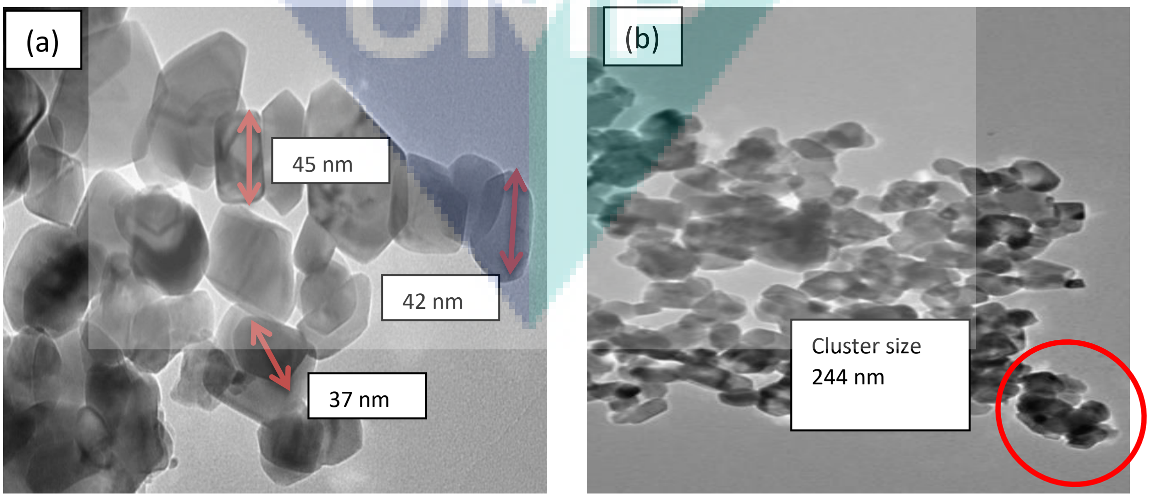

Figure 4.1: TEM micrographic image for TiO_2 nanofluid, magnification: (a)100 nm, (b) 200 nm

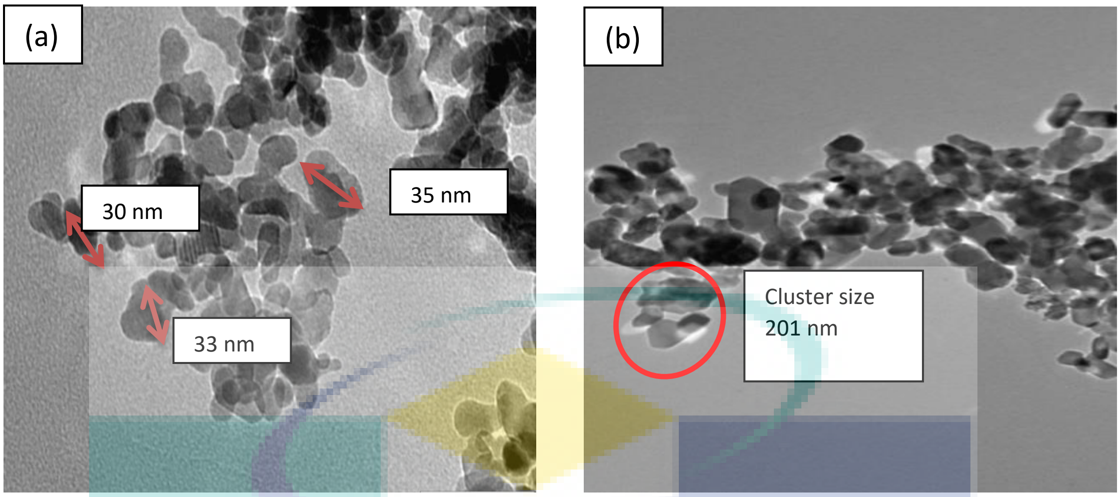

Figure 4.2: TEM micrographic image for TiO_2/ZnO nanofluid, magnification: (a)100 nm, (b) 200 nm

4.2.2 Sedimentation Observation

Figure 4.3a shows the sample preparation of TiO_2 while Figure 4.3b shows the sample preparation of TiO_2/ZnO. Sundar et al. (2012), observed that their Fe_3O_4 nanoparticles dispersed in a water-ethylene glycol mixture is stable up to one month. After more than one month of observation, the nanofluid displayed small amount of sedimentation for all base fluid due to gravitational forces (Sundar et al., 2013).

The samples of preparation of TiO_2 and TiO_2/ZnO were analysed after one month to observe the sedimentation. Figure 4.3c shows the sedimentation for TiO_2 nanofluid, and Figure 4.3d shows the sedimentation for TiO_2/ZnO nanofluid. Sedimentation were found in both the examples, yet the sedimentation is discovered lesser in TiO_2/ZnO nanofluid than TiO_2 nanofluid. This phenomenon occurs due to stronger van der Waals interaction in in TiO_2/ZnO nanofluid than TiO_2 nanofluid. Sarafraz, Hormozi, and Kamalgharibi (2014) likewise specified in their paper that sedimentation of nanofluids happen because of the very strong van der Waals interaction. With the sedimentation method the stability of nanofluid can be investigated and also the concentration of supernatant will be the deciding factor to determine whether the nanofluid is stable or not. Henceforth, it can be concluded that the TiO_2/ZnO nanofluid is more stable than TiO_2 nanofluid.

Some of the challenges faced by suspended particles are such as agglomeration and rapid settling of particles in fluid (Hadadian, Samiee, Ahmadzadeh, & Goharshadi, 2013). The importance of high durability and better stability of suspensions are related with enhancement of heat transfer. The preparation of nanofluids for this research used the sonication process as a control measure of nanofluid stability. Duangthongsuk and Wongwises (2008) appeared in their paper that a longer sonication process time could create more steady nanoparticles without agglomeration, the test solution in different volume concentration and same volume ratio of base fluid (EG :W) after preparation and observation for one month. Although no surfactant was used during the preparation of the nanofluids, the solution is in stable condition with minimum sedimentation observed for up to one month. It was observed to be stable during the thermos-physical properties study and the force convection experiment. Similar findings were also found by Duangthongsuk and Wongwises (2008). They found that the ultrasonic process prolongs the nanofluids stability up to three months. Maheshwary and Nemade (2015), conducted deeper investigations on the effect of using the sonication process to ZrO_2/ H_2O.Astounding, the nanofluid showed positive enhancement of thermal conductivity reflects that went through the sonication process are appropriate for cooling application.

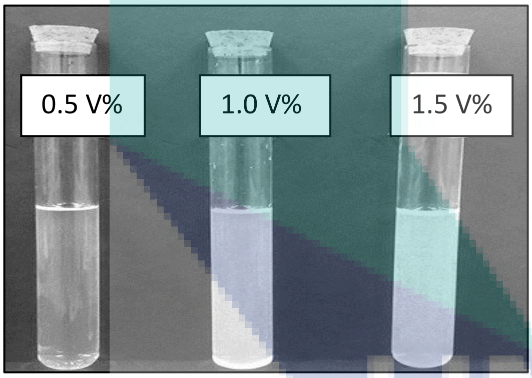

Figure 4.3a: Sample preparation TiO_2

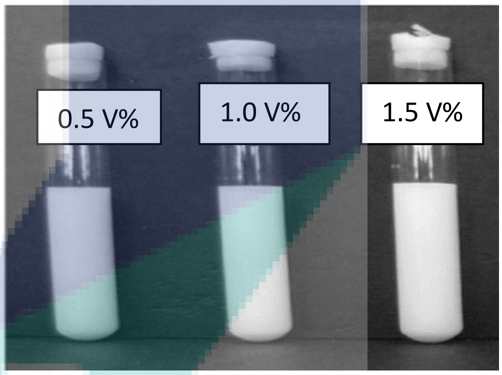

Figure 4.3b: Sample preparation TiO_2/ZnO

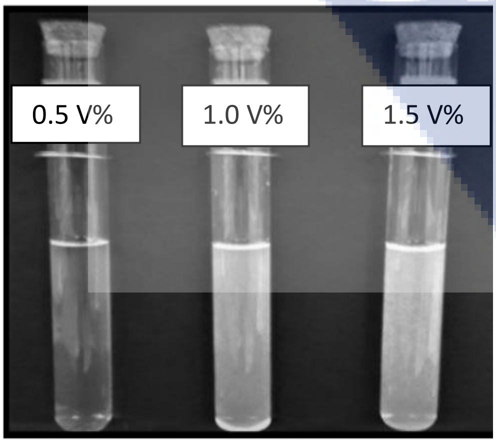

Figure 4.3c: After 1 month TiO_2

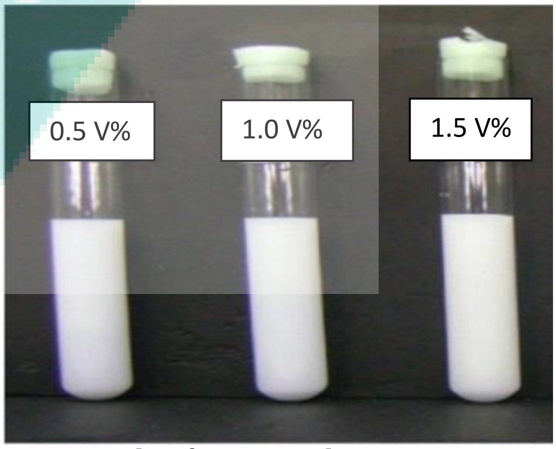

Figure 4.3d: After 1 month TiO_2/ZnO

4.2.3 UV-VIS Spectrophotometer Evaluation

Absorbance drop evaluation is another stability validation method used to prove stable of nanofluid scientifically. Foremost, peak absorbance wave length need to be determined for all the volume concentration and the outcomes are as appeared in Figure 4.4. From the diagram, it is noticed that the peak absorbance for entire volume concentration occurs at wavelength of 288 nm for TiO_2 in the interim for TiO_2/ZnO occurs at wavelength 250 nm. In this manner, this peak wavelength value is used in Shimadzu UV-2600 Spectrophotometry to measure absorbance drop for one month. The absorbance drop evaluation is estimated for the lowest volume concentration (0.5%) and highest volume concentration (1.5%) as delineates in Figure 4.5 and Figure 4.6 respectively.

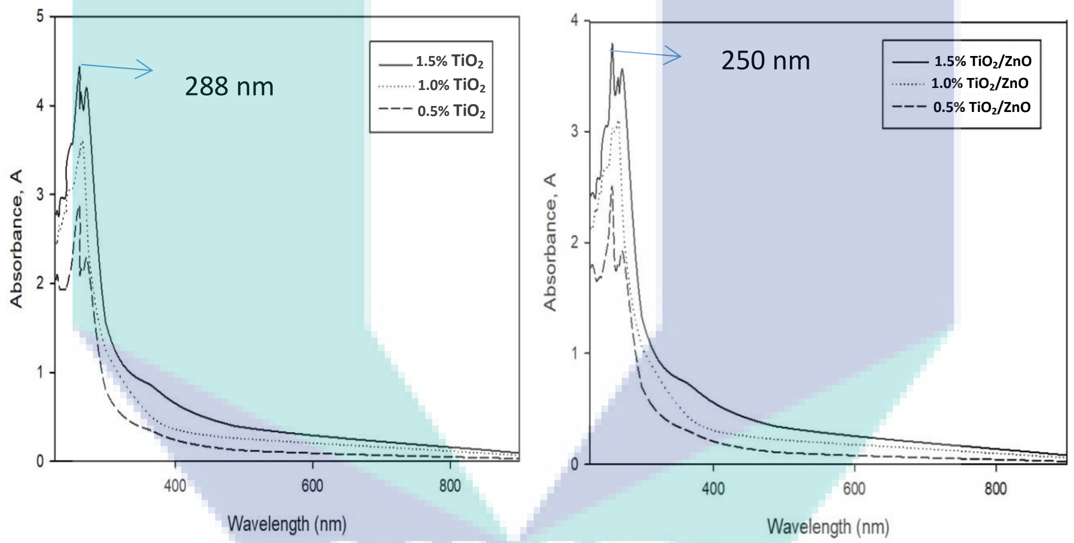

Figure 4.4: Peak absorbance value for all the volume concentration of TiO_2 and TiO_2/ZnO

Graph in Figure 4.5 shows absorbance drop for 0.5% volume concentration of TiO_2 and TiO_2/ZnO. The deliberate absorbance drop after one month is 7.62% for TiO_2/ZnO and 6% for TiO_2. According to F. Sharif, Arjmand, Moud, Sundararaj, and Roberts (2017) the absorbance drop more than 30% after a month demonstrate that nanofluid is instable. Thus, dispersion of nanocellulose in EGW produces a highly stable nanofluid. Meanwhile, absorbance drop for 1.5% volume concentration as illustrates in Figure 4.6. It achieves absorbance drop of 3% for TiO_2/ZnO and 2% for TiO_2 after one month of evaluation. Subsequently, TiO_2/ZnO nanofluid with lowest volume concentration records the highest absorbance drop contrasted to highest

TiO_2/ZnO nanofluid volume concentration (Mehrali et al., 2014). This best clarification for this phenomenon is known as effect of adjacent particle. Once colloidal suspension is achieved, base fluid creates an upward stream which pushes the nanoparticle and prevents it from falling due to gravity acceleration. Accordingly, the upward stream impact is greater in high concentration nanofluid compared to low concentration nanofluid which reduces absorbance drop in the colloidal suspension (Richardson & Zaki, 1954).

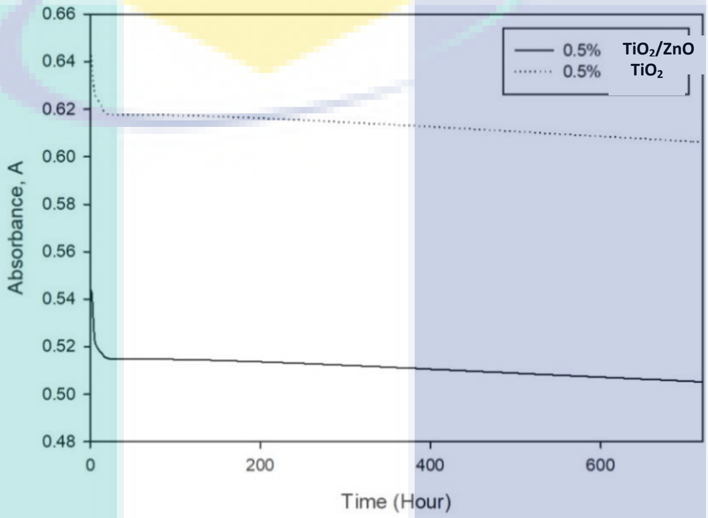

Figure 4.5: Absorbance drop for volume concentration 0.5% of TiO_2 and TiO_2/ZnO after one month of nanofluid preparation

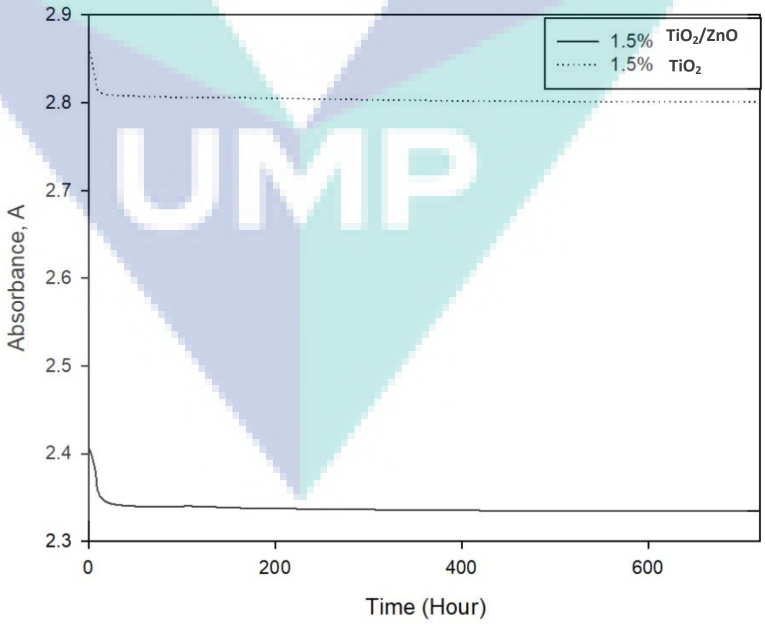

Figure 4.6: Absorbance drop for volume concentration 1.5% for TiO_2 and TiO_2/ZnO after one month of nanofluid preparation

4.2.4 Thermal Conductivity of Nanofluid

Figure 4.7 shows the thermal conductivity of TiO_2 nanofluid and TiO_2/ZnO nanofluid in volume concentration (0.5 vol %, 1.0 vol % and 1.5 vol %) measured at the range of 10 ºC to 60 ºC. The experimental result of thermal conductivity was validated with Eq. (3.3). Figure 4.7 shows that the thermal conductivity TiO_2/ZnO and TiO_2 nanofluids increased with an increase in temperature. This is a direct result of the TiO_2/ZnO and TiO_2 nanoparticles are rapidly mobilized at high temperature. The most astounding thermal conductivity of all the volume concentration of TiO_2/ZnO and TiO_2 nanofluid is obtained at 60 ºC in the interim, the least thermal conductivity acquires at 10 ºC. The result shows that, the thermal conductivity of the TiO_2/ZnO nanofluid is greatly improved than TiO_2 nanofluid as far as all the volume concentration (0.5 vol %, 1.0 vol % and 1.5 vol %). This is because of the stochastic motion of TiO_2/ZnO nanoparticles are higher than TiO_2 nanoparticles. S. K. Das et al. (2006) likewise specified that the stochastic motion of nanoparticles is the explanation of thermal conductivity enhancement at high temperature.

Madhesh and Kalaiselvam (2014) used hybrid nanofluid (Cu- TiO_2/Water) as coolant in their experimentation where they found the nanofluid improved the thermal conductivity and increasing temperature of fluid. K. Madhesh et al. stated that thermal conductivity of 0.69 W/m.K achieved at maximum concentration of 1% and temperature of 353. Additionally they also stated that the thermal conductivity of (Cu-TiO_2/Water) hybrid nanofluid in counter flow heat exchanger as capacity of temperature and volume concentration. The thermal conductivity of (ZnO-TiO_2/EG) hybrid nanofluid can be anticipated by utilizing correlation of Esfe et al. (2014).

Epifani, Giannini, Tapfer, and Vasanelli (2000) additionally proposed a condition for expectation of effective thermal conductivity of (TiO_2-SiO_2/EG and water) hybrid nanofluid having settled centralization of nanoparticles at 1%, while volume proportions of TiO_2 and SiO_2 nanoparticles were fluctuated in the way 20:80, 40:60, 50:50, 60:40 and 80:20. Most and least improvement in thermal conductivity was accomplished for volume proportion of 20:80 and 50:50 separately. Hussein, Bakar, Kadirgama, and Sharma (2013) found that expansion of TiO_2-SiO_2 nanoparticles prompted increase in thermal conductivity of base liquid and proposed relationship for forecast of thermal conductivity. Greatest improvement in thermal conductivity acquired was 22.8%. The thermal conductivity was most extreme at highest concentration and temperature.

Impact on thermal conductivity of (Cu-TiO_2/EG and water) hybrid nanofluid by pH (Iranidokht, Hamian, Mohammadi, & Shafii, 2013), weight concentration and sonication time were been studied by Hussein et al. (2013) . In their research, they found increase in sonication time and weight concentration of nanoparticle will increase the thermal conductivity of hybrid nanofluid. When Cu TiO_2 nanoparticles were added to neutral base fluid, the thermal conductivity improved greatly. Megatif, Ghozatloo, Arimi, and Shariati-Niasar (2016) yielded comes about with respect to thermal performance of (TiO_2-CNTs/water) hybrid nanofluid in shell and tube heat exchanger. Diverse thermo-physical properties were additionally estimated by different concentration. Thermal conductivity of 0.2% CNTs-TiO_2 hybrid nanofluid was 2.5% more prominent than CNTs nanofluid.

Through their research of (TiO_2-SiO_2/water and EG) hybrid nanofluid in circular tube, Hussein et al. (2013) evaluated nanofluid thermo physical properties at 30 ºC. They found out that when they increase the concentration from 2 to 3%, the thermal conductivity of nanofluid increase 3.7%. They also found that increment in concentration of (TiO_2-FMWCNTs/water) nanofluid will increase the thermal conductivity. However, they stated that when they increase the temperature the effective thermal conductivity increased up to 52 ºC. Further increment in the temperature caused the effective thermal conductivity to reduce.

Sajid and Ali (2018) revealed that decorated MWCNTs-Ag nanofluid was 0.16–8.02% better than undecorated through their research on hybrid nanofluid contained MWCNTs decorated Ag nanoparticles. The also stated that the thermal conductivity was at its highest when MWCNT refluxed for 1 h, 40 ºC and 4% mass ratio of Ag. Harandi, Karimipour, Afrand, Akbari, and D'Orazio (2016) stated that the thermal conductivity directly proportional with MWCNTs ratio in hybrid nanofluid during their research on thermal conductivity of (Al_2O_3- MWCNTs/water) hybrid nanofluid. They also found that spherical shape particles showed better thermal conductivity than cylindrical shape nanoparticles.

In. Baghbanzadeh, Carbone, Cozzoli, and Kappe (2011) research, they assessed various different concentrations and ratios of nanoparticle to observe the thermal conductivity of nanofluid. Due to poor thermal conductivity of silica the hybrid nanofluid perform lower thermal conductivity than MWCNTs nanofluid. Though the research the conclude that the thermal conductivity for MWCNTs nanofluid > Hybrid nanofluid (50:50) > Hybrid nanofluid (80:20) > silica nanofluid. Tahat and Benim (2017) stated that the efficiency of solar collector improved up to 45% when applying hybrid nanofluid in flat plate during their investigation on thermal properties of (CuO-Al_2O_3/water and EG) hybrid nanofluid. The measured data has been validated by comparing the obtained experimental data with the data from American Society of Heating, Refrigerating and Air Conditioning Engineers (ASHRAE). Based on the validation processes, it is noticed that the agreement between the experimental data and validation data from ASHRAE is very good. This has been proved when amount of deviation of experimental data from the data of ASHRAE is less than 10 percent

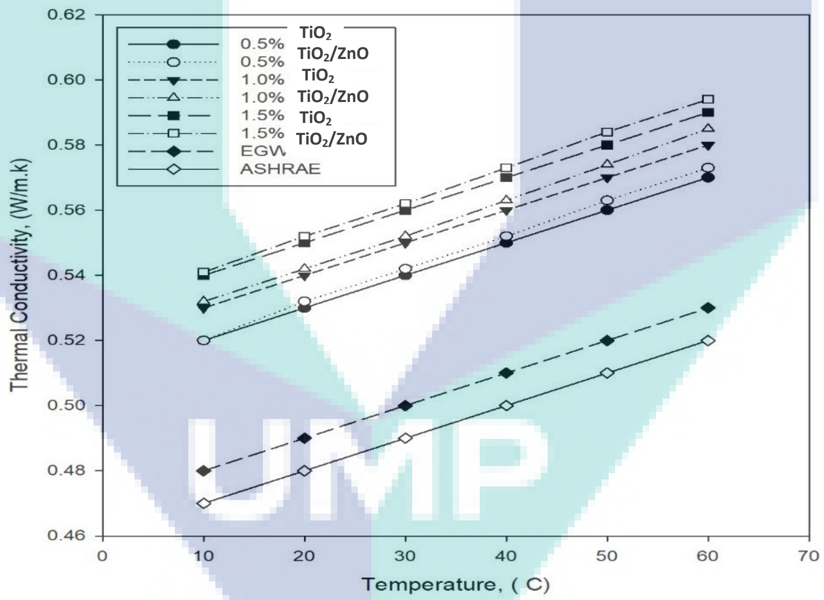

Figure 4.7: Thermal conductivity

4.2.5 Viscosity of Nanofluid

Different concentrations of nanofluids and EGW were prepared to measure the viscosity. Volume concentrations of 0.5%, 1.0 %, and 1.5 % were tested at three distinct temperatures at 30 ºC, 50 ºC and 70 ºC. Figure 4.8 shows the viscosity reading of EGW, TiO_2 and TiO_2/ZnO nanofluids of various volume concentrations. From the results, it can be concluded that the viscosity is inversely proportional to the temperature. The viscosity decreases as the temperature increases. But the viscosity increases as the volume concentration of the nanofluids increases.

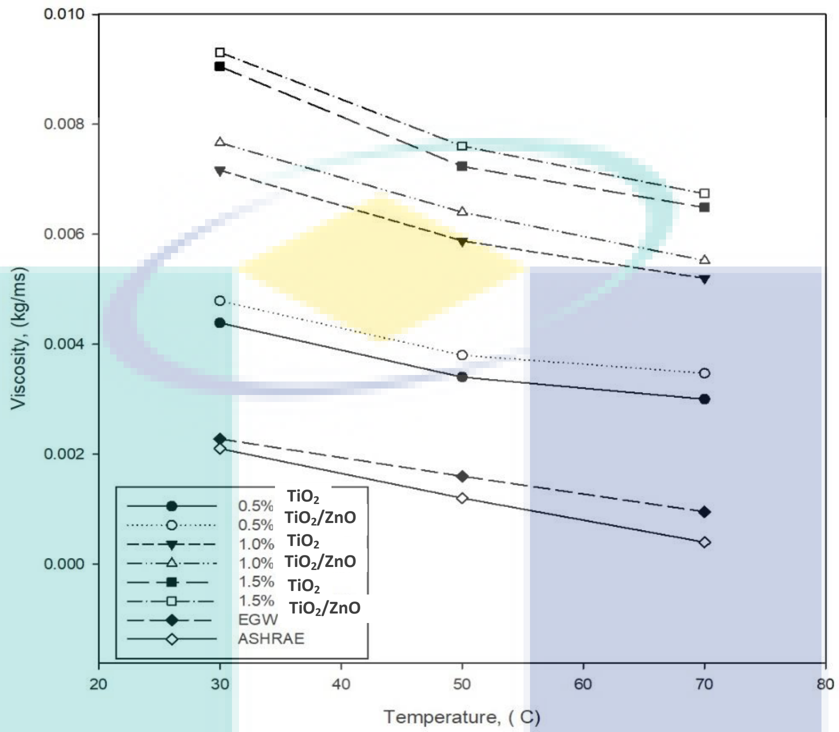

Figure 4.8: Viscosity of various volume concentrations.

Volume concentration of 1.5% of TiO_2 and TiO_2/ZnO nanofluids exhibit maximum value of viscosity at temperature of 30 ºC. Meanwhile, the minimum value of viscosity is obtained with volume concentration of 0.5% at the temperature of 70 ºC for TiO_2 and TiO_2/ZnO nanofluids. Due to the weakening of the inter particles and inter molecule adhesion forces as the temperature of nanofluid increasing, the viscosity is decreasing (Azmi, Hamid, Mamat, Sharma, & Mohamad, 2016). The free volume in the nanofluid structure will increase and the internal friction forces between molecules decreases. As the volume concentration affects the fluid internal shear stress, the viscosity increases. From the results obtained, the EGW recorded much lower viscosity compared to TiO_2 and TiO_2/ZnO nanofluid.

When the viscosity of a fluid is lower pump requires lower amount of power consumption to run the fluid. Thus, it is more convenient when pump in a cooling system consume less power to circulate or delivers coolant from storage tank system. Hence nanofluid exhibiting lower viscosity is more sufficient to be use as machining coolant. The measured data has been validated by comparing the obtained experimental data with the data from American Society of Heating, Refrigerating and Air Conditioning Engineers (ASHRAE). Based on the validation processes, it is noticed that the agreement between the experimental data and validation data from ASHRAE is very good. This has been proved when amount of deviation of experimental data from the data of ASHRAE is less than 10 percent.

4.2.6 Density

Adjacent to thermal conductivity and viscosity, force convention analysis also required the specific heat and density of nanofluids. Along these lines, the two properties were acquired using mixture relations which are commonly used by researchers. This mixture relationship was also considered by Pak and Cho (1998) in their convection heat transfer investigation. The density of nanofluids increases as the particle loading increase in each base fluid, however as the temperature increase, the density slightly decreases. Yiamsawas, Mahian, Dalkilic, Kaewnai, and Wongwises (2013), conducted experimental investigate by comparing the mixture relationship for density with experimental data. They found that their data is in good term with relation within 7%. Tough, the evaluated specific heat capacity for nanofluids decreased with the increase of particles concentration.

Decrement of specific heat capacity of nanofluids was expected the ascent in thermal diffusivity (Sharman, Dewes, & Aspinwall, 2001). From the Figure 4.9 the maximum density measured for TiO_2 and TiO_2/ZnO nanofluid are at 30 ºC with volume concentration of 1.5%. Meanwhile, the lowest density obtained for TiO_2 and TiO_2/ZnO nanofluid are at 70 ºC with volume concentration of 0.5 %. Overall, for TiO_2 the density varies from 1061.72 kg/m^3 to 1045.01 kg/m^3 for 0.5% volume concentration from 30 ºC to 70 ºC. At 1.0% volume concentration the density varies from 1068.50 kg/m^3 to 1052.91 kg/m^3 from 30 ºC to 70 ºC. Density varies from 1074.52 kg/m^3 to 1059.29 kg/m^3 is measured for volume concentration of 1.5% from 30 ºC to 70 ºC. For TiO_2/ZnO nanofluid, the density varies from1065.52 kg/m^3 to 1049.31 kg/m^3 for 0.5% volume concentration from 30 ºC to 70 ºC. At 1.0% volume concentration the density varies from 1072.50 kg/m^3 to 1056.88 kg/m^3 from 30 ºC to 70 ºC. The density varies from 1078.72 kg/m^3 to 1062.88 kg/m^3 is acquired for volume concentration 1.5% from 30 ºC to 70 ºC. Density results reveal that it has a decline trend with temperature and increasing trend with volume concentration.

The measured data has been validated by comparing the obtained experimental data with the data from American Society of Heating, Refrigerating and Air Conditioning Engineers (ASHRAE). Based on the validation processes, it is noticed that the agreement between the experimental data and validation data from ASHRAE is very good. This has been proved when amount of deviation of experimental data from the data of ASHRAE is less than 10 percent

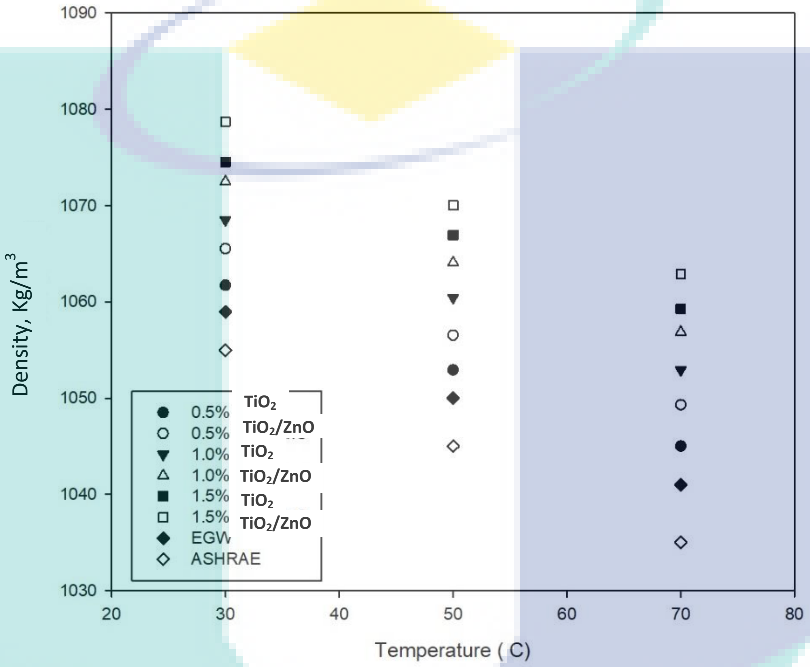

Figure 4.9: Density of various volume concentrations.

4.2.7 Specific Heat Capacity

Specific heat capacity is another crucial thermophysical property that determines heat transfer performance. Thus, measurement of specific heat capacity for EGW, TiO_2, and TiO_2/ZnO nanofluid at varying temperature and volume concentration is as portrays in Figure 4.10. The maximum specific heat capacity achieved for TiO_2 and TiO_2/ZnO nanofluid is at 90 ºC with volume concentration of 0.5%. In the interim, the minimum specific heat capacity achieved for TiO_2 and TiO_2/ZnO nanofluid is at 30 ºC with volume concentration 1.5 %.

Overall, for TiO_2 nanofluid with 0.5% volume concentration, specific heat capacity of 3511 J/kg.ºC - 3900 J/kg.ºC is obtained, from 30 ºC to 90 ºC. For TiO_2 nanofluid with 1.0% volume concentration, specific heat capacity of 3368 J/kg.ºC - 3668 J/kg.ºC is achieved, from 30 ºC to 90 ºC. For TiO_2 nanofluid with 1.5% volume concentration, specific heat capacity of 3201 J/kg.ºC - 3500 J/kg.ºC is obtained from 30 ºC to 90 ºC. For TiO_2/ZnO nanofluid with 0.5% volume concentration, specific heat capacity of 3561 J/kg.ºC - 3946 J/kg.ºC is measured from 30 ºC to 90 ºC. For TiO_2/ZnO nanofluid with 1.0% volume concentration, specific heat capacity of 3428 J/kg.ºC - 3748 J/kg.ºC is measured from 30 ºC to 90 ºC. For TiO_2/ZnO nanofluid with 1.5% volume concentration, specific heat capacity of 3299 J/kg.ºC - 3580 J/kg.ºC is measured from 30 ºC to 90 ºC.

In conclusion, TiO_2/ZnO nanofluid with 0.5% volume concentration has better specific heat capacity than EGW and TiO_2 nanofluid. This is because, the capability of TiO_2/ZnO nanofluid with 0.5% volume concentration to absorb energy in the form of heat is greater than EGW and TiO_2 nanofluid (Ali et al.,2015). The measured data has been validated by comparing the obtained experimental data with the data from American Society of Heating, Refrigerating and Air Conditioning Engineers (ASHRAE). Based on the validation processes, it is noticed that the agreement between the experimental data and validation data from ASHRAE is very good. This has been proved when amount of deviation of experimental data from the data of ASHRAE is less than 10 percent

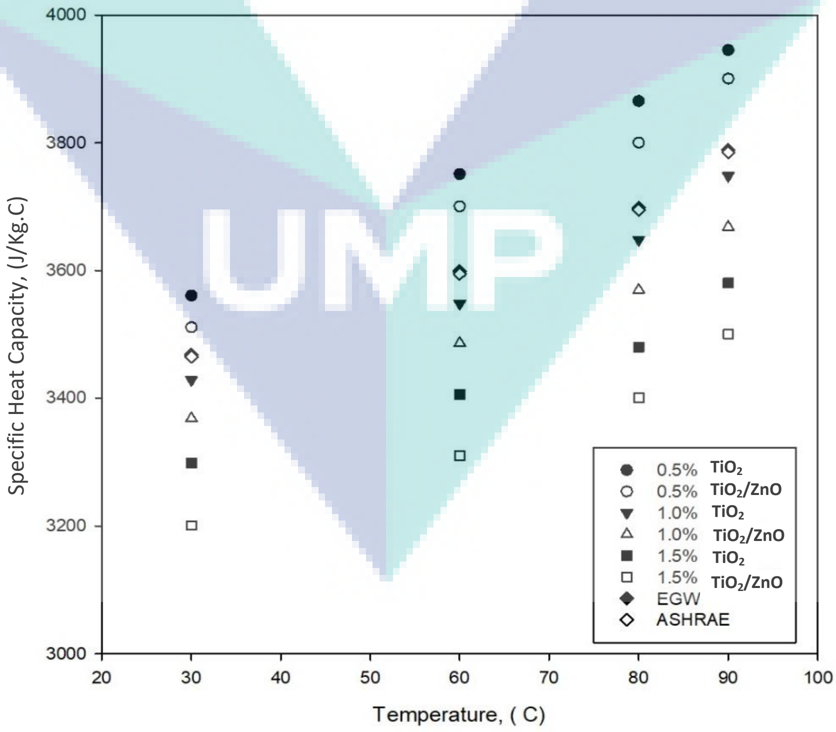

Figure 4.10: Specific Heat Capacity of various volume concentrations.

4.3 Surface Roughness

After the first pass of milling experiment which is 180 mm of cutting, the surface roughness reading is used to generate the full linear equation Eq. (4.1). The linear equation generated by statistical method is used to predict the surface roughness of milling experiment conducted expressed as:

$$\text{Roughness} = 0.2019 - 0.000042 \text{ Cutting Speed} + 0.419 \text{ Feed Rate} + 329 \text{ Depth of Cut} \quad (4.1)$$

Generally, the increase in feed rate and axial depth of cut will cause the surface roughness to increase. The increases in feed rate will increases the average surface roughness. This is a result of the increases in friction force between the workpiece and cutting tool interface. This friction force will increases the temperature in the cutting zone. In this way, the shear strength of the material reduces and it behaves in ductile form. The sticky in nature of steel material is the reason for the increased surface roughness. On the other hand, the decrease in cutting speed will cause increases in surface roughness (Alauddin, El Baradie, & Hashmi, 1996). At lower cutting speed the tendency of BUE is much higher on the edge of tool and it would affect the surface integrity. The feed rate has the most predominant impact on the surface roughness, trailed by the axial depth and the cutting speed. This situation can be explained by the decrease in cutting forces resulting from the decrease in feed rate. Smaller cutting forces cause less vibration and provide better surface roughness. Another factor to consider is cutting speed. Besides that, Sun, Brandt, and Dargusch (2009), stated that the increase in cutting force resulting from the increase in feed rate. Larger cutting force cause high vibration and provide worse surface roughness.

It is comprehended that an increase in cutting speed enhances surface quality. This outcome bolsters the contention that sufficiently high cutting speeds reduce cutting forces together with the effect of natural frequency and vibration, giving better surface roughness (Sturesson, Håkansson, & Claesson, 1997). Thus, a better surface roughness can be acquired by employing high cutting speed, low axial depth and low feed rate (Choudhury & El-Baradie, 1999). This can be seen, at experimental 11 in Figure 4.11 where the roughness at high cutting speed and low federate produces better surface roughness. The surface roughness for EGW is 0.195 µm, for TiO_2 the surface roughness is 0.146 μm and for TiO_2/ZnO the surface roughness is 0.121 μm when the cutting speed used is 2500 rpm (high cutting speed) and the federate is 0.02 mm/tooth (low federate). The surface roughness for nanofluid is superior to the EGW due to the better thermal properties of nanofluid as heat transfer fluid compared to ordinary fluids (Murshed et al., 2005).

In the case of machining, nanofluid acts as a heat transfer medium in the cutting zone. Therefore, the heat generated in cutting zone has been dissipated by the nanofliud since the ability of the nanofluid to carry away the heat. Subsequently, the surface quality of workpiece will be better when there is less burning in the cutting zone. Murshed et al. (2008), stated that the effective of thermal conductivity increases as the Brownian motion between the nanoparticle in based liquid cause a stronger transport of heat compare to sole heat conduction. But in nanofluid wise, TiO_2/ZnO has better thermal conductivity and specific heat capacity than TiO_2. Hence the surface roughness for TiO_2/ZnO is much better than TiO_2 at high cutting speed and low federate.

Muthusamy, Kadirgama, Rahman, Ramasamy, and Sharma (2016) found that the combination of cutting speed 2500 rpm and feed rate of 0.04 mm/tooth would give the lowest surface roughness for hard steel milling hardened steel material. Öktem, Erzurumlu, and Kurtaran (2005) created a surface roughness model which concluded that the significant of cutting speed and feed rate on the surface roughness is much greater than the influence of axial depth of cut. Bouzid, Zghal, and Sai (2004) found a high value of cutting speed used with a small value of feed rate would enhance the roughness of the machined Duplex stainless steel surface. They also found that an optimal value of depth of cut was more dependent on the material characteristics and the machine dynamics.

Meanwhile, in Figure 4.11, with combination of low cutting speed and low federate the roughness produces for EGW is (0.290 μm), for TiO_2 nanofluid is (0.221 μm) and for TiO_2/ZnO nanofluid is (0.184μm). In the interim, combination of low cutting speed and high federate produces high surface roughness for EGW is (0.303 μm), for TiO_2 nanofluid is (0.227 μm) and for TiO_2/ZnO nanofluid is (0.189 μm) which indicates the influences of federate towards surface roughness.

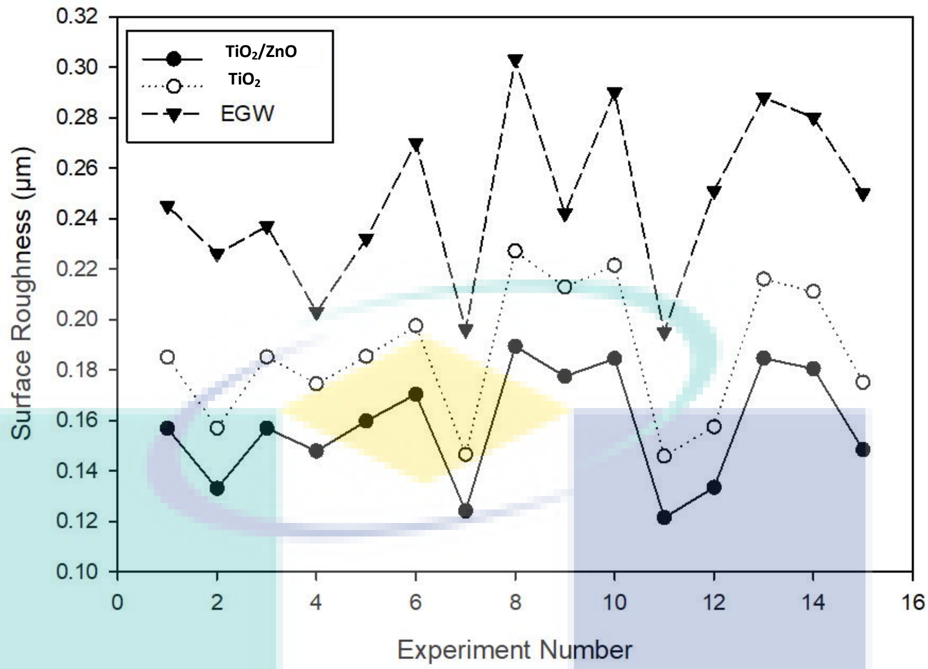

Figure 4.11: Experimental result of surface roughness

In conclusion, end-milling experiment conducted with ethylene glycol based TiO_2/ZnO nanofluid produced better surface roughness compare with end-milling experiment conducted with EGW (about 38%) and TiO_2 nanofluid (about 17%). The range of surface roughness for TiO_2/ZnO nanofluid experiments are from 0.121 µm to 0.189 µm, and for TiO_2 nanofluid is from 0.146 µm to 0.227 µm. Meanwhile the milling experiment conducted with EGW produce roughness range from 0.195 µm to 0.303 µm. Figure 4.12 shows the average surface roughness value obtained from experimentation and the value predicted by the linear model. It shows that the predicted values are in good agreement with the experimental value for TiO_2/ZnO nanofluid experiment. This indicates that the predicted linear model is useful to predict value of surface roughness. The adequacy of linear model is verified using the analysis of variance (ANOVA) at a level of confident of 95 %.

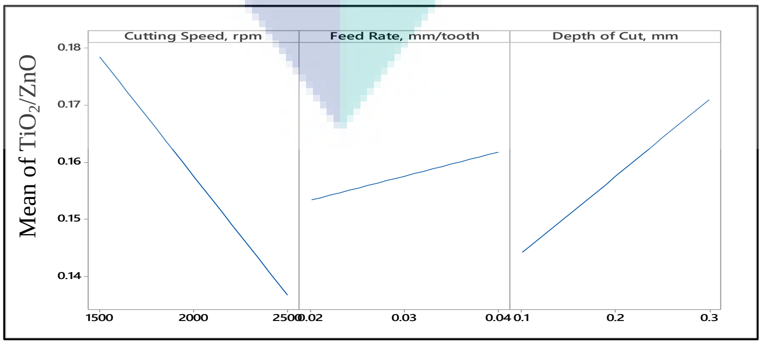

Figure 4.12: Experimental result of surface roughness predicted by linear mode

As shown in Table 4.2, the probability (P-value) is not significant with lack of fit (>0.05) for both experiment. Meanwhile, F-static for the model is 1.99 for TiO_2/ZnO nanofluid experiment. This implies that the Lack of Fit is not significant relative to pure error. This indicates that the linear model could fit and adequate (Kadirgama, Noor, et al., 2008). With the aid of the linear model equation, the contour of the average surface roughness has been plotted for TiO_2/ZnO nanofluid experiment. Figure 4.13 shows the surface roughness contours at different axial depth of cut, feed rate and cutting speed. It is obvious that the finest surface roughness occur at high cutting speed, low feed rate and low axial depth of cut for both set of experiment. Figure 4.14 shows the error between actual and predicted data for surface roughness, the average is 7 % of error.

Table 4.2: ANOVA Table

Source	DF	F-Value	P-Value
Model	3	7.77	0.005
Linear	3	7.77	0.005
Cutting Speed, rpm	1	16.11	0.002
Feed Rate, mm/tooth	1	0.65	0.437
Depth of Cut, mm	1	6.54	0.027
Error	11		
Lack-of-Fit	9	1.99	0.379
Pure Error	2		
Total	14		

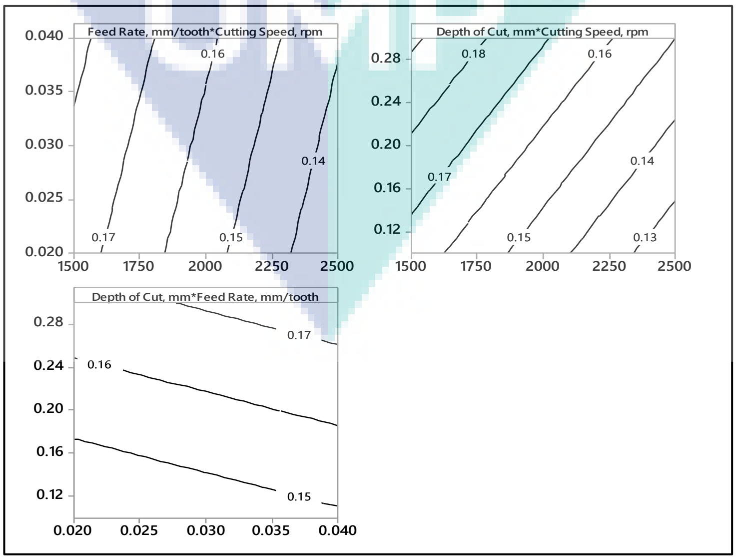

Figure 4.13: Surface roughness contours

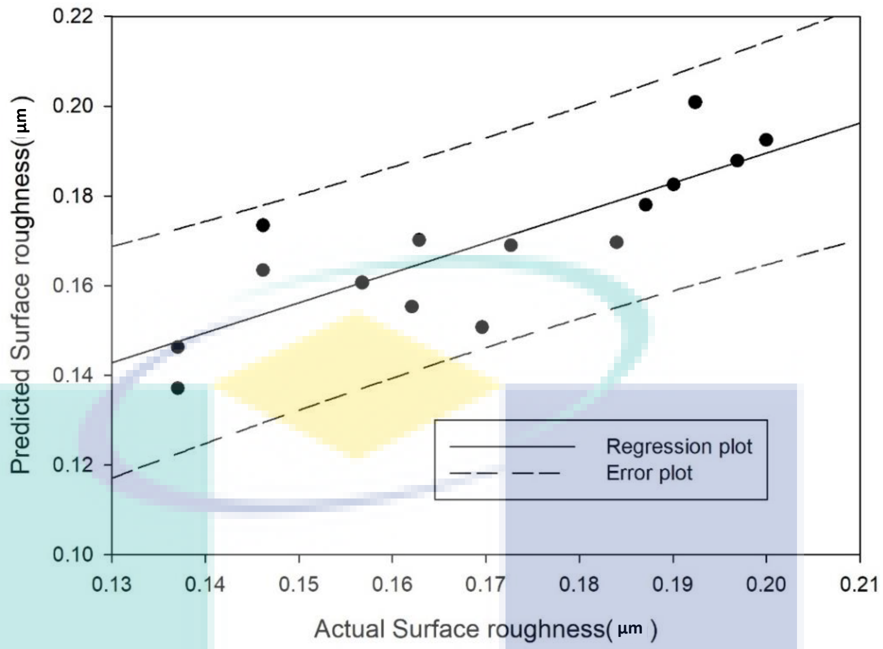

Figure 4.14: Error between actual and predicted surface roughness

4.4 Tool Life

Field and Kahles, 1971 stated that tool life can be found from the expression below:

$$Tool\ life = \frac{TL}{F_m} \tag{4.2}$$

where F_m is the feed rate in mm/min and TL is the total length to reach flank wear criterion 0.3 mm.

Tool life = 99.74 - 0.01660 Cutting Speed - 1209 Feed Rate - 1.9 Depth of Cut (4.3)

Equation 4.2 and Equation 4.3 demonstrates that the instrument life increments with the decline of cutting speed, feed rate and axial depth of cut. Equation 4.3 is generated from statistical method. Undeniably feed rate is the most overpowering parameter than axial depth of cut and cutting speed which influences the tool life. Subsequently, the tool life can be prolonging by lower the cutting speed, lower feed rate and lower axial depth for end-milling process. The comparable outcome was found by Alauddin et al. (1997) where stated that decrement in tool life were caused by an increment in cutting speed, feed rate and axial depth of cut. Korkut, Kasap, Ciftci, and Seker (2004), expressed that tool life diminish drearily with the increasing of cutting speed. This shows feed rate is the most predominant parameter which adds to the tool failure, which cause by the increment on temperature in shear zone. Consequently, high temperature frequently brings about tool wear for example plastic deformation. Those components debilitate the cutting tool material and add to the wear progression on the edge of the instrument.

On other hand, tool life for EGW, TiO_2 nanoluid, and TiO_2/ZnO nanofluid decreases when there is increases in cutting speed in all experiments Dearnley and Grearson (1986) stated that the intact area between chip-tool is lesser during high cutting speeds, which leads to a convergence of high temperature and plastic deformation happens as the temperature is getting high and the cutting tool tends to lose their strength. These will likewise contribute and increment in the thermal gradient as thermal crack generation rate increases which lead to tool wear. Eldem and Barrow (1976) stated that increment in cutting speed accelerates thermally activated wear mechanisms in addition to generating more intense mechanical impact. Similar trends were also reported by Vivancos, Luis, Ortiz, and González (2005) when machining hardened steel at higher cutting speed. Furthermore, because the longer time contact position (high cutting speed) between the tool and workpiece will cause high temperature in the cutting zone, the constituents Ni will harden the workpiece, and then tool life will be reduced. Thus, the tendency of tool wear to increase with increasing cutting is found to be predominant. According to S. Sharif (1999) failure modes of the cutting tools when machining at higher cutting speed conditions were dominated by severe flank wear, excessive chipping and catastrophic failure which were mainly due to combination of adhesion, diffusion and plastic deformation wear mechanisms.

It can likewise be seen that there is a noteworthy increase in tool life when there is reduction in axial depth of cut. From Figure 4.15, it can be concluded that the influence of axial depth of cut on tool life is very little. This outcome upheld by Astakhov (2006) where expressed that the tool life rate shouldn't change dramatically as there is increment in the axial depth of cut. The past findings expressed that the average temperature remains unaltered even the axial depth of cut increases the contact stresses at the tool-chip intact area. Hence, the high axial depth of cut will not alternate the tool life rate if the milling process is carried out at optimum feed rate and cutting speed.

Besides that, Figure 4.15 show that all the end-milling experiment with TiO_2/ZnO nanofluid produces highest tool life, then followed by TiO_2 nanofluid which produces slightly low tool life then TiO_2/ZnO nanofluid compare with EGW which produces lowest tool life. From Figure 4.15, the highest tool life was achieved at experiment 10 where the cutting speed is 1500 rpm (lowest) and the feed rate is 0.02 mm/tooth (lowest). The highest tool life stated for EGW is 32.59 minutes, for TiO_2 is 49.18 minutes, and for TiO_2/ZnO is 60.72 minutes at experiment 10. The TiO_2/ZnO nanofluid as coolant increases the tool life by 28.13 minutes than EGW.

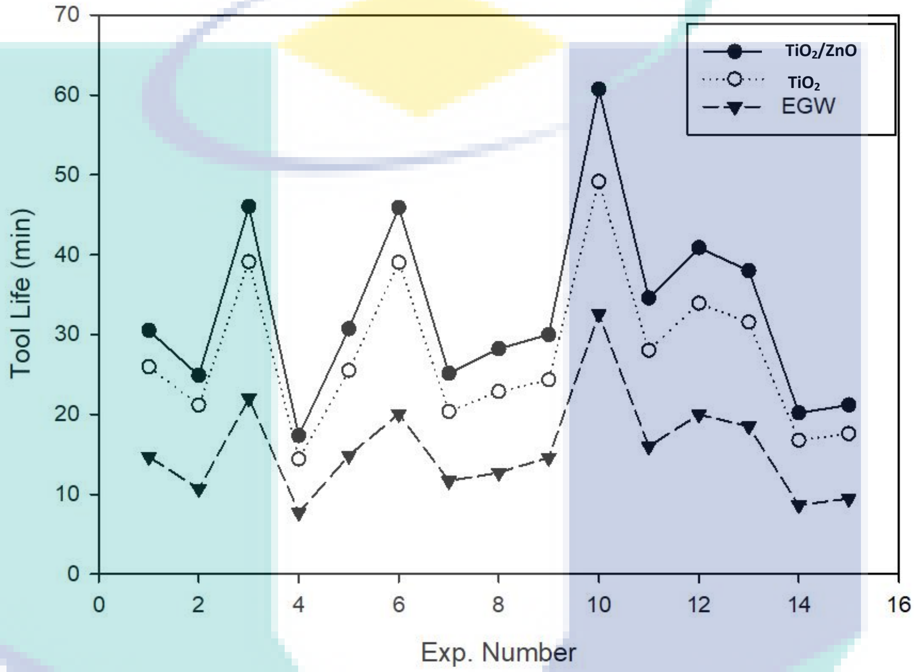

Figure 4.15: Tool life for TiO_2, TiO_2/ZnO and EGW

By using TiO_2/ZnO nanofluid as coolant, the tool life can be prolonged and the wear can be reduced. This can be credited to the superb execution of nanofluid as a heat transporter in tool-chip intact area. Higher wear rate occurs when there is a convergence of high temperature at the edge of the flank. In any case, utilizing TiO_2/ZnO nanofluid as cutting fluid will decrease the temperature infiltrate into cutting tool because of the high heat transfer rate of TiO_2/ZnO nanofluid. The heat transfer potential is improved by the higher surface region of nanoparticles since the heat transfer happens on the surface region of the particle (Murshed et al., 2005).

Figure 4.16 shows the tool life value obtained from experimentation and the value predicted by the linear model. It shows that the predicted values are in good agreement with the experimental value for TiO_2/ZnO nanofluid experiment. This indicates that the predicted linear model is useful to predict value of tool life. The adequacy of the linear model is verified using ANOVA at level of confident 95 %. As shown in Table 4.3, the P-value of linear model for tool life were 0.323 for TiO_2/ZnO nanofluid experiment. Hence, the P-value is not significant with the lack-of-fit since the value is more than 0.05. Figure 4.17 shows the tool life contours at three different combination of axial depth of cut for TiO_2/ZnO nanofluid experiment. It is clearly noticeable that the increase in cutting speed and feed rate will reduce the tool life. Figure 4.18 shows the error between actual and predicted data for tool life, the average is 11 % of error.

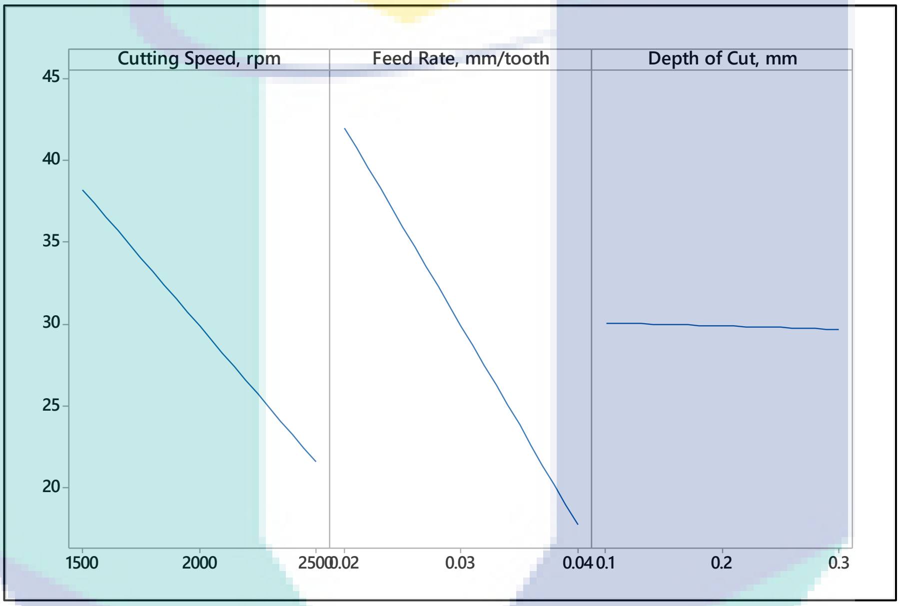

Figure 4.16: Experimental result of tool life predicted by linear model

Table 4.3: ANOVA Table

Source	DF	Adj SS	Adj MS	F-Value	P-Value
Model	3	1719.96	573.32	47.31	0
Linear	3	1719.96	573.32	47.31	0
Cutting Speed, rpm	1	551.29	551.29	45.49	0
Feed Rate, mm/tooth	1	1168.38	1168.38	96.42	0
Depth of Cut, mm	1	0.3	0.3	0.02	0.878
Error	11	133.3	12.12		
Lack-of-Fit	9	132.61	14.73	43.13	0.323
Pure Error	2	0.68	0.34		
Total	14	1853.26			

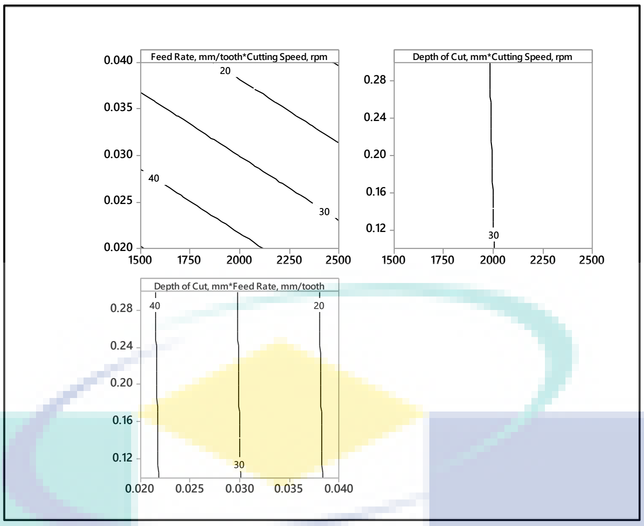

Figure 4.17: Tool life contours

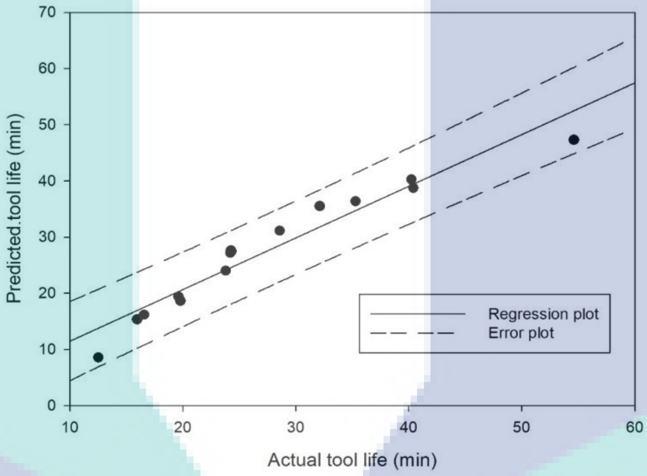

Figure 4.18: Error between actual and predicted tool life

4.5 Multi-Objective Optimization

Machining response needs to be optimized with three properties so that it will indicate the optimum parameters (Cutting speed, federate and axial depth of cut) for surface roughness and tool life. The optimize criteria was selected as maximum tool life and minimum surface roughness.

The optimization produces 8 solutions that meet with the criteria with different desirability as shown in Figure 4.19. It shows that solution one produce the optimum structure parameters that produce maximum tool life and minimum surface roughness are cutting speed= 2166, Feedrate = 0.02 and axial depth of cut = 0.1. It produces tool life = 37.07 min and surface roughness = 0.14502 µm. The desirability is nearly 1 (0.713), and it satisfy the goal of the optimization.

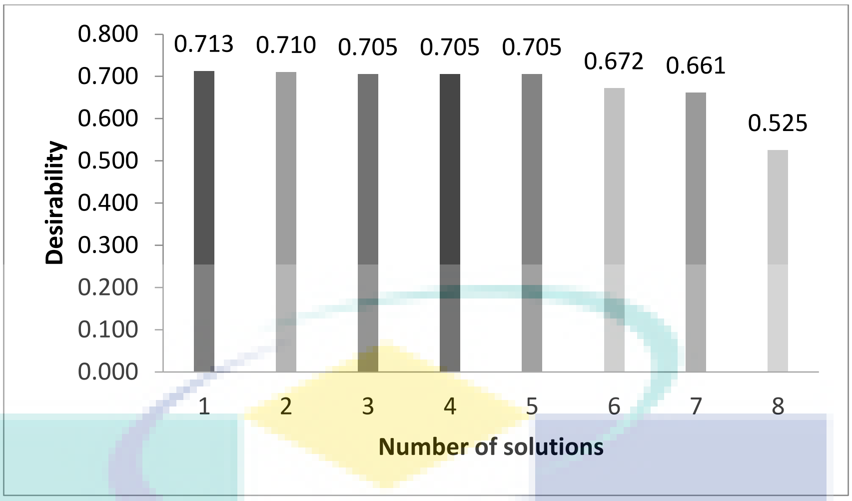

Figure 4.19: The desirability of the optimum parameters

4.5.1 Optimization validation

Table 4.4 shows the optimization value of tool life and surface roughness for actual experimental value and statistical model value. The highest desirable value parameters selected and experiment run to compare the experimental and statistical method value. Cutting speed used for experiment is 2200 rpm, feed rate 0.02 mm/tooth and axial depth of cut 0.1 mm. The error percentage between the statistical model and actual experimental value is below 5% for tool life and surface roughness.

Table 4.4: Optimization value of tool life and surface roughness for actual experimental value and statistical model value

Parameters	Experimental value	Statistical value
Cutting speed, rpm	2200	2166
Feed rate, mm/tooth	0.02	0.02
Axial depth of cut, mm	0.1	0.1
Tool life, minute	35.29	37.07
Surface roughness, µm	0.1381	0.1452

4.6 Morphology Analysis on Tool Wears

Figure 4.20, Figure 4.21 and Figure 4.22 exhibits the assortment in flank wear width with milling distance in end-mill SUS 304 stainless steel under EGW, TiO_2, and TiO_2/ZnO nanofluid. From the result, it is noted that as the milling distance increasing the flank wears increasing as well. The comparable pattern was found in a recent research carried out by Liew. The milling distance will be preceded until the point that the wear achieved the ISO 8688-2-1989 (E) wear criterion, flank wear ≥ 0.3 mm. From Figure 4.20, Figure 4.21 and Figure 4.22, it can be seen that Experiment 4 (cutting speed 2500 rpm, feed rate 0.04 mm/tooth and axial depth of cut 0.2 mm) having the highest flank wear rate meanwhile, Experiment 10 (cutting speed 1500 rpm, feed rate 0.02 mm/tooth and axial depth of cut 0.2 mm) have the lowest flank wear rate for EGW, TiO_2, and TiO_2/ZnO nanofluid.

The highest flank wear reach the failure criterion at milling distance around 780 mm for EGW, around 1280 mm for TiO_2, and around 1390 mm for the TiO_2/ZnO nanofluid. The lowest flank wear reach the failure criterion around 990 mm for EGW, around 1620 mm for TiO_2 nanofluid, and around 1780 mm for TiO_2/ZnO nanofluid. These results show the influence of cutting speed and feed rate on the flank wear. The flank wear increases as the cutting speed and flank wear increases. As indicated by Thamizhmanii and Hasan, high heat produced on the flank area will affect the arrangement of flank wear. According to Dearnley and Grearson, high heat will produce on the tool-chip interface when high cutting speed and feed rate used. Thus the tool tip will be softening by the high heat produced which ending increases the wear. In this manner, the flank wear rate is considerably higher at high cutting speed and feed rate.

From the experimental results, TiO_2/ZnO nanofluid shows better results than TiO_2 nanofluid and EGW. TiO_2/ZnO nanofluid reaches the failure criterion at longest milling distance than TiO_2 nanofluid and EGW. Thus, it can be concluded that TiO_2/ZnO nanofluid have a great enchantment on flank wear rate for milling hard material. Khandekar et al. (2012), found similar results as the flank wear rate is lower when using nanofluid as cutting fluid. This occurs due to TiO_2/ZnO nanofluid improved conduction, convection and wettability compare to TiO_2 nanofluid and EGW. TiO_2/ZnO nanofluid sustain for a longer period as it contains superior properties in cooling and lubrication retain cutting tool the hardness. Cutting tool materials generally undergo severe changes in thermal and mechanical properties when machining nickel-based alloys. The applied stresses and temperatures generated at the cutting edge greatly influence the flank wear rate, hence the tool life. Notching at the tool nose and axial depth of cutting region is the prominent failure mode when machining nickel-based alloys. This is caused by the combination of high temperature, high workpiece strength, work hardening, abrasive chips, etc. (Khamsehzadeh, 1991). In general, the mode of tool failure throughout this work was flank wear, notching or wear at the tool nose. Figure 4.23 shows SEM for EGW at milling distance of 900 mm (cutting speed 2500 rpm, feed rate 0.04 mm/tooth and axial depth of cut 0.2 mm). The flank wear occurs on EGW at milling distance 900 mm can be seen in Figure 4.23. Meanwhile there are no traces of flank wears on TiO_2 and TiO_2/ZnO nanofluid at milling distance of 900 mm.

Due to rubbing of the tool on the flank side with work material and movement of the chips on the rake face, the formation of flank wear occurs. The friction between the flank side of the tool and machine which led to flank wear will cause the tool wear. The tool wear mainly depends on the work material, tool geometry, cutting parameters and also cutting fluid. When using EGW as cutting fluid, because of the lower thermal heat properties, at high temperature the heat produced at the tool-work material is not transferred efficiently. By using the TiO_2 and TiO_2/ZnO nanofluid the heat produced at tool-work material interface can be reduced drastically because of the good thermal heat properties of nanofluid as heat transfer. From the results, when using TiO_2 nanofluid the milling distance to reach flank wear criteria is improved 55.55% than EGW as a cutting fluid. Meanwhile hybrid TiO_2/ZnO improved 80% in milling distance to reach flank wear criteria than EGW. Hybrid TiO_2/ZnO is much better than TiO_2 nanofluid and EGW in terms of thermal heat properties which cause flank wear occurs at much longer distance for TiO_2/ZnO than TiO_2 nanofluids.

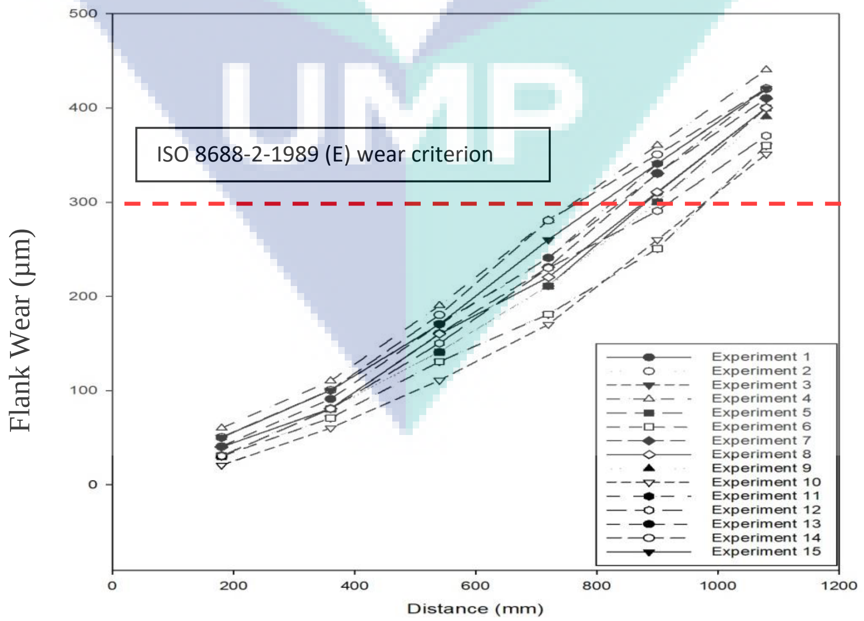

Figure 4.20: Progression of flank wear by distance for milling with EGW

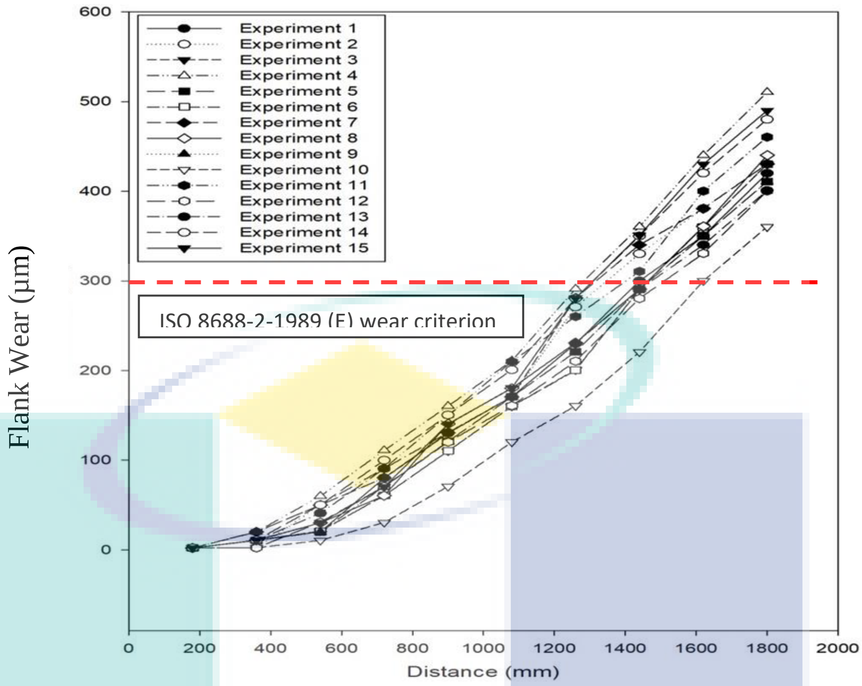

Figure 4.21: Progression of flank wear by distance for milling with TiO_2

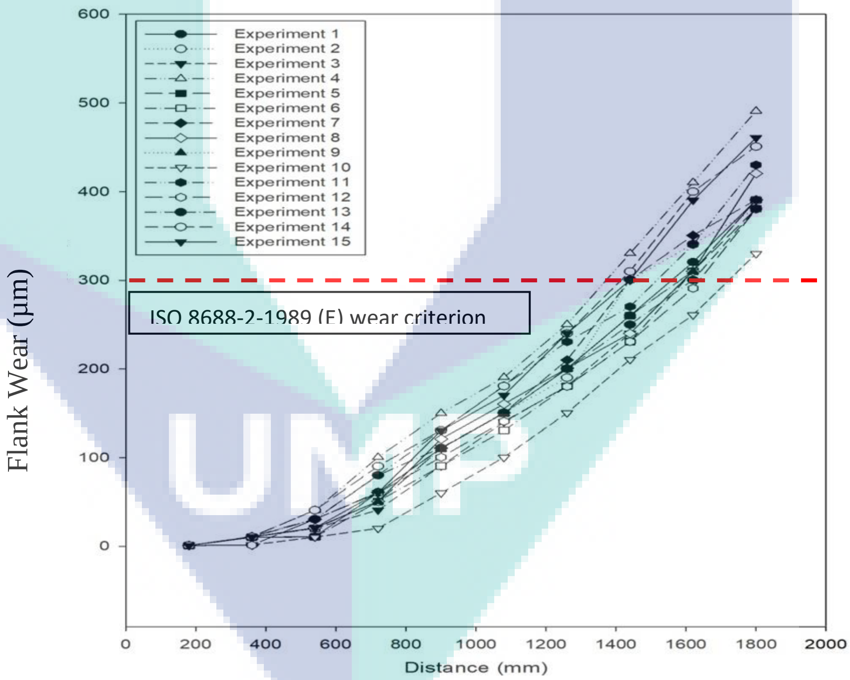

Figure 4.22: Progression of flank wear by distance for milling with TiO_2/ZnO

Chipping wear formed initially on the tip of the cutting edge, on a height that equals half of the axial depth of cut. This is because the yielding temperature is greatest on tip of the cutting edge (Ulutan & Ozel, 2011). From Figure 4.24, it can be seen that EGW has heavier chipping while TiO_2 nanofluid with less chipping at a milling distance of 900 mm (cutting speed 2500, feed rate 0.02, axial depth of cut 0.1). Meanwhile there is no trace of chipping wear at milling distance of 900 mm when using TiO_2/ZnO nanofluid as cutting fluid. Therefore, it can be obviously seen that TiO_2/ZnO nanofluid function as an extraordinary coolant in preventing the chipping wear. This is because of the better thermal conductivity of TiO_2/ZnO nanofluid compare to EGW and TiO_2.

TiO_2/ZnO nanofluid reduces the heat generated on the cutting zone hence the chipping was reduced extremely. From the Figure 4.25, milling distance at 900 mm (cutting speed 2500, feed rate 0.02, axial depth of cut 0.1), it can be clearly seen that the coating on flank face for EGW was piled off and expose the carbide structure. For TiO_2 nanofluid the coating pilled off lesser than EGW. Meanwhile TiO_2/ZnO nanofluid has a little coating piled off on the flank face compared to EGW and TiO_2 nanofluid.

According to Liao and Shiue (1996), they stated that during high speed milling of stainless steel with water soluble coolant the coating layer of cutting insert will pilled of. But with using nanofluid, the coating pilled of can be reduced due to an inpermanent layer formed on the flank face by nanofluid. Figure 4.26 and Figure 4.27 shows the intefacial layer formed by TiO_2/ZnO nanofluid and TiO_2 nanofluid respectively. For the TiO_2/ZnO nanofluid, solid Ti and Zn nanoparticles layer has been embedded into tiny holes on the cutting edge and act as additional layer to shield the cutting tool. For TiO_2 nanofluid, solid Ti layer embedded and act as additional layer. Electron dispersive X-ray (EDX) analysis on the edge of cutting insert was conducted to determine the composition of the layer.

Figure 4.26 shows the present of Ti and Zn particles in the interfacial layer formed. While Figure 4.27 shows the present of Ti particles in the intefacial layer. The formed impermanent layer will protects the cutting insert early stage of cutting process. This layer is found to be the interfacial layer which is formed by the solid Ti nanoparticle which acts as a thermal bridge during the milling process (Koo & Kleinstreuer, 2004). TiO_2/ZnO nanofluid forms a better impermanent layer than TiO_2 nanofluid which is far more better in reducing the coating of tool pilled off.

Adhesion were the main tool wear mechanisms seen in the present work, which is clearly demonstrated by the adhered workpiece material and the formation of a built-up edge (BUE) on the tool flank as shown in Figure 4.28. A BUE is formed due to the high pressure generated during cutting and the high chemical affinity of the tool and workpiece material. Similar observations have been made by Sharman et al. (2001). When ball nose end milling Inconel 718 they found that the main wear mechanism was adhesion and reported BUE formation and plucking of the tool coating. This led to the exposure of the tungsten carbide substrate and subsequently rapid wear of the tool.

Liao and Shiue (1996) studied the wear of tungsten carbide tools in turning Inconel 718. They proposed a mixed wear mechanism consisting of material adhesion, diffusion and material removal, explaining both the observations made by Sharman et al. (2001) and results of the present experiments. This mechanism involved the diffusion of iron and nickel into the binder phase of the carbide tool, weakening the bond between the tungsten carbide particles and facilitating attrition. This resulted in an easier removal of carbide tool particles during break off of the built-up edge and subsequent repeated exposure of the low wear resistant cobalt phase to the cutting process (Sharman et al., 2001).

Using EGW for milling, crack was found formed at the region where the coating has been removed as shown in Figure 4.29. The crack formed on the flank face was parallel to the cutting edge. Cracks appear on the flank face at milling distance below than 1m when end-mill stainless steel. The main reason for the cracks to occur is the mechanical impact between the cutting tool and workpiece. These cracks are referred as mechanical crack which spread to the rake face. Milling with nanofluid shows the cutting tool can withstand for longer distance than milling with EGW.

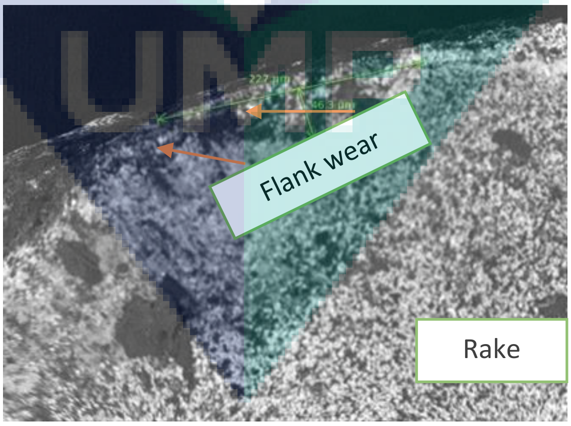

Figure 4.23: SEM of EGW, magnification 500 µm, 2000 cutting speed, 0.02 feed rate, 0.1 axial depth

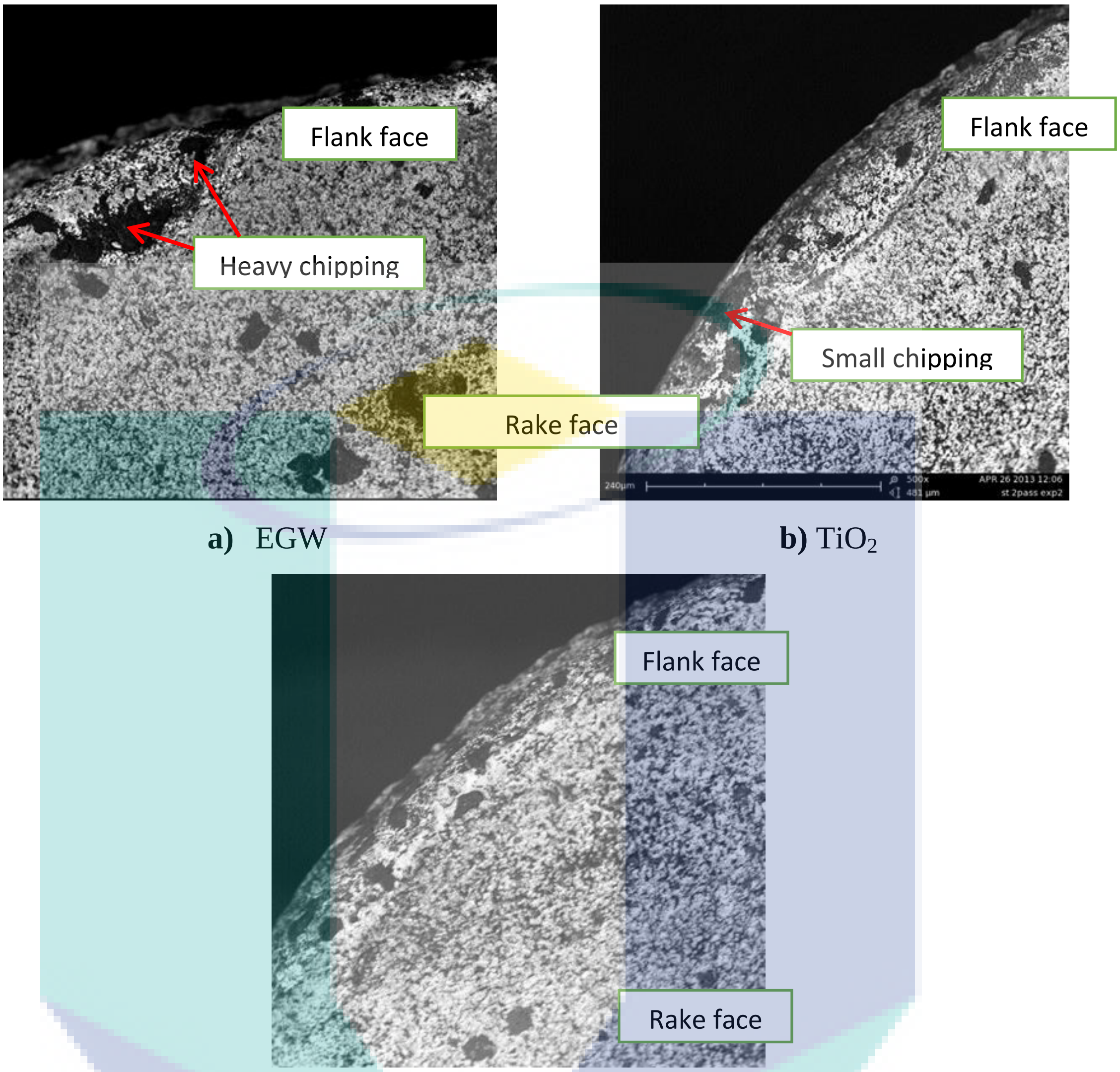

a) EGW **b)** TiO_2

C) TiO_2/ZnO

Figure 4.24: SEM of EGW, TiO_2 and TiO_2/ZnO, magnification 500 µm (2500 cutting speed, 0.02 feed rate, 0.1 axial depth) distance 900 mm

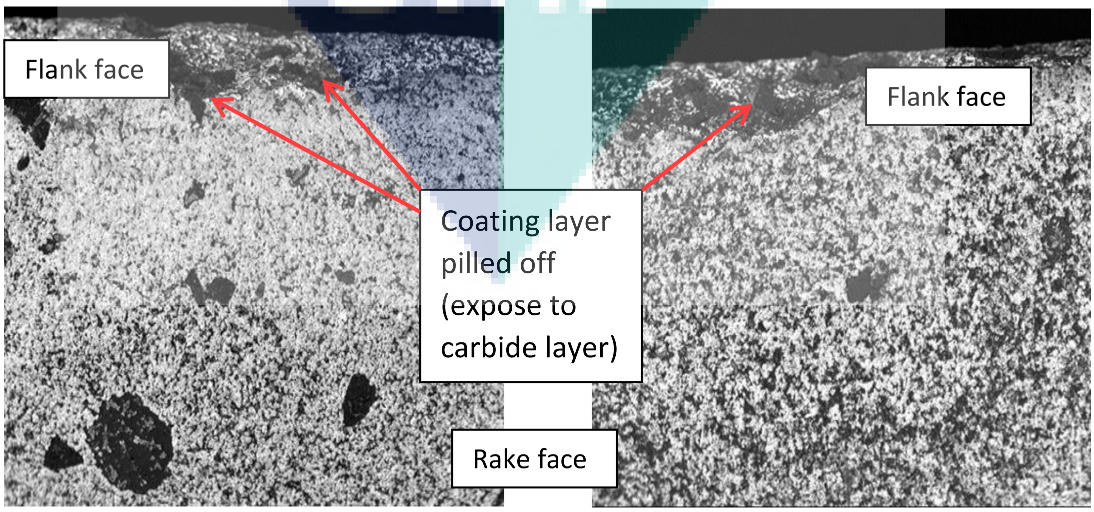

a) EGW **b)** TiO_2

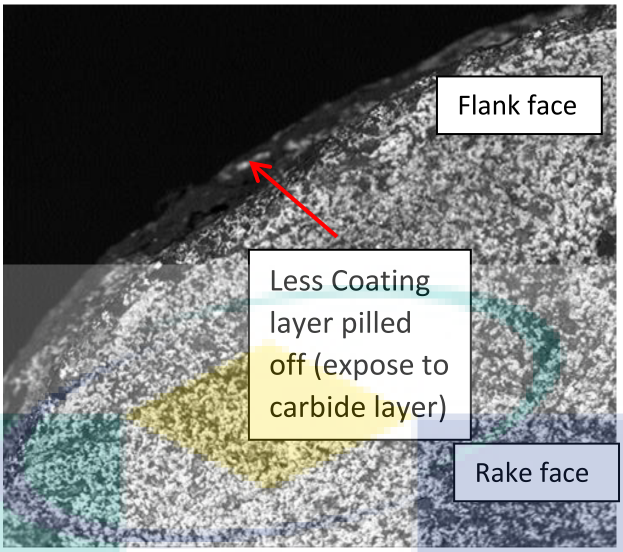

c) TiO_2/ZnO

Figure 4.25: SEM of EGW, TiO_2 and TiO_2/ZnO, magnification 500 µm (2500 cutting speed, 0.02 feed rate, 0.1 axial depth) distance 900 mm

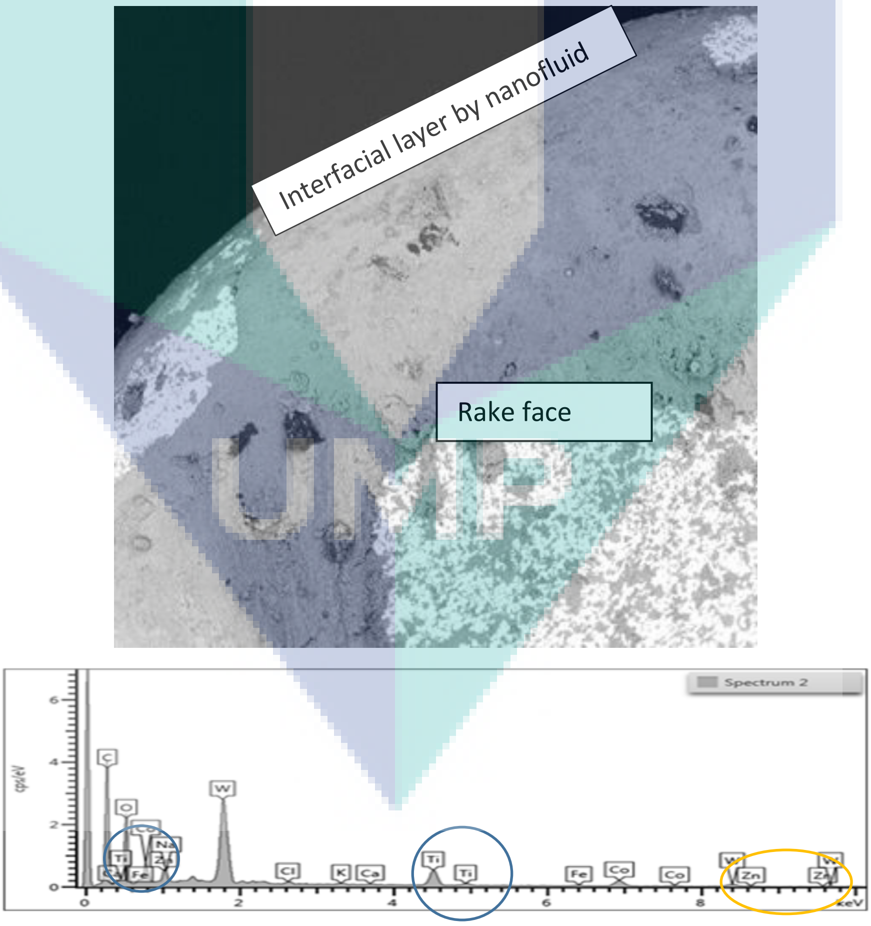

Figure 4.26: SEM and EDX of TiO_2/ZnO

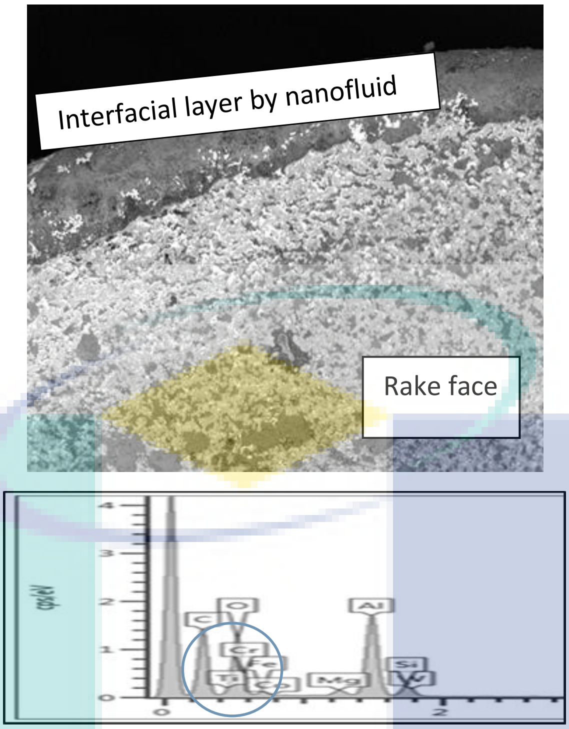

Figure 4.27: SEM and EDX of TiO_2

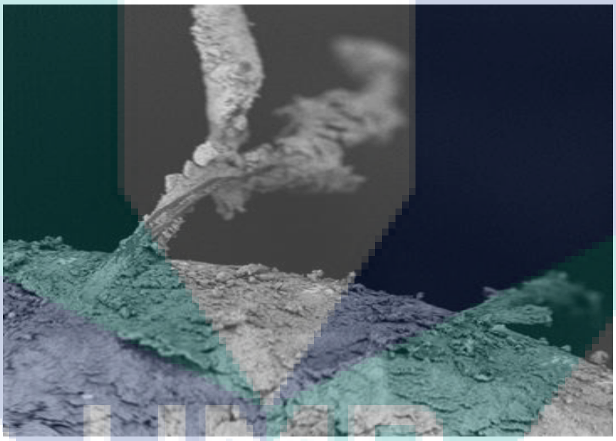

Figure 4.28: BUE with EGW

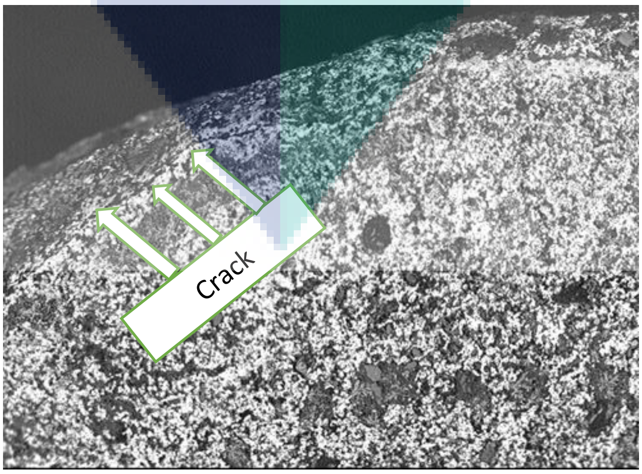

Figure 4.29: Crack for EGW

4.7 Chips Formation

The chips found in the study are classified into two types. Type I: unstable chip and type II: critical chip. Type I and II chips are generated by a process with chatter of different severity. All chips are obtained from the machining process when the tool is within its wear criteria to exclude the effect of tool wear. Figure 4.30 shows an unstable chip. The surface texture shows lot of waving. Sometimes it is the result of adiabatic shear occurring in the work material. Similar unstable chips observed by Ning, Rahman, and Wong (2001). Chatter serves as a source of uneven surface roughness and the finished surface will consist of alternate unburnished (dull) and burnished (shiny) regions (Ning et al., 2001). This mechanism of chip formation differs significantly from that of stable cutting. This type of chips mainly found in TiO_2 and EGW. When chattering is developed fully, the cutting edge is no longer moving in the way as that in stable cutting, but vibrates while it is rotating.

Type II chip is known as a critical chip. The resulting chip shown in Figure 4.31 is wavy and nearly symmetrical, resembling a harmonic or sine wave. According to Yuan Ning et al. the chatter marks are different compared to those of unstable chip. This kind of chip formation is also noted for its in-cut segment area and cutter movement which distinguishes itself from the unstable and that of stable cutting. This type of chip is composed of a number of connected (more or less) elements. In end-milling, it is found as a consequence of self-excited vibration (Ning et al., 2001). It is accompanied by cyclic variations of undeformed chip thickness (cutting depth), as well as shear, rake angle, and clearance angle. Mainly found in Hybrid nano.

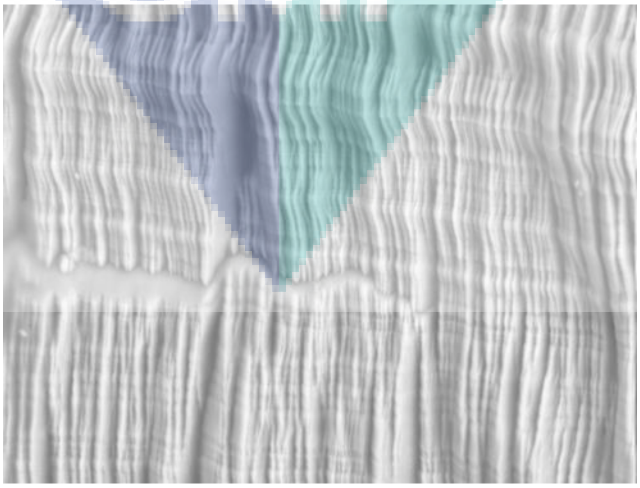

Figure 4.30: Unstable chip in EGW and TiO_2

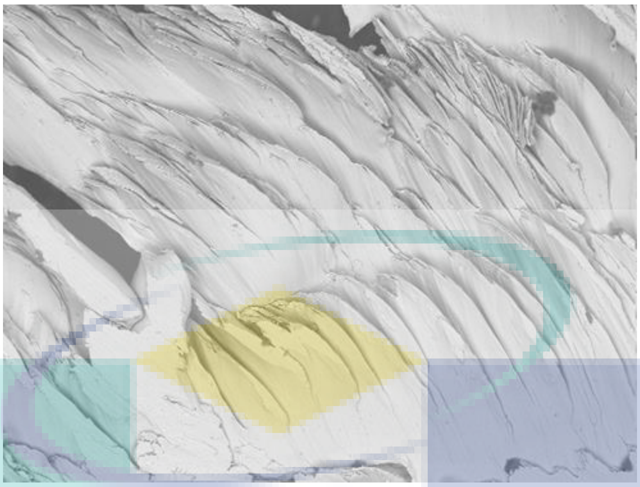

Figure 4.31: Critical chip

4.8 Analysis of Wear Mechanism

Abou-El-Hossein and Yahya (2005) stated that BUE (Figure 4.32) can simply formed at low cutting speed during machining ductile material such as austenite stainless steel. This is due to diffusion wear took place at the tool-chip interface and cause the element from the workpiece transfer to the insert rake face. According to W Grzesik (2009) carbon and metal particles transfer into insert rake face in the form of chips generated during the milling process. In same period, atoms of alloying element of the workpiece material diffuse into the rake face and react with insert coating to degrade further. According to previous researcher by Jawaid et al. (2000), attrition wear (Figure 4.33) is a removal of grains or agglomerates of tool material due to intermittent adhesion between the tool and the workpiece as a result of the irregular chip flow and the breaking of a partially stable BUE. Significant plucking of tool particles when milling steel material can be reasonably associated with attrition wear. The attrition behavior can be described as the cyclic adhesion and removal of workpiece and chip material from the tool, which also causes removal of tool particles (Jawaid et al., 2000).

On the other hand, the milling testing with nano particle base coolant the insert exhibits a micro-wear mechanism. Figure 4.32 shows the massive adhesion which contributes to BUE. However, this BUE is not in stable state since many cutting insert exhibits this phenomenon. The adhesion of the workpiece material on the rake face of the milling insert can form a strong shield on the layer of the milling insert after the TiN coated layer has been removed. The adhered layer will act as superfluous layer to shield the cutting insert since layer containing Ti nanoparticle. In most cases, the adhering metal was found mainly on the rake face rather than on the flank face after the tools had failed (Jawaid et al., 2000).

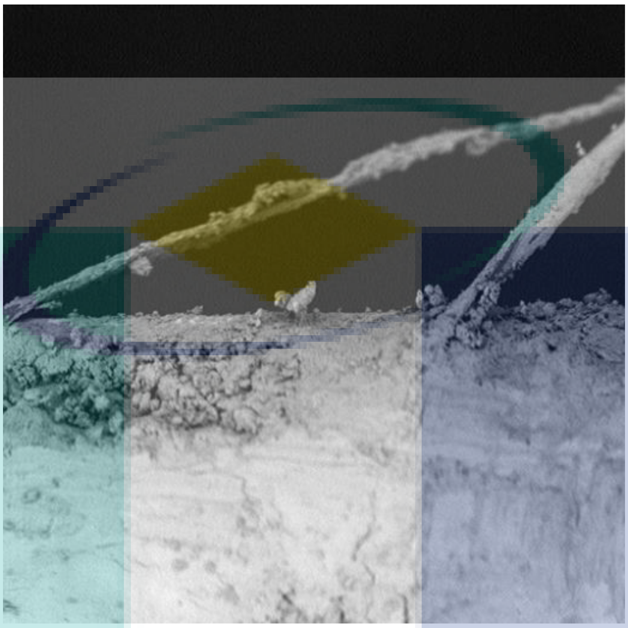

Figure 4.32: SEM of BUE for EGW

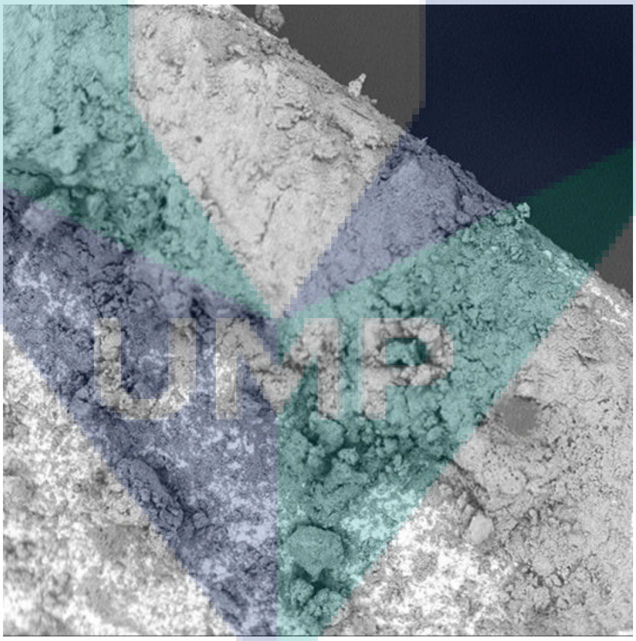

Figure 4.33: Attrition wear

CHAPTER 5

CONCLUSION AND RECOMMENDATION

5.1 Conclusion

In the present study, linear mathematical model were developed to predict milling parameter for TiN coated carbide insert under three different milling environments which using water soluble coolant EGW, ethylene glycol based TiO_2 nanofluid and ethylene glycol based TiO_2/ZnO hybrid nanofluid as cutting fluid. The predicted linear model used to find the optimum milling parameter for minimize the surface roughness and maximize the tool life based on RSM. The experimental results were compared with the predicted result. It can be summarized from the results and discussion as follows:

1. Hybrid nanofluid and single nanofluid's thermal conductivity higher than EGW 13% and 11%. Hybrid nanofluid recorded 12% more than single nanofluid Viscosity. Hybrid nanofluid and single nanofluid Density slightly higher than EGW about 0.75% and 0.5%. Hybrid nanofluid and single nanofluid specific heat capacity higher than EGW about 30% and 22%

2. The models between cutting parameters and response for surface roughness and tool life have been established. For surface roughness the error for the predicted value vs the actual value is 7%. Meanwhile for tool life the error for the predicted value vs the actual value is 11%. High cutting speed, low feed rate and low axial depth will provide fine surface roughness. Low cutting speed and Low feed rate will increase the tool life.

3. For the surface roughness by using single nanofluid TiO_2, the surface roughness increase by 23.7% while using Hybrid nanofluid TiO_2/ZnO it increases better by 36.5% than EGW. By using single nanofluid TiO_2 the tool life has been increased about 50.1% while the Hybrid nanofluid, TiO_2/ZnO increases much more better about 86 % than EGW. For the flank wear, single nanofluid exceeds 60% length than EGW Hybrid nanofluid 80% more than EGW.

4. The multi objective optimization for the parameters has been established. Where the optimum cutting speed= 2166 rpm, Feedrate = 0.02 mm and axial depth of cut = 0.1 mm which produces tool life = 37.07 min and surface roughness = 0.1452 µm. The desirability is nearly 1 (0.713), and it satisfy the goal of the optimization.

5.2 Contribution of the Thesis

1. This thesis contributes the data of machining with TiN tool to the manufacturing industry. This data can be used by the industry during the milling operation of this alloy in order to save the total testing cost and time. Also, the tool life can be predicted by using the equation developed and the optimum parameters required to produce products with good surface roughness can be found.

2. Development of the hybrid nanocoolant TiO_2/ZnO which have a good thermal conductivity and viscosity. This hybrid nanocoolant will extend the tool life and reduce the wear mechanism.

3. This thesis also contributes to the automobile parts and electrical appliance since It has good resistance of corrosion and heat, while also excellent in mechanical properties.

5.3 Recommendation

This present work can be proposed for further work in following area:

- The related approach to be used to predict the other milling response such as cutting force, cutting temperature. Analysis of cutting tool temperature and workpiece temperature is important to predict the amount of heat has been dissipated in the cutting zone when milling with nanofluid and hybrid nanofluid. Therefore, infrared camera is suggested to be used to measure the temperature distribution on the workpiece and cutting tool. Besides that, the similar project can be proposed to predict the cutting parameter for other steel material.

- In addition, the machining process with nanofluid and hybrid nanofluid can recommend with turning and grinding. The identical approach is used to determine the effect of nanofluid and hybrid nanofluid in turning and grinding to reduce the difficulty that associate with heat.
- Machining response can be studied for different type of nanoparticle used to prepare the nanofluid and hybrid nanofluid. On the other hand, the study of cutting response also can be conducted by using different size of nanoparticle.

REFERENCES

Aberoumand, S., & Jafarimoghaddam, A. (2016). Mixed convection heat transfer of nanofluids inside curved tubes: An experimental study. *Applied Thermal Engineering, 108*, 967-979.

Abou-El-Hossein, K., & Yahya, Z. (2005). High-speed end-milling of AISI 304 stainless steels using new geometrically developed carbide inserts. *Journal of materials processing technology, 162*, 596-602.

Abu-Nada, E., & Oztop, H. F. (2009). Effects of inclination angle on natural convection in enclosures filled with Cu–water nanofluid. *International Journal of Heat and Fluid Flow, 30*(4), 669-678.

Afrand, M. (2017). Experimental study on thermal conductivity of ethylene glycol containing hybrid nano-additives and development of a new correlation. *Applied Thermal Engineering, 110*, 1111-1119.

Afrand, M., Toghraie, D., & Ruhani, B. (2016). Effects of temperature and nanoparticles concentration on rheological behavior of Fe3O4–Ag/EG hybrid nanofluid: an experimental study. *Experimental Thermal and Fluid Science, 77*, 38-44.

Alauddin, M., El Baradie, M., & Hashmi, M. (1995). Computer-aided analysis of a surface-roughness model for end milling. *Journal of materials processing technology, 55*(2), 123-127.

Alauddin, M., El Baradie, M., & Hashmi, M. (1996). Optimization of surface finish in end milling Inconel 718. *Journal of materials processing technology, 56*(1-4), 54-65.

Alauddin, M., El Baradie, M., & Hashmi, M. (1997). Prediction of tool life in end milling by response surface methodology. *Journal of materials processing technology, 71*(3), 456-465.

Altintas, Y. (2012). *Manufacturing automation: metal cutting mechanics, machine tool vibrations, and CNC design*: Cambridge university press.

Angayarkanni, S., & Philip, J. (2015). Review on thermal properties of nanofluids: Recent developments. *Advances in colloid and interface science, 225*, 146-176.

Anijdan, S. M., Madaah-Hosseini, H., & Bahrami, A. (2007). Flow stress optimization for 304 stainless steel under cold and warm compression by artificial neural network and genetic algorithm. *Materials & design, 28*(2), 609-615.

Astakhov, V. P. (1998). *Metal cutting mechanics*: CRC press.

Astakhov, V. P. (2006). *Tribology of metal cutting* (Vol. 52): Elsevier.

Atkins, A. (2003). Modelling metal cutting using modern ductile fracture mechanics: quantitative explanations for some longstanding problems. *International Journal of Mechanical Sciences, 45*(2), 373-396.

Avila, R., & Abrao, A. (2001). The effect of cutting fluids on the machining of hardened AISI 4340 steel. *Journal of Materials Processing Technology, 119*(1), 21-26.

Azmi, W., Hamid, K. A., Mamat, R., Sharma, K., & Mohamad, M. (2016). Effects of working temperature on thermo-physical properties and forced convection heat transfer of TiO 2 nanofluids in water–Ethylene glycol mixture. *Applied Thermal Engineering, 106*, 1190-1199.

Baghbanzadeh, M., Carbone, L., Cozzoli, P. D., & Kappe, C. O. (2011). Microwave-assisted synthesis of colloidal inorganic nanocrystals. *Angewandte Chemie International Edition, 50*(48), 11312-11359.

Bailey, J., Jeelani, S., & Becker, S. (1976). Surface integrity in machining AISI 4340 steel. *Journal of engineering for industry, 98*(3), 999-1006.

Balint, D., & Hutchinson, J. (2005). An analytical model of rumpling in thermal barrier coatings. *Journal of the Mechanics and Physics of Solids, 53*(4), 949-973.

Baradie, M. E. (1993). Surface roughness model for turning grey cast iron (154 BHN). *Proceedings of the Institution of Mechanical Engineers, Part B: Journal of Engineering Manufacture, 207*(1), 43-54.

Bawa, H. (1995). *Workshop Technology*: Tata McGraw-Hill India.

Behrens, B.-A., Doege, E., Reinsch, S., Telkamp, K., Daehndel, H., & Specker, A. (2007). Precision forging processes for high-duty automotive components. *Journal of materials processing technology, 185*(1-3), 139-146.

Benardos, P., & Vosniakos, G.-C. (2003). Predicting surface roughness in machining: a review. *International journal of machine tools and manufacture, 43*(8), 833-844.

Bjurka, E. (2012). Analyze of insert geometries, wear types and insert life in milling.

Boothroyd, G. (1988). *Fundamentals of metal machining and machine tools* (Vol. 28): Crc Press.

Boubekri, N., & Shaikh, V. (2015). Minimum quantity lubrication (MQL) in machining: Benefits and drawbacks. *Journal of Industrial and Intelligent Information, 3*(3).

Bouzid, W., Zghal, A., & Sai, L. (2004). Taguchi Method For Design Optimisation of Milled Surface Roughness. *Materials Technology*, *19*(3), 159-162.

Box, G. E., & Draper, N. R. (1987). *Empirical model-building and response surfaces*: John Wiley & Sons.

Bruni, C., d'Apolito, L., Forcellese, A., Gabrielli, F., & Simoncini, M. (2008). Surface roughness modelling in finish face milling under MQL and dry cutting conditions. *International Journal of Material Forming*, *1*(1), 503-506.

Budak, E. (1992). Flexible milling force model for improved surface error predictions. *Proc. 1992 Engineering system Design and Analysis, Istanbul, Turkey*, *47*, 89.

Byrne, G., Dornfeld, D., & Denkena, B. (2003). Advancing cutting technology. *CIRP Annals*, *52*(2), 483-507.

Chandrasekar, M., Suresh, S., & Bose, A. C. (2010). Experimental investigations and theoretical determination of thermal conductivity and viscosity of Al2O3/water nanofluid. *Experimental Thermal and Fluid Science*, *34*(2), 210-216.

Chen, W. (2000). Cutting forces and surface finish when machining medium hardness steel using CBN tools. *International journal of machine tools and manufacture*, *40*(3), 455-466.

Chen, X., Engle, K. M., Wang, D. H., & Yu, J. Q. (2009). Palladium (II)-catalyzed C-H activation/C-C cross-coupling reactions: versatility and practicality. *Angewandte Chemie International Edition*, *48*(28), 5094-5115.

Choi, S., Singer, D., & Wang, H. (1995). Developments and applications of non-Newtonian flows. *ASME FED*, *66*, 99-105.

Choudhury, I., & El-Baradie, M. (1999). Machinability assessment of inconel 718 by factorial design of experiment coupled with response surface methodology. *Journal of materials processing technology*, *95*(1-3), 30-39.

Cormier, M. J., Young, W. A., Johnson, J. A., & Daddona, P. E. (2011). Microprojection array having a beneficial agent containing coating. In: Google Patents.

Coromant, S. (1994). *Modern metal cutting*: Sandvik Coromant.

Das, B., Chattopadhyay, P., Upadhyay, A., Gupta, K., Mandal, M., & Karak, N. (2014). Biophysico-chemical interfacial attributes of Fe 3 O 4 decorated MWCNT nanohybrid/bio-based hyperbranched polyurethane nanocomposite: an antibacterial wound healing material with controlled drug release potential. *New Journal of Chemistry*, *38*(9), 4300-4311.

Das, S. K., Choi, S. U., & Patel, H. E. (2006). Heat transfer in nanofluids—a review. *Heat transfer engineering, 27*(10), 3-19.

Davis, J. R. (1995). *ASM specialty handbook: tool materials*: ASM international.

De Oliveira, A. J., & Diniz, A. E. (2009). Tool life and tool wear in the semi-finish milling of inclined surfaces. *Journal of materials processing technology, 209*(14), 5448-5455.

Dearnley, P., & Grearson, A. (1986). Evaluation of principal wear mechanisms of cemented carbides and ceramics used for machining titanium alloy IMI 318. *Materials Science and Technology, 2*(1), 47-58.

Deshmukh, S., & Sangawar, V. (2016). One-step synthesis of polyethylene microspheres using a modified chemical route for pulmonary drug delivery. *Journal of Taibah University for Science, 10*(4), 485-489.

Dewes, R., Ng, E., Chua, K., Newton, P., & Aspinwall, D. (1999). Temperature measurement when high speed machining hardened mould/die steel. *Journal of materials processing technology, 92*, 293-301.

Dhar, N., Kamruzzaman, M., & Ahmed, M. (2006). Effect of minimum quantity lubrication (MQL) on tool wear and surface roughness in turning AISI-4340 steel. *Journal of materials processing technology, 172*(2), 299-304.

Diniz, A., & Ferreira, J. (2003). Influence of refrigeration/lubrication condition on SAE 52100 hardened steel turning at several cutting speeds. *International journal of machine tools and manufacture, 43*(3), 317-326.

Duangthongsuk, W., & Wongwises, S. (2008). Effect of thermophysical properties models on the predicting of the convective heat transfer coefficient for low concentration nanofluid. *International Communications in Heat and Mass Transfer, 35*(10), 1320-1326.

Dureja, J., Gupta, V., Sharma, V. S., & Dogra, M. (2009). Design optimisation of flank wear and surface roughness for CBN-TiN tools during dry hard turning of hot work die steel. *International Journal of Machining and Machinability of Materials, 7*(1-2), 129-147.

Eastman, J. A., Choi, S., Li, S., Yu, W., & Thompson, L. (2001). Anomalously increased effective thermal conductivities of ethylene glycol-based nanofluids containing copper nanoparticles. *Applied physics letters, 78*(6), 718-720.

El-Khabeery, M., & Fattouh, M. (1989). Residual stress distribution caused by milling. *International journal of machine tools and manufacture, 29*(3), 391-401.

Eldem, S., & Barrow, G. (1976). Tool life in interrupted turning operations. *Isr. J. Technol.*, *14*(4), 172-178.

Endres, J. (2002). *The effects of corner radius on tool flank wear.* Paper presented at the Proceedings of the 2002 NSF Design, Service and Manufacturing Grantees and Research Conference, San Juan, Puerto Rico.

Epifani, M., Giannini, C., Tapfer, L., & Vasanelli, L. (2000). Sol–gel synthesis and characterization of Ag and Au nanoparticles in SiO2, TiO2, and ZrO2 thin films. *Journal of the American Ceramic Society*, *83*(10), 2385-2393.

Esfe, M. H., Saedodin, S., Bahiraei, M., Toghraie, D., Mahian, O., & Wongwises, S. (2014). Thermal conductivity modeling of MgO/EG nanofluids using experimental data and artificial neural network. *Journal of Thermal Analysis and Calorimetry*, *118*(1), 287-294.

Ezugwu, E., Wang, Z., & Machado, A. (1999). The machinability of nickel-based alloys: a review. *Journal of materials processing technology*, *86*(1-3), 1-16.

Farkas, P. (1972). A method of coating diamond particles with metal. In: Google Patents.

Fuh, K.-H., & Wu, C.-F. (1995a). A proposed statistical model for surface quality prediction in end-milling of Al alloy. *International journal of machine tools and manufacture, 8*(35), 1187-1200.

Fuh, K.-H., & Wu, C.-F. (1995b). A residual-stress model for the milling of aluminum alloy (2014-T6). *Journal of materials processing technology, 51*(1-4), 87-105.

Furner, J. M., Yahya, N., & Duffy, M. L. (2005). Teach mathematics: Strategies to reach all students. *Intervention in school and clinic*, *41*(1), 16-23.

Gautier, G., Priarone, P. C., Rizzuti, S., Settineri, L., & Tebaldo, V. (2015). A contribution on the modelling of wire electrical discharge machining of a γ-TiAl alloy. *Procedia CIRP*, *31*, 203-208.

Ghadimi, A., Saidur, R., & Metselaar, H. (2011). A review of nanofluid stability properties and characterization in stationary conditions. *International Journal of Heat and Mass Transfer*, *54*(17-18), 4051-4068.

Giovanola, J. H. (1988). Adiabatic shear banding under pure shear loading part i: direct observation of strain localization and energy dissipation measurements. *Mechanics of Materials*, *7*(1), 59-71.

Gökkaya, H. (2010). The Effects of Machining Parameters on Cutting Forces, Surface Roughness, Built-Up Edge (BUE) and Built-Up Layer (BUL) During Machining

AA2014 (T4) Alloy. *Strojniski Vestnik/Journal of Mechanical Engineering, 56*(9).

Gorlenko, O. (1981). Assessment of surface roughness parameters and their interdependence. *Precision Engineering, 3*(2), 105-108.

Grzesik, W. (2008). *Advanced machining processes of metallic materials: theory, modelling and applications*: Elsevier.

Grzesik, W. (2009). Wear development on wiper Al2O3–TiC mixed ceramic tools in hard machining of high strength steel. *Wear, 266*(9-10), 1021-1028.

Gupta, M. K., Sood, P., & Sharma, V. S. (2016). Optimization of machining parameters and cutting fluids during nano-fluid based minimum quantity lubrication turning of titanium alloy by using evolutionary techniques. *Journal of Cleaner Production, 135*, 1276-1288.

Hadadian, M., Samiee, S., Ahmadzadeh, H., & Goharshadi, E. K. (2013). Nanofluids for heat transfer enhancement–a review. *Physical chemistry research, 1*(1), 1-33.

Harandi, S. S., Karimipour, A., Afrand, M., Akbari, M., & D'Orazio, A. (2016). An experimental study on thermal conductivity of F-MWCNTs–Fe3O4/EG hybrid nanofluid: effects of temperature and concentration. *International Communications in Heat and Mass Transfer, 76*, 171-177.

Hasegawa, M., Seireg, A., & Lindberg, R. (1976). Surface roughness model for turning. *Tribology international, 9*(6), 285-289.

Henglein, A. (1993). Physicochemical properties of small metal particles in solution:" microelectrode" reactions, chemisorption, composite metal particles, and the atom-to-metal transition. *The Journal of Physical Chemistry, 97*(21), 5457-5471.

Hill, W. J., & Hunter, W. G. (1966). A review of response surface methodology: a literature survey. *Technometrics, 8*(4), 571-590.

Hong, I., & Koo, C. H. (2005). Antibacterial properties, corrosion resistance and mechanical properties of Cu-modified SUS 304 stainless steel. *Materials Science and Engineering: A, 393*(1-2), 213-222.

Hoyle, G. (1964). Recent developments in high-speed steels. *Metallurgical Reviews, 9*(1), 49-91.

Hsien, W. L. Y. (2015). Utilisation of Vegetable Oil, Solid Lubricant, Mist Lubrication, Minimum Quantity Lubrication (MQL) in Machining. In *Towards Green Lubrication in Machining* (pp. 19-31): Springer.

Hussein, A. M., Bakar, R. A., Kadirgama, K., & Sharma, K. (2013). Experimental measurement of nanofluids thermal properties. *International Journal of Automotive and Mechanical Engineering, 7*, 850.

Inspektor, A., Oles, E., & Bauer, C. (1997). Theory and practice in diamond coated metal-cutting tools. *International Journal of Refractory Metals and Hard Materials, 15*(1-3), 49-56.

Iranidokht, V., Hamian, S., Mohammadi, N., & Shafii, M. B. (2013). Thermal conductivity of mixed nanofluids under controlled pH conditions. *International Journal of Thermal Sciences, 74*, 63-71.

Jawaid, A., Sharif, S., & Koksal, S. (2000). Evaluation of wear mechanisms of coated carbide tools when face milling titanium alloy. *Journal of materials processing technology, 99*(1-3), 266-274.

Jayal, A. D., & Balaji, A. (2009). Effects of cutting fluid application on tool wear in machining: Interactions with tool-coatings and tool surface features. *Wear, 267*(9), 1723-1730.

Kadirgama, K., Abou-El-Hossein, K., Mohammad, B., Noor, M., & Sapuan, S. (2008). Prediction of tool life by statistic method in end-milling operation. *Scientific Research and Essays, 3*(5), 180-186.

Kadirgama, K., Noor, M., & Rahman, M. (2008). Optimization of surface roughness in end milling on mould aluminium alloys (AA6061-T6) using response surface method and radian basis function network. *Jourdan Journal of Mechanical and Industrial Engineering, 2*(4).

Kakaç, S., & Pramuanjaroenkij, A. (2016). Single-phase and two-phase treatments of convective heat transfer enhancement with nanofluids–A state-of-the-art review. *International Journal of Thermal Sciences, 100*, 75-97.

Khamsehzadeh, H. (1991). *Behaviour of ceramic cutting tools when machining superalloys.* University of Warwick,

Khandekar, S., Sankar, M. R., Agnihotri, V., & Ramkumar, J. (2012). Nano-cutting fluid for enhancement of metal cutting performance. *Materials and Manufacturing Processes, 27*(9), 963-967.

Khuri, A. I., & Cornell, J. A. (1996). *Response surfaces: designs and analyses* (Vol. 152): CRC press.

Kishawy, H., & Elbestawi, M. (1998). Effects of edge preparation and cutting speed on surface integrity of die materials in hard machining. *Proc Int Mech Eng Congr Exp MED, 8*, 269-276.

Kiyak, M., & Çakır, O. (2007). Examination of machining parameters on surface roughness in EDM of tool steel. *Journal of materials processing technology, 191*(1-3), 141-144.

Kline, W., DeVor, R., & Shareef, I. (1982). The prediction of surface accuracy in end milling. *Journal of engineering for industry, 104*(3), 272-278.

Konermann, L., & Douglas, D. (1997). Acid-induced unfolding of cytochrome c at different methanol concentrations: electrospray ionization mass spectrometry specifically monitors changes in the tertiary structure. *Biochemistry, 36*(40), 12296-12302.

Koo, J., & Kleinstreuer, C. (2004). A new thermal conductivity model for nanofluids. *Journal of Nanoparticle Research, 6*(6), 577-588.

Korkut, I., Kasap, M., Ciftci, I., & Seker, U. (2004). Determination of optimum cutting parameters during machining of AISI 304 austenitic stainless steel. *Materials & design, 25*(4), 303-305.

Kumar, S. A., Meenakshi, K. S., Narashimhan, B., Srikanth, S., & Arthanareeswaran, G. (2009). Synthesis and characterization of copper nanofluid by a novel one-step method. *Materials Chemistry and Physics, 113*(1), 57-62.

Lawal, S., Choudhury, I., & Nukman, Y. (2012). Application of vegetable oil-based metalworking fluids in machining ferrous metals—a review. *International Journal of Machine Tools and Manufacture, 52*(1), 1-12.

Lee, P.-H., Nam, J. S., Li, C., & Lee, S. W. (2012). An experimental study on micro-grinding process with nanofluid minimum quantity lubrication (MQL). *International Journal of Precision Engineering and Manufacturing, 13*(3), 331-338.

Lee, S., Choi, S.-S., Li, S., and, & Eastman, J. (1999). Measuring thermal conductivity of fluids containing oxide nanoparticles. *Journal of Heat transfer, 121*(2), 280-289.

Liao, Y., & Shiue, R. (1996). Carbide tool wear mechanism in turning of Inconel 718 superalloy. *Wear, 193*(1), 16-24.

Lima, J., Avila, R., Abrao, A., Faustino, M., & Davim, J. P. (2005). Hard turning: AISI 4340 high strength low alloy steel and AISI D2 cold work tool steel. *Journal of materials processing technology, 169*(3), 388-395.

Liu, C., & Barash, M. (1982). Variables governing patterns of mechanical residual stress in a machined surface. *Journal of engineering for industry, 104*(3), 257-264.

Lu, W., Wei, Z., Gu, Z.-Y., Liu, T.-F., & Park, J. (2014). Tuning the structure and function of metal–organic frameworks via linker design. *Chemical Society Reviews, 43*(16), 5561-5593.

M'Saoubi, R., Outeiro, J., Chandrasekaran, H., Dillon Jr, O., & Jawahir, I. (2008). A review of surface integrity in machining and its impact on functional performance and life of machined products. *International Journal of Sustainable Manufacturing, 1*(1-2), 203-236.

Madhesh, D., & Kalaiselvam, S. (2014). *Energy efficient hybrid nanofluids for tubular cooling applications.* Paper presented at the Applied Mechanics and Materials.

Maheshwary, P., & Nemade, K. (2015). Enhancement in heat transfer performance of ZrO2/H2O nanofluid via ultrasonication time. *International Journal on Recent and Innovation Trends in Computing and Communication (IJRITCC), 3*(2), 35-37.

Manjunathaiah, J., & Endres, W. J. (2000). A new model and analysis of orthogonal machining with an edge-radiused tool. *Journal of Manufacturing Science and Engineering, 122*(3), 384-390.

Masmali, M., & Mathew, P. (2016). *Geometric Chip Analysis of Helical End Milling Based on a Variable Flow Stress Machining Theory.* Paper presented at the Proc. 6th International Conference on Industrial Engineering and Operations Management, Kuala Lumpur, Malaysia: IEOM Society International.

Matsumoto, Y., Barash, M., & Liu, C. (1986). Effect of hardness on the surface integrity of AISI 4340 steel. *Journal of engineering for industry, 108*(3), 169-175.

Matsumoto, Y., Hashimoto, F., & Lahoti, G. (1999). Surface integrity generated by precision hard turning. *CIRP Annals-Manufacturing Technology, 48*(1), 59-62.

McEachron, R., Connors, E. J., & Slutz, D. E. (1993). Multi-layer metal coated diamond abrasives with an electrolessly deposited metal layer. In: Google Patents.

Mead, R., & Pike, D. (1975). A biometrics invited paper. A review of response surface methodology from a biometric viewpoint. *Biometrics, 31*(4), 803-851.

Megatif, L., Ghozatloo, A., Arimi, A., & Shariati-Niasar, M. (2016). Investigation of laminar convective heat transfer of a novel TiO2–carbon nanotube hybrid water-based nanofluid. *Experimental Heat Transfer, 29*(1), 124-138.

Mehrali, M., Sadeghinezhad, E., Latibari, S. T., Kazi, S. N., Mehrali, M., Zubir, M. N. B. M., & Metselaar, H. S. C. (2014). Investigation of thermal conductivity and rheological properties of nanofluids containing graphene nanoplatelets. *Nanoscale research letters, 9*(1), 15.

Melkote, S., & Thangaraj, A. (1994). An enhanced end milling surface texture model including the effects of radial rake and primary relief angles. *Journal of engineering for industry, 116*(2), 166-174.

Minea, A. A. (2017). Hybrid nanofluids based on Al2O3, TiO2 and SiO2: numerical evaluation of different approaches. *International Journal of Heat and Mass Transfer, 104*, 852-860.

Mintsa, H. A., Roy, G., Nguyen, C. T., & Doucet, D. (2009). New temperature dependent thermal conductivity data for water-based nanofluids. *International Journal of Thermal Sciences, 48*(2), 363-371.

Mishra, A., & Prasad, T. (1985). Residual stresses due to a moving heat source. *International Journal of Mechanical Sciences, 27*(9), 571-581.

Mital, A., & Mehta, M. (1988). Surface finish prediction models for fine turning. *The International Journal Of Production Research, 26*(12), 1861-1876.

Montgomery, D. C. (2017). *Design and analysis of experiments*: John wiley & sons.

Munkhbayar, B., Tanshen, M. R., Jeoun, J., Chung, H., & Jeong, H. (2013). Surfactant-free dispersion of silver nanoparticles into MWCNT-aqueous nanofluids prepared by one-step technique and their thermal characteristics. *Ceramics International, 39*(6), 6415-6425.

Muraka, P., Barrow, G., & Hinduja, S. (1979). Influence of the process variables on the temperature distribution in orthogonal machining using the finite element method. *International Journal of Mechanical Sciences, 21*(8), 445-456.

Murshed, S., Leong, K., & Yang, C. (2005). Enhanced thermal conductivity of TiO2—water based nanofluids. *International Journal of Thermal Sciences, 44*(4), 367-373.

Murshed, S., Leong, K., & Yang, C. (2008). Investigations of thermal conductivity and viscosity of nanofluids. *International Journal of Thermal Sciences, 47*(5), 560-568.

Muthukrishnan, N., & Davim, P. (2011). Influence of coolant in machinability of titanium alloy (Ti-6Al-4V). *Journal of Surface Engineered Materials and Advanced Technology, 1*(1), 9-14.

Muthusamy, Y., Kadirgama, K., Rahman, M., Ramasamy, D., & Sharma, K. (2016). Wear analysis when machining AISI 304 with ethylene glycol/TiO 2 nanoparticle-based coolant. *The International Journal of Advanced Manufacturing Technology*, *82*(1-4), 327-340.

Najiha, M., Rahman, M., & Kadirgama, K. (2015). Machining performance of aluminum alloy 6061-T6 on surface finish using minimum quantity lubrication. *International Journal of Automotive and Mechanical Engineering, 11*, 2699.

Najiha, M., Rahman, M., & Kadirgama, K. (2016). Performance of water-based TiO2 nanofluid during the minimum quantity lubrication machining of aluminium alloy, AA6061-T6. *Journal of Cleaner Production, 135*, 1623-1636.

Ng, E.-G., Aspinwall, D., Brazil, D., & Monaghan, J. (1999). Modelling of temperature and forces when orthogonally machining hardened steel. *International journal of machine tools and manufacture, 39*(6), 885-903.

Ning, Y., Rahman, M., & Wong, Y. (2001). Investigation of chip formation in high speed end milling. *Journal of materials processing technology, 113*(1-3), 360-367.

Öktem, H., Erzurumlu, T., & Kurtaran, H. (2005). Application of response surface methodology in the optimization of cutting conditions for surface roughness. *Journal of materials processing technology*, *170*(1-2), 11-16.

Okushima, K., Kakino, Y., Hagihara, S., & Hashimoto, N. (1971). A stress analysis in the orthogonal cutting by photo elasto-plasticity method. *Bulletin of Japan Society of Precision Engineering*(1), 1.

Ostwald, P. F., & Munoz, J. (2008). *Manufacturing processes and systems*: John Wiley & Sons.

Ouchi, C. (2001). Development of steel plates by intensive use of TMCP and direct quenching processes. *ISIJ international*, *41*(6), 542-553.

Oxley, P. L. B. (1989). *The Mechanics of Machining: An Analytical Approach to Assesing Machinability*: Ellis Horwood.

Ozcelik, B., & Bayramoglu, M. (2006). The statistical modeling of surface roughness in high-speed flat end milling. *International journal of machine tools and manufacture*, *46*(12-13), 1395-1402.

Pak, B. C., & Cho, Y. I. (1998). Hydrodynamic and heat transfer study of dispersed fluids with submicron metallic oxide particles. *Experimental Heat Transfer an International Journal*, *11*(2), 151-170.

Parashar, B. N., & Mittal, R. (2002). *Elements of manufacturing processes*: PHI Learning Pvt. Ltd.

Philip, J., & Shima, P. (2012). Thermal properties of nanofluids. *Advances in colloid and interface science*, *183*, 30-45.

Philip, J., Shima, P., & Raj, B. (2008). Evidence for enhanced thermal conduction through percolating structures in nanofluids. *Nanotechnology, 19*(30), 305706.

Pozhar, L. A. (2000). Structure and dynamics of nanofluids: Theory and simulations to calculate viscosity. *Physical Review E, 61*(2), 1432.

Pozhar, L. A., & Gubbins, K. E. (1997). Quasihydrodynamics of nanofluid mixtures. *Physical Review E, 56*(5), 5367.

Rahman, M., Kadirgama, K., & Ab Aziz, A. S. (2014). Artificial Neural Network Modeling of Grinding of Ductile Cast Iron Using Water Based SiO2 Nanocoolant. *International Journal of Automotive & Mechanical Engineering, 9*.

Rahman, M., Kumar, A. S., & Salam, M. (2002). Experimental evaluation on the effect of minimal quantities of lubricant in milling. *International journal of machine tools and manufacture*, *42*(5), 539-547.

Reen, O. W. (1966). Cutting tool material. In: Google Patents.

Ren, H., & Altintas, Y. (2000). Mechanics of machining with chamfered tools. *Journal of Manufacturing Science and Engineering*, *122*(4), 650-659.

Research, G. V. (June 2018). Metal Working Fluids Market Worth $14.54 Billion by 2025. *Metal Working Fluids Market*.

Richardson, J., & Zaki, W. (1954). The sedimentation of a suspension of uniform spheres under conditions of viscous flow. *Chemical Engineering Science, 3*(2), 65-73.

Sajid, M. U., & Ali, H. M. (2018). Thermal conductivity of hybrid nanofluids: A critical review. *International Journal of Heat and Mass Transfer, 126*, 211-234.

Sarafraz, M., Hormozi, F., & Kamalgharibi, M. (2014). Sedimentation and convective boiling heat transfer of CuO-water/ethylene glycol nanofluids. *Heat and Mass Transfer, 50*(9), 1237-1249.

Sarkar, J., Ghosh, P., & Adil, A. (2015). A review on hybrid nanofluids: recent research, development and applications. *Renewable and Sustainable Energy Reviews, 43*, 164-177.

Schuldt, S., Arnold, G., Kowalewski, J., Schneider, Y., & Rohm, H. (2016). Analysis of the sharpness of blades for food cutting. *Journal of Food Engineering, 188*, 13-20.

Senevirathne, S., & Ranaweera, R. (2018). Investigation of effects of Cutting Speed on Tool Wear with Optimum Temperature MQL Aerosol.

Shao, G., Kibira, D., & Lyons, K. (2010). *A virtual machining model for sustainability analysis.* Paper presented at the ASME 2010 International Design Engineering Technical Conferences and Computers and Information in Engineering Conference.

Sharif, F., Arjmand, M., Moud, A. A., Sundararaj, U., & Roberts, E. P. (2017). Segregated hybrid poly (methyl methacrylate)/graphene/magnetite nanocomposites for electromagnetic interference shielding. *ACS applied materials & interfaces, 9*(16), 14171-14179.

Sharif, S. (1999). *Face milling of titanium coated alloys using coated and uncoated carbide tools.* Coventry University,

Sharma, K., Sarma, P., Azmi, W., Mamat, R., & Kadirgama, K. (2012). Correlations to predict friction and forced convection heat transfer coefficients of water based nanofluids for turbulent flow in a tube. *Int. J. Microscale Nanoscale Therm. Fluid Transport Phenom, 3*(4), 1-25.

Sharman, A., Dewes, R. C., & Aspinwall, D. K. (2001). Tool life when high speed ball nose end milling Inconel 718™. *Journal of materials processing technology, 118*(1-3), 29-35.

Shaw, M. C., & Cookson, J. (2005). *Metal cutting principles* (Vol. 2): Oxford university press New York.

Shintani, K., Ueki, M., & Fujimura, Y. (1989). Optimum tool geometry of CBN tool for continuous turning of carburized steel. *International journal of machine tools and manufacture, 29*(3), 403-413.

Smith, S. (1991). An Over View of Modeling and Simulaiton of Milling Process. *Trans of ASME, J. Eng. for Ind., 113*, 169-175.

Sodavadia, K., & Makwana, A. (2014). Experimental investigation on the performance of coconut oil based nano fluid as lubricants during turning of AISI 304 austenitic stainless steel. *Int. J. Adv. Mech. Eng, 4*(1), 55-60.

Stefanescu, D. M., Upadhya, G., & Bandyopadhyay, D. (1990). Heat transfer-solidification kinetics modeling of solidification of castings. *Metallurgical Transactions A, 21*(3), 997-1005.

Stirnimann, J., & Kirchheim, A. (1997). *New Cutting Force Dynamometers for High Precision-Machining.* Paper presented at the Industrial Tooling Conference, Southampton.

Sturesson, P.-O., Håkansson, L., & Claesson, I. (1997). Identification of the Statistical Properties of the Cutting Tool Vibration in a Continuous Turning Operation: Correlation to Structural Properties. *Mechanical Systems & Signal Processing, 11*(3), 459-499.

Sun, S., Brandt, M., & Dargusch, M. (2009). Characteristics of cutting forces and chip formation in machining of titanium alloys. *International journal of machine tools and manufacture, 49*(7-8), 561-568.

Sundar, L. S., Ramana, E. V., Singh, M., & De Sousa, A. (2012). Viscosity of low volume concentrations of magnetic Fe3O4 nanoparticles dispersed in ethylene glycol and water mixture. *Chemical physics letters, 554*, 236-242.

Sundar, L. S., Ramana, E. V., Singh, M. K., & Sousa, A. C. (2014). Thermal conductivity and viscosity of stabilized ethylene glycol and water mixture Al2O3 nanofluids for heat transfer applications: An experimental study. *International Communications in Heat and Mass Transfer, 56*, 86-95.

Sundar, L. S., Singh, M. K., & Sousa, A. C. (2013). Thermal conductivity of ethylene glycol and water mixture based Fe3O4 nanofluid. *International Communications in Heat and Mass Transfer, 49*, 17-24.

Sundaram, R., & K Lambert, B. (1981). Mathematical models to predict surface finish in fine turning of steel. Part II. *The International Journal Of Production Research, 19*(5), 557-564.

Suresh, S., Venkitaraj, K., Selvakumar, P., & Chandrasekar, M. (2011). Synthesis of Al2O3–Cu/water hybrid nanofluids using two step method and its thermo physical properties. *Colloids and Surfaces A: Physicochemical and Engineering Aspects, 388*(1-3), 41-48.

Sutherland, J., & Devor, R. E. (1986). An improved method for cutting force and surface error prediction in flexible end milling systems. *Journal of engineering for industry, 108*(4), 269-279.

Tahat, M. S., & Benim, A. C. (2017). *Experimental Analysis on Thermophysical Properties of Al2O3/CuO Hybrid Nano Fluid with its Effects on Flat Plate Solar Collector.* Paper presented at the Defect and diffusion forum.

Taraman, K. (1974). Multi machining output—multi independent variable turning research by response surface methodology. *International Journal of Production Research, 12*(2), 233-245.

Teng, T.-P., Cheng, C.-M., & Pai, F.-Y. (2011). Preparation and characterization of carbon nanofluid by a plasma arc nanoparticles synthesis system. *Nanoscale research letters*, *6*(1), 293.

Thiele, J. D., & Melkote, S. N. (1999). Effect of cutting edge geometry and workpiece hardness on surface generation in the finish hard turning of AISI 52100 steel. *Journal of materials processing technology*, *94*(2-3), 216-226.

Thiele, J. D., Melkote, S. N., Peascoe, R. A., & Watkins, T. R. (2000). Effect of cutting-edge geometry and workpiece hardness on surface residual stresses in finish hard turning of AISI 52100 steel. *Journal of Manufacturing Science and Engineering*, *122*(4), 642-649.

Tieu, A., Fang, X., & Zhang, D. (1998). FE analysis of cutting tool temperature field with adhering layer formation. *Wear*, *214*(2), 252-258.

Timofeeva, E. V., Gavrilov, A. N., McCloskey, J. M., Tolmachev, Y. V., Sprunt, S., Lopatina, L. M., & Selinger, J. V. (2007). Thermal conductivity and particle agglomeration in alumina nanofluids: experiment and theory. *Physical Review E*, *76*(6), 061203.

Trent, E., & Wright, P. (1991). Heat in Metal Cutting. *Metal Cutting, 3rd Ed. Butterworth Heinemann, Oxford, UK*, 57-85.

Ulutan, D., & Ozel, T. (2011). Machining induced surface integrity in titanium and nickel alloys: A review. *International journal of machine tools and manufacture*, *51*(3), 250-280.

Usui, E., & Shirakashi, T. (1982). Mechanics of machining—from descriptive to predictive theory. *On the Art of Cutting Metals—75 Years Later*, *7*, 13-35.

Vajjha, R. S., & Das, D. K. (2009). Experimental determination of thermal conductivity of three nanofluids and development of new correlations. *International Journal of Heat and Mass Transfer*, *52*(21-22), 4675-4682.

Vivancos, J., Luis, C., Ortiz, J., & González, H. (2005). Analysis of factors affecting the high-speed side milling of hardened die steels. *Journal of materials processing technology*, *162*, 696-701.

Wei, X., Zhu, H., Kong, T., & Wang, L. (2009). Synthesis and thermal conductivity of Cu2O nanofluids. *International Journal of Heat and Mass Transfer*, *52*(19-20), 4371-4374.

Wilborn, E. (2014). Nanofluid enhancement of mineral oil and thermal properties instrument design.

Wu, D., & Matsumoto, Y. (1990). The effect of hardness on residual stresses in orthogonal machining of AISI 4340 steel. *Journal of engineering for industry, 112*(3), 245-252.

Xia, Y., Yang, P., Sun, Y., Wu, Y., Mayers, B., Gates, B., . . . Yan, H. (2003). One-dimensional nanostructures: synthesis, characterization, and applications. *Advanced materials*, *15*(5), 353-389.

Yang, J., Ding, Y., Chen, G., & Li, C. (2007). Synthesis of conducting polyaniline using novel anionic Gemini surfactant as micellar stabilizer. *European polymer journal*, *43*(8), 3337-3343.

Yazid, M., CheHaron, C., Ghani, J., Ibrahim, G., & Said, A. (2011). Surface integrity of Inconel 718 when finish turning with PVD coated carbide tool under MQL. *Procedia Engineering*, *19*, 396-401.

Yiamsawas, T., Mahian, O., Dalkilic, A. S., Kaewnai, S., & Wongwises, S. (2013). Experimental studies on the viscosity of TiO2 and Al2O3 nanoparticles suspended in a mixture of ethylene glycol and water for high temperature applications. *Applied energy*, *111*, 40-45.

Yu, W., & Xie, H. (2012). A review on nanofluids: preparation, stability mechanisms, and applications. *Journal of nanomaterials, 2012*, 1.

Yu, W., Xie, H., Chen, L., & Li, Y. (2010). Investigation on the thermal transport properties of ethylene glycol-based nanofluids containing copper nanoparticles. *Powder technology*, *197*(3), 218-221.

Zhou, X., Wang, D., Liu, X., Zhang, D., Qu, S., Ma, J., . . . Liu, W. (2015). 3D-imaging of selective laser melting defects in a Co–Cr–Mo alloy by synchrotron radiation micro-CT. *Acta Materialia*, *98*, 1-16.

Zhu, H.-t., Lin, Y.-s., & Yin, Y.-s. (2004). A novel one-step chemical method for preparation of copper nanofluids. *Journal of colloid and interface science, 277*(1), 100-103.

LIST OF PUBLICATIONS

1. M. Hussein, Lingenthiran, K. Kadirgamma, M. M. Noor, "Palm oil based nanofluids for enhancing heat transfer and rheological properties",Heat and Mass transfer, 2018, 5, 1-7, Q2 = IF = 1.92

2. K.Kadirgama, K.Anamalai, K.Ramachandran, Lingenthiran, D.Ramasamy, M.Samykano," Thermal analysis of SUS 304 stainless steel using ethylene glycol/nanocellulose-based nanofluid coolant", International Journal of Advanced Manufacturing Technology, Volume 97, Issue 5-8, 1 July 2018, Pages 2061-2076, Q1, IF = 2.94

3. L.Samylingam, K.Anamalai K.Kadirgama M.Samykano D.Ramasamy M.M.Noor.Najafi M.M.Rahman Hong Wei Xian Nor Azwadi Che Sidik Thermal analysis of cellulose nanocrystal-ethylene glycol nanofluid coolant, International Journal of Heat and Mass Transfer Volume 127, Part B, December 2018, Pages 173-181 Q1, IF = 3.94

4. Anamalai, K., Samylingam, L., Kadirgama, K., Ramasamy, D., ,"Multi-objective optimization on the machining parameters for bio-inspired nanocoolant" Journal of Thermal Analysis and Calorimetry, 2018, Article in press, Q2, IF = 1.81

5. Kaaliarasan Ramachandran, Kumaran Kadirgama, Devarajan Ramasamy, Mahendran Samykano, Lingenthiran Samylingam, Faris Tarlochan, Gholamhassan Najafi, Evaluation of Specific Heat Capacity and Density for Cellulose Nanocrystal-based Nanofluid, Journal of Advanced Research in Fluid Mechanics and Thermal Sciences 51, Issue 2 (2018) 169-186, Q1, IF = 0.146